NASA Technical Memorandum 74097

Aerodynamic Characteristics of Airplanes at High Angles of Attack

Joseph R. Chambers and Sue B. Grafton
Langley Research Center
Hampton, Virginia

National Aeronautics
and Space Administration

Scientific and Technical Information Office

1977

SUMMARY

The paper provides an introduction to, and a broad overview of, the aerodynamic characteristics of airplanes at high angles of attack. The discussion includes (1) some important fundamental phenomena which determine to a large extent the aerodynamic characteristics of airplanes at high angles of attack; (2) static and dynamic aerodynamic characteristics near the stall; (3) aerodynamics of the spin; (4) test techniques used in stall/spin studies; (5) applications of aerodynamic data to problems in flight dynamics in the stall/spin area; and (6) the outlook for future research in the area. Stalling and spinning are flight dynamic problems of importance to all aircraft, including general aviation airplanes, commercial transports, and military airplanes. The emphasis in the paper, however, is placed on military configurations and the principal aerodynamic factors which influence the stability and control of such vehicles at high angles of attack.

INTRODUCTION

The present paper has been prepared to provide an introduction to, and a broad overview of, the aerodynamic characteristics of airplanes at high angles of attack. (See the references contained herein for more detailed information.) Such aerodynamic inputs are required for analysis of flight dynamic problems in the high-angle-of-attack regime, where large-amplitude, nonlinear effects predominate. The aerodynamic phenomena involved are extremely complex and generally unpredictable when existing theoretical methods are used. This situation is in marked contrast to the state of the art for low-angle-of-angle conditions, for which the knowledge and understanding of aerodynamics have become refined to the point that theoretical and semiempirical prediction methods are now used routinely to provide satisfactory estimates of stability derivatives for subsonic and supersonic flows.

The discussion includes (1) some important fundamental phenomena which determine to a large extent the aerodynamic characteristics of airplanes at high angles of attack; (2) static and dynamic aerodynamic characteristics near the stall; (3) aerodynamics of the spin; (4) test techniques used in stall/spin studies; (5) applications of aerodynamic data to problems in flight dynamics in the stall/spin area; and (6) the outlook for future research in the area.

Stalling and spinning are flight dynamic problems of importance to all aircraft, including general aviation airplanes, commercial transports, and military airplanes. The emphasis herein, however, is placed on military configurations, and the major aerodynamic factors which influence the stability and control of such vehicles at high angles of attack. Shown in figure 1 is a sketch which depicts the relative ranges of angle of attack for the cruise, high-angle-of-attack, stall, and spin flight regimes for a typical jet fighter.

Experience has shown that aerodynamic characteristics of airplanes at high-angle-of-attack/stall/spin conditions are extremely nonlinear with respect to static motion variables (angles of attack and sideslip) and dynamic motion variables (angular rates); and the magnitude and sense of many important parameters fluctuate rapidly with small increments of angle of attack. Such characteristics are especially prevalent in the lateral-directional axes, as discussed in subsequent sections of this paper. It is shown that these nonlinear effects are strongly dependent upon complex aerodynamic flow fields and the particular airplane configuration under consideration; as a result the state of the art for theoretical predictions of high-angle-of-attack aerodynamics is extremely poor and in marked contrast to the state of the art for linear derivatives. Much wind-tunnel testing is therefore required to insure satisfactory behavior of airplanes at high angles of attack.

SYMBOLS AND NOMENCLATURE

b wing span

c wing chord

$\bar{c}$ mean aerodynamic chord

C_D drag coefficient, $\frac{F_D}{q_\infty S}$

C_L lift coefficient, $\frac{F_L}{q_\infty S}$

C_l rolling-moment coefficient, $\frac{M_X}{q_\infty S b}$

$C_{l_p} = \frac{\partial C_l}{\partial \frac{pb}{2V}}$

$C_{l_\beta} = \frac{\partial C_l}{\partial \beta}$

$C_{l_{\dot{\beta}}} = \frac{\partial C_l}{\partial \frac{\dot{\beta} b}{2V}}$

C_m pitching-moment coefficient, $\frac{M_Y}{q_\infty S \bar{c}}$

$C_{m,i}$ inertial pitching-moment coefficient

$$C_{m_q} = \frac{\partial C_m}{\partial \frac{q\bar{c}}{2V}}$$

$$C_{m_{\dot{\alpha}}} = \frac{\partial C_m}{\partial \frac{\dot{\alpha}\bar{c}}{2V}}$$

C_n yawing-moment coefficient, $\frac{M_Z}{q_\infty S b}$

$$C_{n_r} = \frac{\partial C_n}{\partial \frac{rb}{2V}}$$

$$C_{n_\beta} = \frac{\partial C_n}{\partial \beta}$$

$$C_{n_{\beta,dyn}} = C_{n_\beta} - \frac{I_Z}{I_X} C_{l_\beta} \sin \alpha$$

$$C_{n_{\dot{\beta}}} = \frac{\partial C_n}{\partial \frac{\dot{\beta}b}{2V}}$$

c_y sectional side-force coefficient, $\frac{\text{Side force per unit length}}{b\rho \frac{V^2}{2}}$

C_Y side-force coefficient, $\frac{\text{Side-force coefficient}}{q_\infty S}$

$$C_{Y_r} = \frac{\partial C_Y}{\partial \frac{rb}{2V}}$$

$$C_{Y_\beta} = \frac{\partial C_Y}{\partial \beta}$$

F_D	drag force
F_L	lift force
g	acceleration due to gravity
i_t	horizontal-tail incidence
I_X, I_Z	moments of inertia about X and Z body axes, respectively
ℓ	model length
m	mass
M	Mach number
M_X	rolling moment
M_Y	pitching moment
M_Z	yawing moment
N	model-to-airplane scale ratio
p, q, r	roll, pitch, and yaw rates, respectively
q_v	dynamic pressure at vertical tail
q_∞	free-stream dynamic pressure
R	Reynolds number
S	wing area
$T_{1/2}$	time to damp to half-amplitude
V	free-stream velocity
w	component of resultant velocity V along Z body axis
W	weight
X, Y, Z	body reference axes
α	angle of attack
β	angle of sideslip
δ_a	aileron deflection
δ_h	horizontal-tail deflection

δ_r	rudder deflection
ϵ	angle of downwash
Λ	wing-sweep angle
μ_b	relative-density coefficient
ν	kinematic viscosity
ν_o	kinematic viscosity at sea level
ρ	air density
ρ_o	air density at sea level
σ	$= \frac{\rho}{\rho_o}$
ϕ	roll angle
ψ	yaw angle
Ω	resultant angular velocity

Nomenclature:

stall angle of attack	value of α for maximum usable lift
post-stall	flight regime at α greater than stall
departure	uncommanded event resulting in complete loss of control
coupling	interaction between longitudinal and lateral-directional axes
post-stall gyration	uncontrolled, nonperiodic motions above stall α
spin	sustained, periodic motions above stall α
pitch-up	aperiodic increase in α due to static instability
wing rock	periodic, limit-cycle roll oscillations
directional divergence (nose slice)	aperiodic divergence in yaw due to lateral-directional instability
deep stall	out of control condition at α greater than stall, with no significant motions other than high rate of descent

FUNDAMENTALS

In order to more fully appreciate and understand the unusual aerodynamic characteristics and flight dynamics of airplanes at high angles of attack, the reader should be aware of some fundamental physical phenomena and nomenclature associated with this flight regime. As indicated in figures 2 and 3, the flow conditions at high angles of attack are extremely complex and involve large regions of stalled flow, low-energy wakes from stalled surfaces, strong vortex flows, and aerodynamic interference between various components of the airframe. Basically, it is this poorly defined flow field which produces the strong nonlinear effects discussed subsequently. It is shown that such flows can have a marked adverse effect on the contributions of the tail surfaces to stability and control, the result being that sudden and complete loss of control and inadvertent spins occur. Additional complicating factors such as aerodynamic hysteresis and time lags in flow reattachment further complicate the situation.

It can be appreciated that the foregoing characteristics tend to be configuration dependent; and indeed, the relative importance of certain aerodynamic parameters at high angles of attack has varied through the years with the evolution of airplane configurations (ref. 1). Figure 4 shows the general evolution in fighter design since World War II. For straight-wing propeller-driven fighters of World War II, a relatively large tail length was typical, and as a result most designs remained longitudinally and directionally stable at the stall. The critical airplane characteristics at high angles of attack were reflected primarily in roll by the stalling and autorotative properties of the unswept wing. Also, these designs have relatively good spin and spin-recovery characteristics. In contrast to this situation, today's jet fighters characteristically utilize a close-coupled, swept-wing design with aft engines and a relatively long, pointed fuselage forebody. Such features tend to promote loss of directional stability and rudder effectiveness at the stall, longitudinal instability, and generally poor spin recovery. In short, the major factors and airframe components which influence high-angle-of-attack behavior of fighters have changed from essentially the wing (for the older designs) to the entire configuration (for current designs). As a result, analysis of aerodynamic characteristics of current fighters is much more complicated, and very few generalities can be made.

For background purposes, some nomenclature commonly used in this research area is presented in "Symbols and Nomenclature."

AERODYNAMIC CHARACTERISTICS NEAR STALL

Longitudinal

Pitch-up.- In a broad sense, propeller-driven fighters of World War II experienced few longitudinal stability problems at high angles of attack. However, the evolution of swept-wing designs with close-coupled tail surfaces resulted in some designs with extremely nonlinear aerodynamic pitching moments at high angles of attack. The phenomena involved loss of stability and control

at high angles of attack and resulted in pitch-up and severe operational constraints and safety hazards.

Considerable research has been directed at studies of pitch-up of airplanes. (See refs. 2 to 10, e.g.) Early research showed that depending on wing geometry and tail location, the pitching moment may in some cases break either nose up or nose down at the stall. It is desirable, of course, to have it break nose down, in order to produce a recovering tendency and to reduce the likelihood of severe loss of lift and control. If the break in pitching moment is nose up, very quick control action is needed to prevent a sharp pitch-up, which could lead to complete stall and potential spin entry.

The aspect ratio and sweep of the wing are especially important in determining whether pitch-up will exist at high angles of attack. The connection between these two factors was first drawn in reference 2, which presented a chart dividing unstable wings (pitch-up) from stable ones on the basis of aspect ratio and sweep. This chart is reproduced here as figure 5. The favorable effect of low aspect ratio is shown as well as the unfavorable effect of sweepback. The latter is due to the spanwise flow of the boundary layer and upwash at the tips, which encourage separation from the tips.

As illustrated in figure 6, tails contribute significantly to pitching-moment nonlinearity at high lift coefficient. This is primarily due to the approach toward or departure from the wing wake by the tail as angle of attack changes. A high tail normally approaches the wake at high lift coefficient, and this, of course, increases $d\varepsilon/d\alpha$ as C_L increases. Tip stalling on swept wings enforces this trend by shifting load inboard - in effect reducing aspect ratio - and by raising the tip vortices, causing closer approach of the tail and the vortex wake. All these effects increase $d\varepsilon/d\alpha$ with increasing C_L; the tail contribution to stability is thereby reduced and pitch-up at high C_L occurs as a result. The problem is further aggravated by loss of dynamic pressure at the tail from impingement on the tail of the wake from the stalled wing. In contrast, the low tail exits the vortex wake of the wing as α increases and enters a region of lower $d\varepsilon/d\alpha$. This stabilizing influence tends to offset the pitch-up tendencies arising from other sources.

Although certain swept-wing airplanes have been plagued with sharp decreases of stability at high lift coefficient due to these effects, it is usually possible to straighten out the C_m versus C_L curves and to control pitch-up by proper tail location, as illustrated in figure 6.

The problem of pitch-up becomes even more severe for highly swept arrow-wing configurations. For example, a recent low-speed wind-tunnel study (ref. 11) of a supersonic cruise vehicle employing the highly swept arrow wing has shown that the angle of attack at which pitch-up occurs can be unacceptably low. Figure 7 shows the low-speed longitudinal stability characteristics of a model of the arrow-wing configuration. Preliminary studies of the basic configuration showed that pitch-up occurred at angles of attack of only about 3°. On the basis of wind-tunnel experience obtained with earlier supersonic cruise configurations, the configuration was modified to incorporate wing leading-edge flaps and Krueger flaps; in addition, the sweep of the outboard wing panels was

reduced without severe degradation of supersonic performance. The modified configuration exhibited a linear, stable variation of pitching-moment coefficient with angle of attack up to $\alpha = 18^{\circ}$, which is well beyond the operational envelope of such a vehicle.

The physical flow phenomenon responsible for the pitch-up is shown in figure 8 for $\alpha = 6^{\circ}$. For the basic configuration, the existence of the wing apex vortices and regions of separated flow on the outboard wing panels is evident. In contrast to this flow situation, the photograph for the modified configuration shows that deflecting the wing leading-edge flaps delayed the formation of the vortex flow and that reducing the sweep of the outboard wing panel and employing the Krueger flap eliminated the regions of separated flow on the outer wing.

Deep stall.- One of the most significant flight dynamic problems related to nonlinear longitudinal aerodynamic characteristics at high angles of attack is the phenomenon known as deep stall. For a number of years, jet fighter airplanes with high horizontal tails have been in use by the armed forces of the United States and other countries. Several of these airplanes have displayed undesirable pitch-up tendencies that have been studied in some detail, as for example, in reference 12. More recently, several T-tail transport designs with engines mounted on the aft end of the fuselage have exhibited a tendency to pitch up into what has been called a deep stall. This is a stall continuing to extremely high angles of attack and from which recovery is difficult or impossible.

The problem is illustrated in figure 9. Immersion of the horizontal tail into the combined wake of the wing, engines, and fuselage occurs at an angle of attack greater than the wing stall angle. At the point where the tail has become immersed in the wake, the wing flow has progressed to a well-developed separation. The net effect is to produce a nonlinear variation of pitching moment with angle of attack that has two ranges of stable trim points, the normal range at a low angle of attack and another range at higher angles of attack, as shown in figure 10. Also shown in figure 10 are the increments of pitching moment produced by full nose-up and full nose-down elevator inputs. The data show that the effectiveness of the elevator decreases markedly at angles of attack beyond wing stall, as a result of the impingement of the low-energy wing wake on the elevators, and that insufficient nose-down control exists for recovery from the deep-stall trim point.

The impact of the deep-stall characteristics on flight motions is shown by the time histories from a piloted-simulator study given in figure 11. On this encounter, the pilot used his usual recovery technique for conventional aircraft (pushing the control column forward). He believed his stall recovery was successful, because the attitude angle came down nearly to the horizontal and the airspeed increased; however, he could not recover from the deep-stall trim condition.

Following several crashes of T-tail airplanes, numerous studies, including wind-tunnel and piloted-simulator investigations, have been made of the problem (refs. 12 to 15). Many of the important factors in deep-stall recovery have been identified:

Pitching moment versus angle of attack
Center-of-gravity location
Elevator effectiveness in stall
Stabilizer effectiveness in stall
Thrust moment
Pitch damping
Inertia in pitch
Lateral-directional stability

Of even more importance is the fact that wind-tunnel tests have shown that certain airframe design modifications can alleviate the problem. In addition, the use of α-limiting control systems, such as automatic stick-pushers, can be employed to constrain the maximum obtainable value of angle of attack and thereby eliminate the pitch-up and attendant deep stall.

The nonlinear longitudinal characteristics listed above cannot be treated in a quantitative sense except by experience and wind-tunnel tests. Certain trends have been established, but these data do not suffice for design. It can be said, however, that the methods of approach and general understanding of nonlinear longitudinal aerodynamics at high angles of attack are fairly well established and significantly more refined than those which exist for the lateral-directional problems which are emphasized in the remaining sections of this paper.

Lateral Directional

Asymmetric stall.- Historically, the problems of lateral-directional stability and control at high angles of attack have been much more troublesome than longitudinal stability problems. The problems involve static and dynamic phenomena with extremely complex and nonlinear characteristics.

As noted earlier, aerodynamic characteristics of airplanes with unswept wings at high angles of attack tend to be predominantly related to characteristics of the wing itself. Two of the flight dynamic problems exhibited by such airplanes near or at the stall include asymmetric stall and autorotation.

The results of a combined flight and wind-tunnel study of asymmetrical stall encountered for the general aviation airplane shown in figure 12 are reported in reference 16. Flight studies of the flying characteristics of the airplane indicated that as the stall was approached, insufficient rudder power was available for trim, and a rapid divergence in roll and yaw occurred at the stall. The conjecture of the pilots who conducted the flight studies was that the airplane lost directional stability or rudder effectiveness at the stall. Studies of the airplane in the Langley full-scale tunnel, however, showed that unsymmetrical wing stalling caused out-of-trim rolling and yawing moments of such a large magnitude that the available control power was insufficient to maintain trim. No loss in effectiveness was found in the controls themselves. The magnitudes of the asymmetrical rolling and yawing moments as determined in the wind-tunnel experiments are illustrated by the results shown in figure 13.

The nature of the stall progression as determined from flow-visualization studies is illustrated in figure 14. Large areas of the left wing are seen to be almost completely stalled, whereas only a small region of stalled flow is evident near the root of the right wing. This unsymmetrical stall did not occur with the propellers removed or in the locked condition, but was evident in varying degrees for all power settings from a windmilling to a full-power condition. The propellers rotated in the same direction and produced asymmetric flow over the wings, which was a factor in the asymmetric stall. Studies of a single-engine version of the airplane did not show the large asymmetry in wing stall.

Autorotation.- The concept of autorotation of an unswept wing is illustrated in figures 15 and 16. Figure 15 shows typical variations of C_L and C_D with α for an airplane with an unswept wing. For angles of attack below the stall (point B), the lift increases with increasing α; the reverse is true for angles of attack beyond the stall. The stall angle of attack varies considerably with the wing section and planform, being of the order of 15° for an unswept wing.

As shown in figure 16, if an unswept wing with forward velocity is subjected to a rate of roll p in the clockwise direction, a chordwise section x-x of the right wing (at a distance y from the wing center line) will encounter an increase of local incidence of py/V, and the corresponding section x'-x' of the left wing will have its incidence decreased by an equal amount.

If the section lift curve is as shown in figure 15, and the wing is operating at point A below the stall, the lift of the downgoing right wing will be increased and that of the upgoing left wing will be decreased, and an opposing, or damping, rolling moment will be produced. Thus, stable damping in roll is provided below the stall. For flight above the stall (point C), the lift of the upgoing wing will be increased relative to the downgoing wing, and a propelling, or autorotative, moment will be produced. This situation results in the basic mechanism of the spin for airplanes with unswept wings.

As shown in figure 17, the propelling aerodynamic rolling moment produced in autorotation is a nonlinear function of roll rate, such that as the spin rate increases, the propelling moments become equal to zero and the wing establishes a steady autorotation in roll.

Static lateral-directional stability.- With the advent of swept-wing, close-coupled jet fighter designs, it became obvious that the high-angle-of-attack flight dynamics of fighters involved factors much more predominant than those contributed directly by the wing. In fact, the general nature of stability and control problems at high angles of attack changed from primarily motions about the roll axis (autorotation) to primarily motions about the yaw axis involving directional instability or divergence. The following discussion (ref. 17) is provided to illustrate the nature of lateral-directional stability and control problems at high angles of attack. The discussion is limited to one airplane configuration, but the general trends are typical of many designs.

A typical directional divergence exhibited by the configuration shown in figure 18 at high angles of attack is illustrated by the time histories presented in figure 19. This figure presents flight recorder traces of the principal flight variables during an accelerated stall at 7620 m (25 000 ft) with the airplane configured for cruise flight (M = 0.4). The maneuver was initiated by rolling to a 60° banked turn to the left and then increasing the angle of attack at an approximately constant rate. As the angle of attack was increased, lightly damped lateral oscillations about the longitudinal body axis (termed "wing rock") became noticeable. At about 44 seconds severe wing rock was experienced; at about 50 seconds the oscillation diverged violently and the airplane entered a $2\frac{1}{2}$-turn spin to the right.

In reference 17, static wind-tunnel force tests were conducted to determine the aerodynamic characteristics of the airplane at high angles of attack. Airframe components were tested individually and in several combinations to determine the contributions of the isolated components to the overall stability characteristics of the airplane and to determine mutual interference effects. The effects of several geometric modifications, or fixes, to the basic configuration were evaluated in an attempt to delay or eliminate lateral-directional instability near the stall.

The results of the investigation indicated that the directional divergence exhibited by the airplane was brought about by a simultaneous loss of directional stability and effective dihedral at high angles of attack. The loss of directional stability resulted from a combination of an adverse sidewash region at the rear of the airplane and a reduced dynamic pressure at the vertical-tail location. The adverse sidewash was generated by the wing-fuselage combination and was related to stalling of the leading wing panel during a sideslip at high angles of attack. The loss of effective dihedral was also attributed to stall of the leading wing panel.

The variations of the static lateral-directional force and moment coefficients with angle of sideslip for angles of attack of 0° and 25° are presented in figure 20. As can be seen, the variations of the lateral-directional coefficients with sideslip become very nonlinear at $\alpha = 25°$, and the concept of stability derivatives for such conditions must include a consideration of the range of sideslip involved. For analysis of stability characteristics, the data are usually analyzed over a sideslip range of about ±5°. Stability derivatives obtained for the present configuration for sideslip angles of ±5° are summarized in figure 21. The data were obtained at Reynolds numbers of 0.5×10^6 and 4.3×10^6. The two sets of data agree fairly well, with the exception of a slightly lower level of directional stability for the higher Reynolds number at moderate angles of attack. Both sets of data indicate a marked decrease in C_{n_β} as angle of attack is increased, C_{n_β} being negative at angles of attack above 22°. The data also indicate that as the angle of attack exceeds 15°, a substantial reduction in effective dihedral occurs. Actually, the loss of directional stability at $\alpha = 22°$ is considered to be especially serious because of the corresponding loss of effective dihedral. This aspect of the problem is discussed in detail subsequently.

Also shown in figure 21 is a vertical hatched region indicating the maximum trim capability of the horizontal tail as determined from static-force tests ($i_t = -21^\circ$). It can be seen that there exists a trimmed-angle-of-attack range of almost 10° for which the airplane is directionally unstable.

The results of a series of tests to evaluate the contributions of various airframe components to C_{n_β} are summarized in figures 22 and 23. Data obtained for the isolated wing and fuselage are presented in figure 22 along with data obtained for the wing-fuselage combination. The data of figure 23 show the effects of the addition of the horizontal- and vertical-tail surfaces to the wing-fuselage combination.

Several points are to be noted from comparisons of the various data. For example, the isolated-wing data W of figure 22 indicate little variation of C_{n_β} with increase in angle of attack. This result is to be expected, inasmuch as little if any leading-edge suction is developed on thin sweptback wings. Also, the isolated-fuselage data F show that the fuselage does not become more unstable until the angle of attack exceeds 28°. The wing-fuselage combination WF, however, shows large unstable variations of C_{n_β} with increasing angle of attack. The magnitudes of C_{n_β} are far greater than those expected by simple addition of the values for the isolated wing and fuselage. This type of aerodynamic phenomenon has been noted in the past for sweptback wing-fuselage combinations at high angles of attack (ref. 18).

As stated in reference 18, the large unstable variations of directional stability which exist relative to the body axes are due largely to wing (or wing-fuselage) induced sidewash over the fuselage afterbody. An additional factor to be considered is the fact that when a swept-wing configuration is sideslipped at high angles of attack, stall of the leading wing panel may significantly affect the flow pattern at the rear of the airplane. This fact is illustrated subsequently by tuft photographs.

The adverse sidewash characteristics exhibited by the wing-fuselage combination might be expected to affect adversely the contribution of the vertical tail to directional stability. The data of figure 23 support this assumption by showing that the vertical-tail contribution to directional stability diminishes markedly as α is increased above 20°, and the tail actually becomes destabilizing at angles of attack above 30°.

In order to evaluate the flow conditions at the vertical-tail location, measurements were made of the dynamic pressure and sidewash angle at the tail location. The results of the tests are shown as functions of angle of attack in figures 24 and 25.

The results of the pressure survey are presented as q_v/q_∞, the ratio of dynamic pressure at the vertical-tail location to the free-stream dynamic pressure. The dynamic-pressure ratio decreases as angle of attack increases above 15°. More specifically, as the stall angle of attack is exceeded, the ratio is reduced to less than 50 percent of the value at $\alpha = 0^\circ$ because of combined shielding of the vertical tail by the fuselage afterbody and impingement of the low-velocity wake of the stalled wing-fuselage combination on the vertical tail.

The results of the sidewash measurements are presented in terms of the sidewash parameter $1 - \frac{\partial\sigma}{\partial\beta}$. At low angles of attack, the data of figure 25 indicate that the sidewash is quite favorable, as has been noted in the past for low-wing configurations. (See refs. 19 to 21.) At angles of attack near the stall, however, the sidewash parameter changes from favorable to unfavorable and, at $\alpha = 30^\circ$. becomes negative, the existence of a destabilizing flow field at the vertical-tail location is thereby indicated.

The foregoing data and analysis show that the primary factor producing loss of directional stability for this particular configuration at angles of attack immediately below the stall (angles in the 15° to 20° range) is adverse sidewash on the fuselage afterbody and on the drooped horizontal tail induced by the wing-fuselage combination. As α is increased above a value of about 20°, the vertical tail enters the adverse sidewash field and the dynamic pressure at the vertical tail is reduced because of shielding by the aft fuselage and/or the stalled wake of the wing. Both these factors contribute to a loss of vertical-tail effectiveness at high angles of attack. The adverse sidewash effect is the predominant effect at angles of attack above 30°, where the tail contribution to directional stability actually becomes negative.

A series of tuft studies were conducted to aid in the interpretation of the static-force test results. Photographs of the tuft patterns as α is increased for sideslip angles of 0° and -10° are presented in figures 26 and 27. At $\alpha = 0^\circ$, sideslip induces a strong favorable sidewash field at the vertical tail, as can be seen by the relative angles of the tufts on the fuselage afterbody. This result is in agreement with the results previously presented regarding variations of $1 - \frac{\partial\sigma}{\partial\beta}$. As the angle of attack is increased, however, the favorable sidewash angle is reduced. At $\alpha = 25^\circ$ and $\beta = -10^\circ$, the tuft patterns indicate a complete stall of the leading wing panel and a reversed-flow region behind the stalled wing panel. This reversed-flow region is evident from the tufts on the fuselage behind the wing, and an extensive region of reversed, or low-velocity, flow in the vicinity of the vertical tail was found by exploring with a tuft on a wand. This reversed-flow region behind the stalled wing and fuselage is evidently the cause of the reduction of q_v/q_∞ at the rear of the model, shown in figure 24, and is a major factor contributing to the directional instability of the wing-fuselage combination and to the loss in vertical-tail effectiveness at high angles of attack. The results of the tuft studies also indicate that stall of the leading wing panel is the cause of the loss of effective dihedral at $\alpha = 15^\circ$. Such a result is a characteristic of swept wings at high angles of attack (ref. 22).

In the past, numerous investigations of lateral-directional dynamic stability at high angles of attack (refs. 23 to 26) have been conducted for configurations having relatively high values of the ratio I_Z/I_X together with appreciable values of the effective-dihedral parameter. As a result of past experience, the parameter $C_{n_{\beta,dyn}}$ is usually used as an indication of direc-

tional divergence at high angles of attack, where $C_{n_{\beta,dyn}} = C_{n_\beta} - \frac{I_Z}{I_X} C_{l_\beta} \sin \alpha$. Negative values of the parameter indicate the existence of directional divergence.

Shown in figure 28 are the variations of C_{n_β} and $C_{n_{\beta,dyn}}$ with angle of attack for the basic configuration. The data show that C_{n_β} and $C_{n_{\beta,dyn}}$ approach zero at a common angle of attack of about 21°. The angle of attack at which $C_{n_{\beta,dyn}}$ becomes negative gives a good approximation of the angle of attack at which the airplane exhibits directional divergence.

Inasmuch as it was determined that the wing-fuselage combination was a major factor leading to directional instability, tests were conducted to modify the basic-wing aerodynamic characteristics by drooping the leading edge of the wing. The results of tests showing the effect of 40° leading-edge droop angle on C_{n_β} and C_{l_β} are presented in figure 29. The data indicate that leading-edge droop produced two very significant and beneficial effects. First, the angle of attack at which directional stability was lost was increased from 22° to 25°, and second, C_{l_β} was maintained at moderate levels up to $\alpha = 40°$. These changes, especially the increase in C_{l_β} at high angles of attack, have important beneficial effects on dynamic lateral-directional stability, as is shown in figure 30. With drooped leading edges, the $C_{n_{\beta,dyn}}$ parameter remained positive (stable) over the angle-of-attack range tested, indicating that the directional divergence might be postponed or eliminated by such a modification.

Simultaneous research was being conducted at NASA on the improved maneuverability afforded by leading-edge slats (ref. 27), and analysis of lateral-directional wind-tunnel data obtained with that modification indicated similar improvements in high-angle-of-attack stability. Flight tests subsequently verified these improvements, and the airplane has been retrofitted with leading-edge slats, as shown in figure 31.

Influence of nose shape.- In view of the limitations imposed on military airplanes by poor stall/spin characteristics and the lack of understanding of factors which determine these characteristics, it is highly desirable to identify geometric features of airplanes which promote inherent spin resistance. As a step toward providing this information, NASA has recently conducted an investigation (ref. 28) to provide some insight into the features affecting the lateral-directional stability characteristics of a high-performance, twin-engine fighter which in operation has exhibited outstanding stall and spin characteristics. These characteristics, which result in an inherent resistance to spins, include positive directional stability through the stall with no

tendency to diverge and no significant adverse yaw due to aileron deflection at high angles of attack.

A wind-tunnel investigation was made with the 0.17-scale model shown in figure 32 in order to define some of the more important geometric and aerodynamic characteristics responsible for the good stall and spin characteristics exhibited by the configuration. The study included wind-tunnel free-flight tests, static-force tests, and dynamic (forced-oscillation) force tests.

One airframe component expected to have significant effects on the stability and control of the model at high angles of attack was the wing. Past studies (refs. 19 and 20) have shown that wing planform characteristics, such as sweepback and taper ratio, can have large effects on lateral-directional stability at high angles of attack. In order to evaluate the effects of wing modifications, a swept wing (similar in planform to that employed by the configuration of ref. 17) and a delta wing were also tested, as shown in figure 33. All wings were of equal area and of relatively equal weights, so that the flight tests were conducted with a constant value of wing loading.

The static directional stability characteristics of the basic configuration are presented in figure 34 in terms of the static stability derivative C_{n_β}. The data show that C_{n_β} was large and positive (stable) at low angles of attack. The magnitude of C_{n_β} decreased markedly when the wing stalled at an angle of attack near 17°; but C_{n_β} became increasingly stable at post-stall angles of attack, in contrast to trends shown by most current fighter configurations. (See ref. 17, e.g.) This unusual increase in directional stability at post-stall angles of attack is expected to be a major beneficial factor resulting in the excellent stall characteristics shown by the configuration.

A number of additional component-buildup tests were conducted to determine the airframe component responsible for the pronounced increase in C_{n_β} exhibited by the configuration beyond wing stall. The data shown in figure 35 indicate the contribution of the vertical tail to C_{n_β}. Two significant results are immediately apparent from these data: First, the tail contribution decreased markedly at angles of attack beyond that for wing stall; and second, when the tail was off, the directional stability continued to increase markedly at angles of attack above 25°, with the result that the model was directionally stable at angles of attack above 31° without a vertical tail.

The decrease in tail contribution to directional stability at angles of attack beyond that for wing stall ($\alpha > 17°$) was due to the fact that the tail became immersed in the low-energy wake for the stalled wing. The fact that the loss in tail effectiveness was the result of loss of dynamic pressure at the tail was shown by tests to determine rudder effectiveness. Such loss in tail effectiveness at high angles of attack is not unusual. The most remarkable, and more significant, characteristic is the large increase in tail-off directional stability at high angles of attack.

Additional tests were made to determine the wing-fuselage component responsible for the stability at high angles of attack. The component found to be responsible was the fuselage forebody, as shown in figure 36, which presents

results of tests conducted with the isolated nose mounted on a balance at a distance ahead of the moment center representative of that for the nose of the basic configuration. The data show that the isolated nose was directionally unstable at low angles of attack, as would be expected. At high angles of attack, however, the isolated nose became directionally stable, and comparison of data for the nose alone and data obtained for the basic configuration with the vertical tail off indicates that virtually all the directional stability of the configuration at angles of attack above 32° was produced by the nose.

The geometric feature probably responsible for the aerodynamic characteristics of the fuselage forebody of the present configuration is the cross-sectional shape indicated in figure 36. As shown in the sketch, the cross section is elliptical in shape, with the major axis horizontal. It has been found in the past investigations (refs. 29 to 31) that a "flattened" nose similar to that of the present configuration tends to produce such stability; the relatively long nose of the present configuration tends to accentuate this effect because of the long moment arm through which side forces produced by the nose can act.

The static directional stability characteristics of the swept- and delta-wing configurations are compared with those of the basic configuration in figure 37. As shown, the swept- and delta-wing configurations have levels of directional stability equal to or higher than those of the basic configuration, and the trends of C_{n_β} at high angles of attack were dominated by the characteristics of the nose, as previously discussed for the basic configuration. It should also be noted that the apparent increase in C_{n_β} for the swept- and delta-wing configurations at low angles of attack was caused by the data-reduction procedure, in which the aerodynamic characteristics were based on the geometric characteristics of the individual wings. When compared for equal wing spans, the values of C_{n_β} for the individual wings are about equal at $\alpha = 0°$. The relative unimportance of the large changes in wing planform for the present configuration underlines the complexity of the flow phenomena at high angles of attack and the increased importance of what might be assumed to be secondary design features, such as fuselage forebody shape.

As pointed out in reference 29, a fuselage forebody which produces a large contribution to static directional stability at high angles of attack will also tend to produce unstable values of damping in yaw. Presented in figure 38 is the variation of the damping-in-yaw parameter $C_{n_r} - C_{n_{\dot\beta}} \cos \alpha$ for the basic configuration as measured in forced-oscillation tests. As shown in figure 38, $C_{n_r} - C_{n_{\dot\beta}} \cos \alpha$ was stable (negative) at angles of attack below stall but became unstable near $\alpha = 28°$ and attained very large unstable values at higher angles of attack. The results of tail-off tests showed that the vertical tail had little effect on the unstable values or trends of the data at high angles of attack. Additional forced-oscillation tests were conducted with components of the model to identify the nose as the cause of the unstable values of $C_{n_r} - C_{n_{\dot\beta}} \cos \alpha$ at high angles of attack.

The physical cause of the unstable damping in yaw is illustrated by the sketches shown in figure 39. In figure 39(a) the configuration is shown in a steady sideslipped condition with the same value of β at both the nose and

the center of gravity. As pointed out previously, for the present configuration, the nose produced a side force which acted through a relatively long moment arm to create a stabilizing yawing moment that tended to reduce the value of β. The sketch in figure 39(b) illustrates the situation for yawing flight, with zero sideslip at the center of gravity. Because the flight path is curved, the nose of the configuration is subjected to a local sideslip angle which produces a side force in a manner similar to that for the static situation. In this case, however, the resulting yawing moment is in a direction which tends to increase the value of yawing velocity and therefore results in unstable values of $C_{n_r} - C_{n_{\dot{\beta}}} \cos \alpha$.

The model was flown in the Langley full-scale tunnel using the free-flight model technique described in a later section, and during the flight tests it was found that the basic model flew smoothly and with little effort by the pilots up to an angle of attack of about 20°. Above $\alpha = 20°$ there was a slight nose wandering, or directional "looseness." The nose wandering, although small, increased the pilot effort required to fly the model smoothly. But the pilot was satisfied with the level of stability and considered that the major cause of the increased pilot effort was a rapid decrease in lateral control effectiveness with increasing angle of attack. At an angle of attack of about 30° the model diverged slowly in yaw against full corrective controls. The yawing motion at the divergence appeared to be a fairly slow rotation about the Z body axis. The swept- and delta-wing configurations exhibited the same general flight characteristics as the basic configuration.

The variations of $C_{n_{\beta,dyn}}$ for the swept- and delta-wing configurations are compared with that for the basic configuration in figure 40. The values of $C_{n_{\beta,dyn}}$ were large and positive for all configurations, and no directional divergence was exhibited. It appears, therefore, that the slow directional divergence exhibited by the model near $\alpha = 30°$ was not predicted by $C_{n_{\beta,dyn}}$ but is probably associated with the unstable values of $C_{n_r} - C_{n_{\dot{\beta}}} \cos \alpha$ (fig. 38) or low rudder effectiveness, neither of which is accounted for in the $C_{n_{\beta,dyn}}$ criterion.

It should be pointed out that the influence of nose shape, which was found to have a large influence on the stability of the present configuration at high angles of attack, may be insignificant for other configurations and may be sensitive to variations in Reynolds number for some shapes. The blending of airframe components for good characteristics at high angles of attack is very configuration dependent and there are few general conclusions to be made. Instead, wind-tunnel test techniques and methods of analysis similar to those discussed must be used early in design stages in order to insure good stall characteristics.

Dynamic derivatives.- The dynamic derivatives produced by rolling, yawing, and pitching are important inputs to problems in flight dynamics at high angles of attack. In addition to providing information regarding the dynamic stability of a configuration, they play an important role in the determination of

automatic control system gains and logic required to optimize handling qualities or prevent loss of control.

At the present time, the most reliable values of dynamic derivatives at high angles of attack are provided by forced-oscillation tests in wind tunnels. This particular testing technique is described in reference 32.

The derivatives measured by the forced-oscillation technique are called oscillatory derivatives, and they represent a combination of the pure damping derivatives and certain linear-acceleration derivatives. That is, the longitudinal oscillatory derivatives contain C_{m_q} (damping in pitch) and $C_{m_{\dot{\alpha}}}$ (damping due to normal acceleration), and the lateral derivatives contain C_{l_p} or C_{n_r} (damping in roll or yaw) with a $\dot{\beta}$ (lateral-acceleration) term. Experience has shown that the use of the combination derivatives gives a more reliable prediction of oscillatory stability characteristics than the use of the pure rate derivatives alone. This is particularly true at the higher angles of attack, where the combination derivative can become large because of the effect of flow separation and lag of flow on the linear-acceleration component of the derivative (refs. 33 to 35).

For example, for an early delta-wing airplane, calculations based on pure rate derivatives predicted a high degree of Dutch roll instability at high angles of attack, whereas free-flight model tests had shown stability. At the time there was no way of knowing which of these two sources of information was correct for this new type of airplane on which there was no experience. The calculation might have been in error because of erroneous assumptions in the equations of motion, and the free-flight model results might not have predicted the correct result because of unknown scale effects. When the airplane was flown, it was found to confirm the results of the free-flight model tests, and it was not until some years later when the forced-oscillation equipment was developed that the source of the error in the calculations was discovered. It was in the use of pure rate derivatives and in neglecting the lateral-acceleration ($\dot{\beta}$) derivatives, which were very important at high angles of attack because of the separated flow on delta wings under these conditions.

A proper theoretical treatment, of course, requires that the pure rate and lateral-acceleration derivatives be separated and included separately in the equations of motion. So far, however, it has not been possible to separate these derivatives with any accuracy. Such separation requires the measurement of one of the derivatives separately, so that it can be subtracted from the combined derivatives measured by the forced-oscillation technique; but the equipment for the measurement of one of the separate derivatives is not at hand. Experience has shown, however, that reasonably good accuracy in dynamic stability calculations can be obtained if the derivatives are used correctly in combined form. The evaluation of the derivatives is relatively straightforward in the low lift-coefficient range, but at lift coefficients near the stall, a serious complication develops. Near the stall, the lag in the alternating increase and decrease in separated flow on the wing surfaces produces moments out of phase with the oscillation and causes the derivatives to become functions of the frequency and amplitude of the oscillation.

Figure 41 shows a typical variation of the damping-in-roll parameter with angle of attack, frequency, and amplitude. It is obvious that one could not have calculated motions correctly unless great care had been taken in choosing the appropriate value of the derivative in the stall range. As an illustration, figure 42 shows the damping of a lateral oscillation as calculated with a range of experimentally determined values for the oscillatory derivative $C_{l_p} + C_{l_{\dot{\beta}}} \sin \alpha$.

Figures 41 and 42 show that it is important to measure the oscillatory stability derivatives at frequencies and amplitudes representative of the motions likely to be encountered by the configuration under study. As an aid in choosing representative values, the natural frequency of a configuration can be approximated through considerations of its mass, inertia, and static characteristics. As far as the amplitude of the oscillation is concerned, most published information to date presents derivatives based only on small-amplitude oscillations. For configurations having high values of inertia and damping, it is likely that small-amplitude derivatives will be appropriate for predicting dynamic likelihood that large-amplitude motions may be encountered. Derivatives measured at large amplitude may be more useful in predicting dynamic stability characteristics in these cases. Most of the difficulties arising from measuring the derivatives at an inappropriate amplitude can be avoided by making the measurements over a range of amplitudes. The results of calculations based on the resulting values of the derivatives may then be compared and interpreted to yield useful accurate predictions of full-scale behavior.

The interpretation of the forced-oscillation tests must include a consideration of Reynolds number effects. The preceding discussion has attempted to point out the large effects that the stall can have on the value of the stability derivatives. Because the variation of stall angle with lift coefficient is a function of Reynolds number, it follows that the dynamic stability characteristics may also change with Reynolds number.

THE SPIN

Mechanics of the Spin

The spin has been defined (ref. 36) as a motion in which an airplane in flight at some angle of attack between the stall and 90° descends rapidly toward the Earth while rotating about a vertical axis. The spinning motion is very complicated and involves simultaneous rolling, yawing, and pitching while the airplane is at high angles of attack and sideslip. Since it involves separated flows in the region beyond the stall, the aerodynamic characteristics of the airplane are very nonlinear and time dependent; and hence, at the present time, the spin is not very amenable to theoretical analyses.

The overall spin maneuver can be considered to consist of the three phases: the incipient spin, the developed spin, and the recovery. An illustration of the various phases of the spinning motion is given in figure 43.

The incipient spin occurs from the time the airplane stalls and rotation starts until the spin axis becomes vertical or nearly vertical. During this

time the airplane flight path is changing from horizontal to vertical, and the spin rotation is increasing from zero to the fully developed spin rate. The incipient spin may occur rapidly and consist of approximately the first two turns. At about the half-turn point, the airplane may be pointed almost straight down, but the angle of attack is usually above that of the stall because of the inclined flight path. (See fig. 43.) As the 1-turn point is approached, the nose comes back up and the angle of attack continues to increase. As the airplane continues to rotate into the second turn, the flight path becomes more nearly vertical, and the pitching, rolling, and yawing motions become more repeatable and approach those of the fully developed spin.

In the developed spin the attitude, angles, and motions of the airplane are somewhat repeatable from turn to turn, and the flight path is approximately vertical. The spin is maintained by a balance between the aerodynamic and inertia forces and moments. The spinning motion is made up of rotation about the airplane center of gravity plus translatory motion of the center of gravity; however, it is primarily a rotary motion and is affected mainly by the moments acting on it.

The third phase, the recovery, is caused by a change in the moments to upset the balance between the aerodynamic and inertia moments. Such a change in the moments is obtained by deflecting the controls of the airplane. The specific control movements required in any particular airplane depend on certain mass and aerodynamic characteristics, which are discussed in reference 36.

As an example of the interaction between aerodynamic and inertial moments in a developed spin, figure 44 shows the balance required about the pitch axis of the airplane. The sketch on the left of figure 44 shows that at spin attitudes, an airplane usually experiences a nose-down aerodynamic pitching moment. This moment is balanced by the inertial moments depicted in the sketch at the right of the figure. In the right-hand sketch, the mass distribution of the airplane has been represented by a system of weights. As the weights rotate about the spin axis, centrifugal forces acting perpendicular to the spin axis create a nose-up inertial pitching moment; and for the steady developed spin, the nose-up inertial moment balances the nose-down aerodynamic moment. The magnitude of the inertial pitching-moment coefficient may be calculated by the expression

$$C_{m,i} = 4\,\frac{I_Z - I_X}{mb^2}\left(\frac{\Omega b}{2V}\right)^2 \frac{b}{c}\,\mu_b \sin 2\alpha$$

The magnitude of the inertial moment is thus dependent on the inertial distribution of the airplane, the nondimensional spin rate, the relative density of the airplane, and the angle of attack. This expression can be used to calculate the magnitude of the inertial pitching moment for a configuration based on mass characteristics and nondimensional spin rates.

Figure 45 presents the variation with angle of attack of the aerodynamic pitching moment for a typical configuration and the calculated inertial

pitching moment (plotted with algebraic sign reversed) based on values of Ω which balance aerodynamic and inertial yawing moments. Points at which the two curves intersect denote potential-steady-spin calculations satisfying the condition of a balance of inertial and aerodynamic moments. As can be seen, two intersection points, denoted A and B, exist. Examination of the characteristics at point A, however, shows this point to be an unstable equilibrium condition, inasmuch as a positive increment of angle of attack at point A creates a larger nose-up inertial moment. Therefore, the angle of attack will continue to increase until the stable conditions of point B are reached. Similar moment balances must be maintained about the lateral and directional axes at similar conditions for a steady spin to exist.

Possibly the most complex and challenging research area in flight dynamics at high angles of attack is a theoretical analysis of the spin. The physical terms in the equations of motion and the general phenomena are known; however, a definition of the complex aerodynamic characteristics of spinning airplanes has not yet been accomplished to the extent that theoretical approaches can be trusted for prediction of critical spin and spin-recovery characteristics. In fact, many of the aerodynamic inputs required for such analyses have not yet been measured in wind tunnels.

Static Aerodynamic Characteristics

Asymmetric yawing moments.- The use of pointed fuselage forebodies for present-day supersonic aircraft can have large effects on the stability and control characteristics of these vehicles at high angles of attack. For extremely high angles of attack, such as those angles associated with post-stall flight and spins, these shapes have been found (ref. 29) to produce large asymmetric yawing moments which can be much larger than the corrective moments produced by deflection of a conventional rudder. These moments may have a predominant effect on stall and spin characteristics and can, in fact, determine the ease and direction in which an airplane may spin. (See ref. 37.) Although the aerodynamic asymmetries produced by sharp noses have been measured in past wind-tunnel investigations of airplane spin characteristics, the basic flow phenomenon was not well understood. As a result, the asymmetries either have often been ignored or have been attributed to poor wind-tunnel flow or significant model asymmetries. Such asymmetries will indeed determine the direction of the yawing moments, but they are not the cause of the large moments.

The results of past investigations such as those of reference 29 have indicated that the large asymmetric yawing moments produced by long, pointed fuselage forebodies are caused by asymmetric shedding of vortex sheets from the nose. As shown in figure 46, flow separation on a long nose at zero sideslip tends to produce a symmetrical pattern of vortex sheets at low angles of attack. This symmetrical flow pattern does not produce any side force on the nose; consequently, no yawing moment is produced. At higher angles of attack, however, the vortices increase in strength; the flow pattern becomes asymmetrical; and the asymmetrical flow produces a side force on the nose which, in turn, produces a yawing moment about the airplane center of gravity.

The investigation in reference 29 indicated the magnitude of such moments for the configuration shown in figure 47. Figure 48 shows the variation of static yawing-moment coefficient C_n with angle of attack at zero sideslip and neutral controls as measured during tests of four separate models of the configuration. The value of C_n remained near zero at low angles of attack, as might be expected. For angles of attack greater than about 30°, however, large excursions of C_n occurred. The magnitudes of the yawing moments are best appreciated by comparison with the value indicated by the dashed line, which indicates the magnitude of C_n produced by a full rudder deflection of 7.5° in the normal, low-angle-of-attack flight range. The out-of-trim moments near $\alpha = 60°$ are several times larger than the moments produced by full-rudder deflection at low angles of attack and are much larger than the moments which would be obtained by rudder deflection at $\alpha = 60°$, because of the marked reduction in rudder effectiveness at high angles of attack due to shielding by the fuselage and wing.

Large out-of-trim yawing moments at high angles of attack have been noted in past investigations of pointed bodies of revolution (refs. 38 to 42), highly swept delta-wing-body combinations (ref. 43), and other airplane configurations. In all cases, the large yawing moments were attributed to asymmetrical shedding of vortex sheets off the long, sharply pointed nose.

Recent wind-tunnel studies (ref. 44) of the tangent-ogive body shown in figure 49 have produced more information on this phenomenon. As shown in figure 50, the data show that the basic tangent-ogive model experienced no significant values of yawing moment at zero sideslip for low angles of attack, as expected. For values of α greater than 40°, however, large asymmetric values of C_n and C_Y were measured. The asymmetries reached maximum values near $\alpha = 55°$ and decreased to near zero values at approximately $\alpha = 65°$. It was found that the data were repeatable to within ±5 percent, and no hysteresis effects were found. It is important to note that the asymmetric values of C_n were primarily positive, or nose right, in sense. These nose-right moments were accompanied by positive values of C_Y (side force to the right). This relationship is an indication of the potential of large side forces on an airplane nose to cause large asymmetric yawing moments at high angles of attack.

The results of tuft flow-visualization tests conducted for the tangent-ogive model at $\beta = 0°$ and $\alpha = 55°$ are shown in figure 51. At this value of α, where the model experienced a maximum asymmetric value of C_n to the right, the tufts show that an asymmetrical pattern of vortex sheets, similar to those indicated by the sketch of figure 46, was shed by the model. One relatively small vortex core was displaced high above and to the left of the model, whereas a large vortex core was located slightly above and to the right of the model. The flow pattern was relatively invariant with time. Although no pressure measurements were made, the data indicated that the large vortex core remained close to the body. The resulting vortex induces flow on the body and creates a side force to the right.

An example of the correlation of the foregoing results with those obtained for conventional airplane configurations is presented in figure 52, where the vortex sheets have been further defined by use of smoke. The photograph shown

at the left of the figure shows the tangent-ogive model at $\alpha = 55^{\circ}$, $\beta = 0^{\circ}$. The photograph at the right of the figure shows similar results obtained for the model of reference 29 at $\alpha = 60^{\circ}$, $\beta = 0^{\circ}$. Both models exhibited large positive asymmetric values of C_n for these test conditions. The flow patterns about the models are very similar in nature. In particular, the small vortex core is seen to separate near the nose of the model and trail horizontally downstream, whereas the large vortex core remains close to the body and extends a considerable length from the nose tip.

An interesting measure of the degree of asymmetry induced by the flow field shown in the previous photographs is afforded by consideration of the inclination of the resultant force within the YZ-plane of the model. Shown in figure 53 is the inclination of resultant force obtained by adding vectorially the side-force and normal-force coefficients at $\beta = 0^{\circ}$. The data show that the resultant force was inclined over 40° from the vertical near $\alpha = 55^{\circ}$.

Past investigations (ref. 37, e.g.) have shown that small strakes placed near the tip of the nose of a pointed body can eliminate or minimize large asymmetric yawing moments at high angles of attack. A series of tests were therefore conducted to determine the effectiveness of strakes for the tangent-ogive body. The strakes tested were placed symmetrically in the XY-plane of the model, and the results are shown in figure 54. The effect of the strakes was to produce a well-defined point of separation which resulted in a symmetrical flow field at all angles of attack and elimination of the asymmetries.

Nose strakes have been incorporated in some current fighter designs for the foregoing reasons as well as for the beneficial effects produced by the strakes on directional stability at high angles of attack. (See fig. 55, e.g.) Additional information on effects of Mach and Reynolds number and nose strakes on asymmetric yawing moments can be found in references 45 and 46.

Stability and control characteristics.- A good appreciation of the violent nature of stall/spin motions and the magnitudes of variations of the important motion parameters is needed to establish the aerodynamic data inputs required to model the motions properly. Figure 56 (from ref. 47) illustrates the types of motion experienced during a flight which includes a departure, spin entry, and a developed oscillatory spin. In this flight, the airplane was flown into a high-g, windup turn during which full aft stick and full aileron were applied. A departure resulted with angle of attack rapidly exceeding 40°, sideslip excursions in excess of ±25°, and yaw rates of over 50 deg/sec. With controls neutralized, the motion settled into a developed, oscillatory spin near $\alpha = 60^{\circ}$ with a yaw rate of 50 deg/sec. This record illustrates the wide range of angle of attack (0° to 90°), sideslip (±40°), rotation rate (in excess of 50 deg/sec), and control-surface deflections (and combinations of deflections) that must be tested to obtain the aerodynamic data needed to model such a large-amplitude motion.

Considerable nonlinearity with angle of attack and sideslip has been found for both longitudinal and lateral-directional static aerodynamic data. Some examples of the degree of nonlinearity with β are shown in figure 57. The upper figure shows the variation of yawing-moment coefficient with sideslip at

$\alpha = 80^\circ$. Note that directional stability varies from highly unstable to highly stable over the β range. The lower figure illustrates the considerable variation of pitching-moment coefficient with sideslip that can occur at high angles of attack. Such large, nose-up changes in C_m with β can produce significant pitch-up tendencies (post-stall motions).

Aerodynamic control characteristics have also been found to exhibit high degrees of nonlinear dependence on angle of attack, sideslip, and control-surface deflections; in addition, deflection of control surfaces can dramatically influence aerodynamic stability. Some of these effects are illustrated in figure 58. The dependence of horizontal-tail effectiveness on tail deflection and sideslip is shown in the top figure for $\alpha = 30^\circ$. The lower left figure illustrates the difference that can occur at spin angles of attack between the moment increments obtained by adding individual control effects (solid line) and those obtained by measuring the moments due to the combined controls (dashed lines). The effect of control deflection on static directional stability is illustrated in the lower right of the figure.

As discussed earlier, the long, pointed fuselage forebody has considerable effect on the static aerodynamic characteristics of current fighters. For example, in reference 29 it was shown that the pointed nose of the design illustrated in figure 47 was responsible for the nonlinear trends of C_n with β at $\alpha = 55^\circ$, as shown in figure 59. The characteristic S-shape of the C_n variation is associated with the separation and attachment pattern of the vortex sheets shed off the nose.

Shown in figure 60 are the variations of the static stability derivatives C_{Y_β} and C_{n_β} with angle of attack for wing-sweep angles of 26°, 50°, and 72.5°. The variation of C_{n_β} with α shows that the directional stability becomes negative, or unstable, for the various wing-sweep angles at angles of attack between 23° and 30°. As the angle of attack was increased above about 50°, the values of C_{n_β} became positive; at an angle of attack of 60°, the values of C_{n_β} were about 4 times as large as the value at $\alpha = 0^\circ$. The large increase in directional stability was accompanied by a large positive change in C_{Y_β} and indicated that the nose of the airplane was responsible for the large yawing moments due to sideslip.

Dynamic aerodynamic characteristics.- Results of small-amplitude, forced-oscillation tests of fighter configurations at spin angles of attack have indicated large, abrupt variations with angle of attack. For example, shown in figures 61 and 62 are results of tests in pitch and yaw for oscillatory amplitudes of $\pm 5^\circ$ for the variable-sweep fighter design of figure 47. The large unstable values of the damping-in-yaw parameter $C_{n_r} - C_{n_{\dot\beta}} \cos\alpha$ shown in figure 62 are especially noteworthy, inasmuch as they further illustrate the phenomena discussed earlier - that a stabilizing fuselage forebody produces unstable damping in yaw.

Experience has indicated that small-amplitude forced-oscillation data provide an insight as to possible autorotative, or prospin, mechanisms; however,

data measured with rotary-spin techniques (discussed later) show that aerodynamic moments, particularly yawing moments, exhibit marked nonlinearities with rate of rotation during conditions experienced by an airplane in a steady spin. Some typical results obtained with this technique are shown in figure 63, where the measured variation of yawing moment with rotation rate $\Omega b/2V$ at $\alpha = 90^\circ$ for two dissimilar current fighter configurations is plotted. Note the highly nonlinear dependence of C_n on $\Omega b/2V$, such that propelling moments are produced at lower rates and damping moments are produced at higher rates. The critical nature of fuselage cross section, Reynolds number, and spin rate on this characteristic is discussed in reference 48.

Aerodynamic control effectiveness measured under rotating conditions has also been found to be as complex as under static conditions. For example, shown in the right part of figure 63 is the measured variation of C_n with $\Omega b/2V$ for two horizontal-tail settings: neutral and full nose-up (-21°). The marked effect of control deflection on the measured aerodynamics is evident. Thus, the same large influence of horizontal-tail deflection on static stability discussed earlier is also evident under rotating conditions. The importance of such data for mathematical studies of spinning is discussed in a later section of this paper.

Additional information relating to nonlinear dynamic data and the flat spin is presented in reference 49.

TEST TECHNIQUES

Introduction

Perhaps the most valuable contribution to an analysis of the stall/spin characteristics of a modern military airplane is an accurate prediction of these characteristics at an early design stage. Unfortunately, standard design procedures which are usually applied with success to conventional unstalled flight are severely limited in application to the stall/spin area because of the relatively complex aerodynamic phenomena previously discussed.

In view of the general lack of understanding of the stall/spin problem, NASA has developed several unique test techniques and facilities for stall/spin studies. For example, the only operational spin tunnel in the United States is located at the NASA Langley Research Center. Because of the specialized techniques involved, much of the stall/spin research for military aircraft and virtually all the dynamic model flight tests related to stall/spin are conducted by NASA.

These studies involve the use of a wide matrix of tools, including conventional wind-tunnel static-force tests, dynamic-force tests, flight tests of dynamic models, theoretical studies, and piloted-simulator studies. The present paper describes three of the more important techniques: (1) flight tests of dynamically scaled models, (2) rotary-balance tests, and (3) piloted-simulator studies.

Dynamic Model Techniques

As a result of the complexity of the stall/spin problem and the lack of proven alternate predictive methods, the most reliable source of information on stall/spin characteristics prior to actual flight tests of the particular airplane has been tests of dynamically scaled airplane models. A properly scaled dynamic model with the proper values of the various aerodynamic and inertial parameters may be thought of as a simulator - albeit subject to some effects of Reynolds and Mach numbers.

NASA has developed several unique dynamic model test techniques for stall/spin studies. This section describes three of the more important test techniques and includes the objectives, advantages, limitations, and area of application of each technique. The techniques are (1) the wind-tunnel free-flight technique, (2) the outdoor radio-controlled model technique, and (3) the spin-tunnel test technique.

Before the techniques are discussed, however, a brief review of model scaling laws is in order to properly introduce the reader to dynamic model testing and to clarify some of the reasons for the test equipment and procedures.

Model scaling considerations.- Dynamic models must be scaled in each of the fundamental units of mass, length, and time in order to provide test results that are directly applicable to the corresponding full-scale airplane at a given altitude and loading condition. Units of length are, of course, scaled from geometric ratios; units of mass are scaled from those of the full-scale airplane on the basis of equal relative-density coefficients; and time is scaled on the basis of equal Froude numbers. As a result of scaling in this manner, the motions of the model are geometrically similar to those of the full-scale airplane, and motion parameters can be scaled by applying the scale factors given in table I.

Some limitations of the dynamic model test techniques are apparent from an examination of the factors given in table I. For example, the model is tested at a value of Reynolds number considerably less than that of the full-scale airplane at comparable flight conditions. A 1/9-scale dynamic model has a Reynolds number only 1/27 that of the corresponding airplane. It should also be noted that although the linear velocities of the model are smaller than full-scale values, the angular velocities are greater than full-scale values. For example, a 1/9-scale model has a flight speed only 1/3 that of the airplane, but it has angular velocities that are 3 times as fast as those of the airplane. Because of the scaling of speed, Mach effects are not represented.

The discrepancy in Reynolds number and Mach number between model and full-scale airplanes can be an important factor which requires special consideration for stall/spin tests. For example, during spin-tunnel tests, there may be present large Reynolds number effects which cause the model to exhibit markedly different characteristics than those associated with correct values of Reynolds number. This point is discussed in detail in a later section on spin-tunnel testing.

The fact that the angular velocities of the model are much faster than those of the airplane poses special problems in controllability of the model for certain techniques. Because the human pilot has a certain minimum response time, it has been found that a single human pilot cannot always satisfactorily control and evaluate dynamic flight models. It is shown in subsequent sections how this control problem is overcome by use of multiple pilots.

As previously discussed, the stall and spin of an airplane involve complicated balances between the aerodynamic and inertial forces and moments acting on the vehicle. In order to conduct meaningful tests with dynamic models, it is important that these parameters be properly scaled. It is therefore mandatory that the scale factors given in table I be used to arrive at a suitable dynamic model. Simply scaling dimensional characteristics without regard to other parameters (as is the case for most radio-controlled hobbyist models) will produce erroneous and completely misleading results. It should also be appreciated that because of the scaling laws, Mach and Reynolds numbers cannot be scaled.

The wind-tunnel free-flight technique.- Each of the model test techniques to be discussed in this paper has a particular area of application within a broad study of stall/spin characteristics for a given airplane configuration. The first technique to be discussed, known as the wind-tunnel free-flight technique, is used specifically to provide information on flight characteristics for angles of attack up to and including the stall for 1g flight. The test setup for this model test technique is illustrated by the sketch shown in figure 64. A remotely controlled dynamic model is flown without restraint in the 9.1- by 18.2-m (30- by 60-ft) open-throat test section of the Langley full-scale tunnel. Two pilots are used during the free-flight tests. One pilot, who controls the longitudinal motions of the model, is located at one side of the test section; the second pilot, who controls the lateral-directional motions of the model, is located in an enclosure at the rear of the test section. The model is powered by compressed air, and the level of the thrust is controlled by a power operator who is also located at the side of the test section.

The cable attached to the model serves two purposes. The first purpose is to supply the model with compressed air, electric power for control actuators, and control signals through a flexible trailing cable which is made up of wires and light plastic tubes. The second purpose of the cable is concerned with safety. A portion of the cable is a steel cable that passes through a pulley above the test section. This part of the flight cable is used to catch the model when a test is terminated or when an uncontrollable motion occurs. The entire flight cable is kept slack during the flight tests by a safety-cable operator, who accomplishes this job with a high-speed pneumatic winch.

The model incorporates limited instrumentation for measurements of motion and control deflections. The instrumentation consists of control-position indicators on each control surface and a three-axis rate-gyro package. The output of the instrumentation is transferred by wires to the location of the test crew, where the data are recorded in time-history form by oscillograph recorders. Motion-picture records from several vantage positions are also made during the flights.

Although it is possible for a single human pilot to fly the model by operating all controls simultaneously, such an arrangement is not suitable for research purposes, because the pilot must concentrate so intently on the task of keeping the model flying satisfactorily that he is not able to evaluate its flight characteristics in sufficient detail. This intense concentration is required for several reasons, one of which (the high angular velocities of the model) was indicated previously in the section on model scaling considerations. Another factor contributing to the difficulty of control is the lack of "feel" in flying a model by remote control. In this technique the human pilot does not sense accelerations as the pilot of an airplane does, and therefore, he must fly with sight cues as the primary source of information. This lack of other cues results in lags in control inputs, which become very significant when attempts are made to fly a model within a relatively restricted area within the tunnel test section. These control problems are especially aggravated during tests of airplane configurations at high angles of attack, where lightly damped lateral oscillations (wing rock), directional divergence (nose slice), and longitudinal instability (pitch-up) are likely to occur.

In the wind-tunnel free-flight technique, each pilot concentrates only on the phase of model motion for which he is responsible. As a result, he is able to fly the model with greater ease and relaxation and can thoroughly evaluate the characteristics of the model. In this manner, the control difficulties inherent in the free-flight technique are largely compensated for.

The wind-tunnel free-flight technique can produce valuable information during studies of flight motions at high angles of attack and at stall. Various phases of a typical investigation would include (1) flights at several values of angles of attack up to and including the stall to evalute dynamic stability characteristics, (2) an evaluation of pilot lateral control techniques at high angles of attack, and (3) an evaluation of the effects of stability augmentation systems.

Studies of dynamic stability characteristics at high angles of attack and at the stall are conducted by varying the tunnel airspeed, the model thrust, and the model angle of attack in steps, in order to trim the model at several values of angle of attack, and noting the resulting dynamic stability characteristics at each trim condition. By simultaneously reducing the tunnel airspeed and increasing the model angle of attack and thrust, the model can be flown through maximum lift, or if the model exhibits a dynamic instability, it can be flown to the point where loss of control occurs. As a result of this type of study, instabilities which could seriously limit the maneuvering capability and endanger the safety of the full-scale airplane are easily and safely identified.

An evaluation of the effect of lateral control inputs at high angles of attack is made by using the lateral-directional controls both individually and in various combinations. This method gives an indication of the relative effectiveness of the controls at high angles of attack as well as an evaluation of adverse yaw characteristics. These tests are important because it is possible for a configuration which is otherwise dynamically stable to experience an out-of-control condition caused by lack of adequate control power or excessive adverse yaw.

The model is equipped with a simplified stability augmentation system in the form of artificial angular rate damping in roll, yaw, and pitch. Air-driven rate gyroscopes are used in conjunction with proportional-type control servos to produce artificial variations in the aerodynamic damping of the model. The effect of stability augmentation about each individual axis is evaluated as part of the free-flight program. At the current time, equipment is being developed to upgrade the capability of the test technique to simulate advanced flight control systems.

The wind-tunnel free-flight technique has several inherent advantages: (1) because the tests are conducted indoors, the test schedule is not subject to weather conditions; (2) the tests are conducted under controlled conditions, and a large number of tests can be accomplished in a relatively short period of time; (3) airframe modifications are quickly evaluated; and (4) models used in the technique are relatively large (1/10 scale for most fighter configurations) and can therefore be used in force tests to obtain static and dynamic aerodynamic characteristics for analysis of the model motions. These aerodynamic characteristics can also be used as inputs for other forms of analysis, such as piloted-simulator studies.

The outdoor radio-controlled model technique.- A significant void of information exists between the results produced by the wind-tunnel free-flight test technique for angles of attack up to and including the stall and the results produced by the spin-tunnel test technique, which defines developed spin and spin-recovery characteristics. The outdoor radio-controlled model technique has, therefore, been designed to supply information on the post-stall and spin-entry motions of airplanes. The technique used at Langley Research Center has been used for a number of years. The Langley radio-controlled model technique consists of launching an unpowered, dynamically scaled, radio-controlled model into gliding flight from a helicopter, controlling the flight of the model from the ground, and recovering the model with a parachute. A photograph showing a typical model mounted on the launching rig of the helicopter is shown in figure 65.

The models used in these tests are made relatively strong to withstand the high landing impact loads of 100g to 150g. They are constructed primarily of fiber glass plastic. The fuselages are 0.64-cm (0.25-in.) thick hollow shells and the wings and tails have solid balsa cores with fiber glass sheet coverings. The model weights vary up to about 890 N (200 lb) for simulation of relatively heavy fighters at an altitude of 9144 m (30 000 ft). Radio receivers and electric-motor-powered control actuators are installed to provide individual operation of all control surfaces and a recovery parachute. Proportional-type control systems are used in this technique.

The instrumentation for the radio-controlled models usually consists of a three-axis linear-accelerometer package, a three-axis rate-gyro package, control-position indicators, and a nose boom equipped with vanes to measure angle of attack, angle of sideslip, and velocity. The signals from the instrumentation are transmitted to the ground via telemetry.

Two ground stations are used for controlling the flight of the model. The control duties are shared by two pilots, since this technique is also

susceptible to the control difficulties previously discussed for the wind-tunnel flight tests. Each ground station is provided with a radio control unit, communications equipment, a motorized tracking unit equipped with binoculars (to assist the pilots in viewing the flight of the model), and motion-picture cameras to photograph the motions of the model for subsequent analysis. A photograph of the tracking and controlling equipment is shown in figure 66. All phases of the test operation are directed by a test coordinator. In addition, magnetic tape recorders on the ground are used to record voice communications between the helicopter, coordinator, and model pilots.

The models are trimmed for approximately zero lift and launched from the helicopter at an airspeed of about 40 knots and an altitude of about 1524 m (5000 ft). The models are allowed to dive vertically for about 5 seconds, after which the horizontal tails are moved to stall the mode. After the stall, various control manipulations may be used; for example, lateral-directional controls may be moved in a direction to encourage any divergence to develop into a spin. When the model has descended to an altitude of about 152 m (500 ft), a recovery parachute is deployed to effect a safe landing.

The outdoor radio-controlled model technique provides information which cannot be obtained from the other test techniques. The indoor free-flight tests, for example, will identify the existence of a directional divergence at the stall, but the test is terminated before the model enters the incipient spin. In addition, only 1g stalls are conducted. The radio-controlled technique can be used to evaluate the effect of control inputs during the incipient spin, and accelerated stalls can be produced during the flights. At the other end of the stall/spin spectrum, spin-tunnel tests may indicate the existence of a flat or nonrecoverable spin mode, but it may be difficult for the airplane to attain this spin mode from conventional flight - the difference being that models in the spin tunnel are launched at about 90° angle of attack with a forced spin rotation. The radio-controlled test technique determines the spin susceptibility of a given airplane by using spin entry techniques similar to those of the full-scale airplane.

During a typical radio-controlled model study, a complete evaluation is made of the effects of various types of control inputs during post-stall motions. For example, the ability of a configuration to enter a developed spin following the application of only longitudinal control (with no lateral-directional inputs) is compared with results obtained when full prospin controls are applied. Recovery from the incipient spin is evaluated by applying recovery controls at various stages of the post-stall motion; for example, controls may be neutralized at varying numbers (or fractions) of turns after the stall. The radio-controlled technique, therefore, determines (1) the spin susceptibility of a configuration, (2) control techniques that tend to produce developed spins, and (3) the effectiveness of various control techniques for recovery from out-of-control conditions. This technique is also being updated to permit simulation of advanced control systems.

There are several limitations of the radio-controlled technique that should be kept in mind. The first, and most obvious, limitation is the fact that the tests are conducted out-of-doors. The test schedule is, therefore, subject to weather conditions, and excessive winds and rain can severely

curtail a program. Another limitation to the technique is that it is relatively expensive. Expensive flight instrumentation is required to record the motions of the model; and the large size of these models requires the use of more powerful and reliable electronic equipment than that used by hobbyists. Costs are compounded by the fact that the model and its electronic equipment frequently suffer costly damage on landing impact. Because of this higher cost and the slow rate at which radio-controlled drop-model tests can be accomplished, this technique is used only in special cases when the simpler and cheaper wind-tunnel and spin-tunnel techniques will not give adequate information. For example, it is used when it is necessary to know whether an airplane can be flown into a particular dangerous spin mode, or when one wants to investigate recovery during the incipient spin. Conversely, most of the exploratory work, such as developing "fixes" for a departure at the stall or investigating a variety of spin-recovery techniques, is done in the wind tunnels.

The spin-tunnel test technique.- The best known test technique used today to study the spin and spin-recovery characteristics of an airplane is the spin-tunnel test technique. The present 6-m (20-ft) Langley spin tunnel has been in operation since 1941, when it replaced a smaller 4.6-m (15-ft) spin tunnel. An external view of the spin tunnel is shown in figure 67, a cross-sectional view is shown in figure 68, and a view of the test section is shown in figure 69. In this tunnel, air is drawn upward by a fan located above the test section. Maximum speed of the tunnel is about 30 m/s (97 ft/sec), resulting in a maximum value of Reynolds number of about 1.96×10^6 per meter (0.6×10^6 per foot). Models are hand launched at about 90° angle of attack, with prerotation, into the vertically rising airstream. The model then seeks its own developed spin mode or modes. For recovery, the tunnel operator deflects the aerodynamic controls on the model to predetermined positions by remote control. Motion-picture records are used to record the spinning and recovery motions.

The models tested in the spin tunnel are normally made of fiber glass and, for fighter airplanes, are usually made to a scale of about 1/30. In a spin-tunnel investigation, the program consists of (1) determination of the various spin modes and spin-recovery characteristics, (2) study of the effect of center-of-gravity position and mass distribution, (3) determination of the effect of external stores, and (4) determination of the size and type of parachute required for emergency spin recovery.

In a typical spin-tunnel test program, tests are made at the normal-loading operating condition for the airplane. The spin and spin-recovery characteristics are determined for all combinations of rudder, elevator, and aileron positions for both right and left spins. In effect, a matrix of both the spin and spin-recovery characteristics is obtained for all control settings for the normal-loading operating condition. These data are used as a base line, and selected spin conditions are tested again with incremental changes to the center of gravity and/or mass conditions. Then, from the effects of these incremental changes, an analysis is made to determine the spin and spin-recovery characteristics that the corresponding airplane is expected to have. Also, the effects of various control positions and deflections are analyzed to determine which control techniques are most effective for recovery. After the spin-recovery characteristics for the normal loading conditions have been determined,

additional tests are made to determine the effects of other loading conditions, of store configurations (including asymmetric stores), and of other items of interest, such as speed brakes and leading- and trailing-edge flaps.

The parachute size required for emergency spin recovery is determined for the most critical spin conditions observed in the spin-tunnel tests and is checked at other conditions throughout the test program. If the parachute size is found to be too small for other conditions, the size is adjusted so that the parachute finally recommended for use on the spin demonstration airplane will be sufficient to handle the most critical spin possible on the airplane for any loading.

Because of the combination of the relatively small scale of the model and the low tunnel speeds, spin-tunnel tests are run at a value of Reynolds number which is much lower than that for the full-scale airplane. Experience has shown that the difference in Reynolds numbers can have significant effects on spin characteristics displayed by models and the interpretation of these results. In particular, past results have indicated that very significant effects can be produced by air flowing across the forward fuselage at angles of attack approaching 90°. These effects are influenced by the cross-sectional shape of the fuselage forebody and may be extremely sensitive to Reynolds number variations, as discussed in reference 48. Particular attention is, therefore, required for documentation of this phenomenon prior to spin-tunnel tests. This documentation has been conducted in the past with the aid of static-force tests over a wide Reynolds number range, as described in the following discussion.

Shown in figure 70 is a plan view of an airplane in a right spin. The arrows along the nose indicate the relative magnitude and sense of the linear sideward velocities along the fuselage due to the spinning rotation. The sketch on the right-hand side of the figure illustrates the sideslip angle at a representative nose location due to the spin rotation. As can be seen, the airplane rate of descent and the sideward velocity at the nose of the airplane combine vectorially to produce a positive sideslip angle β at the nose. It has been found that sideslip on the nose of an airplane at spin attitudes can produce large forces, and these forces in turn produce large moments, because the length between the nose and the center of gravity of modern military airplanes tends to be relatively large. If, in a right spin (as shown in fig. 70), positive (nose-right) yawing moments are produced by the nose due to the effective sideslip angle, then the nose is producing prospin, or autorotative, moments. If, on the other hand, negative (nose-left) values of yawing moment are produced by the nose, then the nose is producing an antispin, or damping, moment.

The sense of the moment actually produced by a particular nose configuration may be very sensitive to the value of Reynolds number. For example, shown in figure 71 is the variation of static yawing-moment coefficient C_n with Reynolds number for a fighter configuration at an angle of attack of 80° and a sideslip angle of 10°. Since, from the information given in figure 70, a positive value of β would be produced at the nose in a right spin, positive values of C_n are prospin and negative values are antispin. Two regions of Reynolds number are of interest: a low value, which is typical of spin-tunnel

tests, and a high value, indicative of the conditions for the full-scale airplane. As can be seen, the values of C_n (which at this angle of attack are produced almost entirely by the nose) tend to be prospin at the spin-tunnel test condition and antispin for the full-scale airplane flight condition. Also shown are data indicating the effect of nose strakes on C_n. The effect of the strakes was to modify the airflow around the nose such that the aerodynamic phenomena produced by the nose at low Reynolds number were similar to those produced at higher Reynolds number.

It has been found during several spin-tunnel investigations that this type of Reynolds number effect did exist for some configurations. The results showed that the model exhibited a nonrecoverable, fast flat spin without corrections for Reynolds number, because of the prospin moments produced by the nose. When strakes were added, satisfactory recoveries from the developed spin were obtained and the model results could be extrapolated to full scale with some confidence. Because of concern over the possible existence of such Reynolds number effects, it is required that a series of static wind-tunnel force tests be conducted for some configurations to insure that adequate simulation of the airplane is provided by the spin-tunnel model. These tests are usually performed in the Ames 12-Foot Pressure Wind Tunnel.

As discussed in the next section of this paper, a rotary-balance test rig recently put into operation in the Ames tunnel provides for the analysis of aerodynamic characteristics during spinning motions at high values of Reynolds number. It is anticipated that this apparatus will ultimately be used for the preliminary Reynolds number investigations required for spin-tunnel tests.

Rotary-Balance Tests

One test technique which has been used to produce much significant information regarding the complex aerodynamic characteristics of airplane configurations during spinning motions is the rotary-balance test technique. In this technique, measurements are made of the aerodynamic forces and moments acting on a wind-tunnel model during continuous 360° spinning motions at a constant angle of attack. Such tests were initially conducted many years ago and identified some of the major factors which infuenced spin characteristics for configurations at that time, such as the autorotative tendencies of unswept wings and certain fuselage cross-sectional shapes. The use of the technique, however, has not kept pace with the rapid evolution in fighter configurations. As a result, little information of this type is available for current fighter configurations which feature long, pointed fuselage noses and blended wing-body arrangements.

Shown in figures 72 and 73 are photographs of rotary-balance test rigs recently put into operation by NASA in the Langley full-scale tunnel and the Ames 12-Foot Pressure Wind Tunnel. Both rigs are capable of providing measurements of six-component data over a range of angle of attack of 45° to 90° and a range of nondimensional spin rate $\Omega b/2V$ of ±0.3.

The apparatus at Langley is designed for tests of the relatively large-scale drop models used for flight tests described in an earlier section of this

paper. Thus, aerodynamic data can be measured for the drop model at the same value of Reynolds number as that obtained in flight tests, and the data can then be used together with conventional static-force data as inputs to theoretical spin-prediction programs for correlation with the results of flight tests. In this manner, the validity of theoretical techniques can be evaluated without the usual complications arising from differences in model configuration and Reynolds number between wind-tunnel tests and flight tests. The apparatus is currently being used for measurements of data for several current military configurations. Tests are conducted to determine the characteristics of the basic configuration, the effects of individual and combined control deflections, the effects of tail surfaces and nose strakes, and the effects of spin radius and sideslip. The foregoing tests are limited to relatively low values of Reynolds number, up to 3.3×10^6 per meter (1×10^6 per foot).

The rotary-balance apparatus presently operational at the Ames Research Center is a modification of an apparatus originally built for testing axisymmetric bodies in the Ames 6- by 6-Foot Supersonic Wind Tunnel. It has just recently been put into operation for conducting basic studies of simple airplanelike configurations and is the forerunner of a new rotary-balance apparatus now under construction. The new apparatus will allow testing of complex model configurations at angles of attack from 0° to 100° and angles of sideslip up to $\pm 30^\circ$ in either the Ames 12-Foot Pressure Wind Tunnel or the Ames 11-Foot Transonic Wind Tunnel. As a result of the pressurization capability of both tunnels, data may be obtained for Reynolds number up to about 29.5×10^6 per meter (9×10^6 per foot). The existing modified rig has been used initially for tests to determine the effects of Reynolds number, angle of attack, and spin rate on the aerodynamic characteristics of airframe components such as pointed noses, various fuselage cross-sectional shapes, and drooped horizontal-tail surfaces.

The two test rigs are used in a coordinated research program between the two NASA centers. Tests at Langley are directed at an understanding of the types of aerodynamic phenomena exhibited by airplane configurations during spins, the mathematical representation of the data in equations of motion, and theoretical evaluations of the effects of the phenomena on spinning motions using the results of dynamic model tests for correlation with theory. Studies at Ames are directed toward an evaluation of the effects of Reynolds number on aerodynamic characteristics, the prediction of rotary data using methods of reference 49, and verification of phenomena observed during tests at Langley.

As discussed in references 50 and 51, the results of these tests have identified several configuration features which can have large effects on the aerodynamic characteristics of modern aircraft during spins. Figure 74 illustrates some of the prospin flow mechanisms which have been identified in these tests. The sketch at the left of the figure indicates the tendency of certain noncircular fuselage cross-sectional shapes to produce autorotative moments for certain values of Reynolds number. This particular phenomenon may be caused by the cross-sectional shape of either the forward or aft fuselage, and configurations are particularly susceptible to this condition for angles of attack corresponding to the flat spin ($\alpha \approx 90^\circ$). The second sketch of figure 74 illustrates a prospin flow mechanism found to exist for a current fighter configuration with drooped horizontal tails (ref. 47). The phenomenon has also been

found to be most pronounced near $\alpha = 90^{\circ}$, but deflection of the horizontal tail as an all-movable control surface has been found to affect spin damping for angles of attack from $\alpha = 45^{\circ}$ to about $\alpha = 80^{\circ}$. The third and fourth sketches illustrate prospin flow mechanisms commonly exhibited by airplane configurations with long, pointed noses for angles of attack between 30° and 70°. As shown by the third sketch, the asymmetric vortices shed off the pointed nose discussed earlier create prospin yawing moments, even for zero rotation rate. Finally, the fourth sketch illustrates that long, pointed noses with certain elliptical cross sections produce large prospin moments as a result of a large contribution of the nose to static directional stability, as discussed earlier. This particular phenomenon is a three-dimensional flow mechanism in contrast to the largely two-dimensional mechanism illustrated by the sketch at the left of the figure. The magnitudes of the moments produced by pointed noses are affected by Reynolds numbers; however, these moments have occurred at the highest values of Reynolds number tested for some configurations.

The results of the tests have also indicated that the aerodynamic moments (particularly yawing and pitching moments) exhibited by current military configurations during spins vary nonlinearly with spin rate. Recent studies (ref. 52, e.g.) have shown that nonlinear moments have a large effect on calculated spin motions and that good agreement is obtained with dynamic model tests for smooth, steady spins when such data are used as inputs for the calculations. On the other hand, use of conventional calculation techniques based on conventional linearized static and dynamic stability derivatives produce completely erroneous results. It appears, therefore, that rotary-balance tests are mandatory for the development of valid mathematical models for spin analysis.

It will be appreciated that the foregoing discussion has been concerned with smooth, steady spins. Experience has shown that many modern military aircraft exhibit large-amplitude oscillatory spins, and more sophisticated wind-tunnel test techniques are required to measure the complex aerodynamics produced by the combined rotary and oscillatory motions.

Simulator Studies

The model test techniques previously discussed have several critical shortcomings. For example, the inputs of the human pilot have been minimized or entirely eliminated. In addition, the use of unpowered models and the space constraints within the wind tunnels do not permit an evaluation of the spin susceptibility of airplanes during typical air-combat maneuvers. Finally, the effects of sophisticated automatic control systems are not usually evaluated because of space limitations within the models at the current time. In order to provide this pertinent information, a piloted simulation test technique has been developed as a logical follow-on to the model tests.

A sketch of the hardware used in this technique is shown in figure 75. The tests are conducted with the Langley differential maneuvering simulator (DMS), which is a fixed-base simulator with the capability of simultaneously simulating two airplanes as they maneuver with respect to one another. A full, wide-angle visual display is provided for each pilot. Two 12.2-m (40-ft)

diameter projection spheres each enclose a cockpit, an airplane-image projection system, and a sky-Earth-Sun projection system. A control console located between the spheres is used for interfacing the hardware and the computer, and it displays critical parameters for monitoring the hardware operation. Each pilot is provided a projected image of his opponent's airplane, showing the relative motions and ranges of the two airplanes by use of a television system. Range and attitude of the target image are controlled by a computer program.

A photograph of one of the cockpits and the target visual display during a typical engagement is shown in figure 76. A cockpit and an instrument display which are representative of current fighter aircraft equipment are used together with a fixed gunsight for tracking. A sophisticated hydraulic control-feel system is used which can be programed to simulate a wide range of characteristics. Although the cockpits are not provided with attitude motion, each cockpit does incorporate a buffet system capable of providing programmable buffet accelerations as high as 1g.

The visual display in each sphere consists of a target image projected onto a sky-Earth-Sun display. The sky-Earth-Sun scene is generated by two point light sources projecting through two hemispherical transparencies, one transparency of blue sky and clouds and the other of terrain features. No provision is made to simulate spatial motions with respect to the sky-Earth scene (such as altitude variation); however, a flashing light located in the cockpit behind the pilot is used as a cue when an altitude of less than 1524 m (5000 ft) is reached. The target-image generation system uses an airplane model mounted in a four-axis gimbal system and a television camera with a zoom lens to provide an image to the target projector within the sphere. The system can provide a simulated range between airplanes from 91.4 m (300 ft) to 13 716 m (45 000 ft) with a 10-to-1 brightness contrast between the target and the sky-Earth background at minimum range.

Additional special effects features of the DMS hardware include simulation of tunnel vision and blackout at high normal accelerations, use of an inflatable anti-g garment for simulation of g-loads, and use of sound cues to simulate wind, engine, and weapons noise as well as artificial warning systems. Additional details on the DMS facility are given in reference 53.

The application of the simulator to the stall/spin area is, of course, dependent on the development of a valid mathematical model of the airplane under consideration. In view of the present lack of understanding of aerodynamic phenomena at spin attitudes, the simulation studies are currently limited to angles of attack near the stall, and fully developed spins are not simulated. Rather, the studies are directed toward an evaluation of the spin susceptibility or stall/departure characteristics of the airplane during typical air-combat maneuvers and the effects of automatic control systems on these characteristics.

Recent studies made with the simulation technique have indicated that it is an extremely valuable tool for stall/spin research. Correlation of results with those obtained from full-scale flight tests for several current fighters has indicated good agreement, particularly with regard to the overall spin resistance of the configurations. In addition, valuable insight as to the effects of various automatic spin-prevention concepts has been obtained. It

is hoped that current research will ultimately result in valid theoretical methods for stall/spin analysis, which in turn will permit an extension of the simulator technique to studies of post-stall motions and the developed spin and spin recovery. A readily apparent application of such a technique would be the development of a procedures trainer for pilot training. This application is deemed especially important, inasmuch as current flight restrictions prohibit intentional spinning of most fighter aircraft and thereby deprive the pilot of training for an emergency which may well be difficult to overcome.

APPLICATIONS

Theoretical Prediction Techniques

Over the years, a number of efforts have been made to calculate the spin-entry, developed-spin, and recovery motions of a variety of fighter airplanes. Unfortunately, most of this work relied solely on limited conventional static and oscillatory aerodynamic data inputs which often did not adequately represent the highly complex flow phenomena associated with flight in the stall/spin regime. As a result of this lack of knowledge of aerodynamics, the correlation of calculated motions with actual flight motions was poor and the credibility of the theoretical prediction techniques was very low.

The previous discussions have attempted to illustrate the extreme complexity of current fighter airplane aerodynamics in the stall/spin regime and to indicate the degree of detail that must be included in an aerodynamic data package used to model stall/spin aerodynamics for use in motion prediction.

Mathematical-model requirements.- Two major elements are required to construct the mathematical model needed to calculate the stall/spin motions - the equations of motion for the vehicle and a representation of the vehicle aerodynamics. Simulation of the large-amplitude, highly coupled motions associated with stall/spin dynamics requires the use of fully nonlinear, six-degree-of-freedom equations of motion. The main difficulty in the formulation of the mathematical model lies with the second requirement - modeling of the vehicle aerodynamics. The model must satisfy two basic requirements: (a) it must be sufficiently comprehensive to cover the wide range of aerodynamic parameter variations (with α, β, . . .) associated with stall/spin motions, and (b) it must accurately represent all the complex high-angle-of-attack aerodynamic phenomena discussed in the previous sections. Unless both these requirements are met, reliable prediction of airplane stall/spin characteristics is not possible.

Unfortunately, no single available test technique can provide all the data necessary to satisfy the basic requirements. Static wind-tunnel test results correctly represent only steady, nonrotating conditions; forced-oscillation data do not account for steady turning flight or for the effects due to a rotating flow field such as that encountered in a spin; and rotary data are valid only for steady spinning conditions. Thus, the problem becomes one of properly combining the different types of data into a workable aerodynamic model. The conventional technique of combining static and forced-oscillation data has been found to provide a generally valid aerodynamic representation through the stall/departure region. However, care must still be taken to

insure that the data are taken at close intervals over a sufficiently wide range of angle of attack, angle of sideslip, and control deflections such that the nonlinearities, rapid variations, and complex interactions described earlier are properly accounted for. In the developed spin region, the presently used technique combines forced-oscillation and rotary data, as developed in reference 54. This method essentially involves separating the airplane angular rates into steady and oscillatory components such that the steady component is used to determine the proper contribution of rotary aerodynamics, and the oscillatory component derived from the forced-oscillation data is used to determine aerodynamic damping. Thus, the method insures that data of each type are applied only to the kinds of motions for which they were measured. It should be noted, however, that this formulation assumes that a rotating flow field has no effect on the forced-oscillation derivatives. The validity of this assumption has not been determined in a rigorous manner, and the use of this technique in predicting oscillatory spin conditions remains to be validated.

Correlation of results.- The degree of correlation obtained between calculated and measured flight stall/spin characteristics has varied with airplane configuration as well as with the types of motion being compared. In general, the best correlation has been obtained in the stall/departure region, where the motions do not contain significantly high steady rotation rates. Recently, fair correlation has been obtained in the steady developed spin region for at least two airplane configurations (ref. 47). Correlation continues to be very poor, however, in the areas of spin entry, incipient spin, and developed oscillatory spin. Representative results obtained in these different regions are presented and discussed in the following sections.

Correlation in the stall/departure region.- The correlation between predicted and actual flight characteristics has generally been good in the stall/departure region. Reference 55 summarizes the fairly good qualitative correlation that has been obtained for a range of past and present configurations by using only the dynamic directional stability parameter $C_{n_{\beta,dyn}}$ and the aileron-effectiveness parameter, both of which rely solely on airplane inertia and static stability and control characteristics.

An example of the degree of quantitative correlation that has been obtained is shown in figure 77. The flight motions shown were measured with the radio-controlled drop-model technique described earlier. The prediction technique which generated the calculated motions incorporated aerodynamic input data obtained from static and forced-oscillation tests. It is evident that the model motions were predicted reasonably well up through the stall and departure. Only when a significant rotation rate had built up at post-stall angles of attack did the measured and calculated motions begin to diverge.

Another example of correlation in the stall is presented in figure 78. The flight data, which were obtained during full-scale tests, show a large-amplitude wing rock occurring in the angle-of-attack region of maximum lift. It is seen that the character of the motion was reasonably well predicted from a comprehensive set of static and oscillatory data measured in the wind tunnel.

Because of the reasonably good degree of correlation obtained in the stall/departure region, the prediction techniques have been used with some confidence in piloted-simulator studies to investigate stall/departure characteristics of particular configurations and to study concepts for the prevention of automatic departure and spin. Some results of these investigations are presented later in this paper.

Correlation in the developed-spin region.- Recent results obtained for two fighter configurations, to be referred to herein as airplanes A and B, will be discussed. For both configurations, a comprehensive set of static, forced-oscillation, and rotary aerodynamic data were measured for use in calculating motions which were then compared with motions obtained in spin tunnel and radio-controlled model tests.

As previously mentioned, earlier attempts at spin prediction generally relied solely on conventional static and oscillatory data for representation of spin aerodynamics. The inadequacy of this technique was documented for both configurations, in that no steady spin of any kind could be computed with only the static and oscillation data as measured. It was found that a steady spin that compared reasonably well with that found experimentally could be obtained by judiciously adjusting selected damping derivatives. However, the adjusted aerodynamics were shown to be nonunique in that essentially the same spin motion could be computed with many different sets of adjusted damping data.

Similar calculations were also made by using the technique of combining rotary and forced-oscillation data discussed earlier. The resulting aerodynamic model gave calculated motions that agreed reasonably well with experimental motions, as shown by the following results for airplane A:

	Calculated	Experimental
α, deg	83.6	83.0
β, deg	2.0	1.5
$\Omega b/2V$	0.187	0.211

For this configuration, which showed a very smooth, steady spin, attempts were made to compute the same motions by using only the rotary data. A divergent oscillatory motion was obtained, indicating that forced-oscillation data are required even in very steady spins. However, the data should perhaps be measured simultaneously with rotary motions so that the flow field is representative of that actually present during a spin. This premise was further indicated in airplane B, which exhibited a slightly more oscillatory steady spin. In this case, a reasonable matching with experimental results was obtained only after the damping in pitch C_{m_q} was increased above the measured values for $\alpha > 75^{\circ}$.

The degree of correlation achieved is illustrated in figure 79, which shows an attempt to match the stall, departure, spin, and recovery motions experienced during a radio-controlled model flight. Except for the degree of oscillation, the data show a fairly good match of the developed-spin motions. The spin-entry and recovery motions, however, were not closely matched and were

simulated only in trends. It should be noted that correlation in these regions would have been even poorer if the entry and recovery motions had shown a higher degree of oscillation.

In concluding this discussion of theoretical prediction techniques, it should be reemphasized that although reasonable confidence has been established in computing stall/departure and steady-spin motions, more work is needed to improve further the aerodynamic models used in the prediction techniques. In the stall/departure region, additional insight into the importance of lateral-acceleration derivatives is required; in addition, techniques for handling non-repeatable static asymmetries should be further examined. Finally, Mach and Reynolds number effects also require further study. In the developed-spin region, the effects of a steady, rotating flow field on oscillatory aerodynamics must be ascertained; also, rotary-balance data are required at larger angle-of-attack and sideslip ranges than presently measured. Additional research in these areas will not only improve predictive capability in the stall/departure/steady-spin regions, but will also aid in the study of motions during spin entry, oscillatory spin, and spin recovery, for which valid predictive techniques are yet to be developed.

Piloted-Simulator Studies

The second major area of work in the stall/spin prediction effort is the use of piloted flight simulation to study the stall/departure characteristics of current fighter configurations and to develop and evaluate concepts for prevention of automatic departure and spin. This simulation effort recognizes the aerodynamic-modeling problems already mentioned and attempts to work in the stall/departure region, where, as previously discussed, the available aerodynamic representations are considered to be reasonably reliable.

Stall/departure simulation research at Langley has been conducted on a fairly broad range of airplane configurations, some of which are illustrated in figure 80. The advantage of studying a diversity of configurations lies in the fact that there exist significant as well as subtle differences in the high-angle-of-attack characteristics of specific configurations. These differences require that caution be observed in trying to apply directly results for one particular airplane to a different one.

The simulation results presented in the following sections illustrate some of the stability and control characteristics exhibited in the stall/post-stall region by many current fighter configurations. During the simulations, several automatic-control concepts were studied and were found to be effective in preventing departures and spins. These concepts are discussed in addition to an evaluation procedure employed to obtain these results.

Description of simulation.- The primary facility used for the stall/departure simulation studies is the Langley differential maneuvering simulator (DMS). Real-time digital simulation techniques and equipment are used in the operation of the DMS. As discussed earlier, fully nonlinear, rigid-body equations of motion are used to compute aircraft motions. The equations employ

nonlinear aerodynamic data as functions of α and β. Typical data ranges are $-10^{\circ} \leq \alpha \leq 90^{\circ}$ and $-40^{\circ} \leq \beta \leq 40^{\circ}$.

Evaluation procedures.- Previous experience with the simulation of fighter stall/spin characteristics (ref. 56) has shown that visual tracking tasks which require the pilot to divert his attention from the instrument panel are necessary to provide realism in studying the possibility of unintentional loss of control and spin entry. Furthermore, earlier studies have shown that mild, well-defined maneuvers can produce misleading results, inasmuch as a configuration that behaves fairly well in such mild maneuvers may be violently uncontrollable in the complex and pressing nature of high-g, air-combat maneuvering (ACM). Finally, for purposes of evaluation in comparing the performance of several configurations, the tasks employed must be repeatable.

The test procedures used in the DMS studies account for the foregoing factors and can generally be divided into two phases. The first involves nontracking tasks in which the evaluation airplane is flown through individual high-angle-of-attack maneuvers, including 1g stalls, windup turns, high-g roll reversals, hammerhead stalls, and coupling maneuvers. These tests allow a comprehensive examination of the overall stability and control characteristics of the airplane at high angles of attack, including conditions involving complex aerodynamic and inertia coupling. In addition, they indicate the types of maneuvers which are the most critical in terms of the departure susceptibility of the airplane.

The second test phase involves tracking of a target airplane through a series of maneuvers representative of ACM. In order to obtain reasonable maneuvers which will force the tracking airplane into maneuvering in the critical high-angle-of-attack regime, the target airplane is programed to have the same thrust and performance characteristics as the evaluation airplane; however, the target airplane is given idealized high-angle-of-attack stability and control characteristics. The target airplane is flown by the evaluation pilot through a series of ACM tasks of varying levels of difficulty while the target's motions are recorded for playback later to drive the target as the task for the evaluation airplane. Results obtained in the first test phase are factored into the generation of these target maneuvers so that the most critical flight conditions will be encountered by the evaluation airplane during tracking. These tracking tasks generally fall into three categories: (a) steady windup turns for steady tracking evaluation; (b) bank-to-bank (or horizontal S) tasks with gradually increasing angle of attack up to maximum α to evaluate rapid rolls and target acquisition; and (c) complex, vigorous ACM tasks to evaluate the susceptibility of the simulated airplane to high-angle-of-attack handling-qualities problems during aggressive maneuvering. These tracking tasks, then, provide the complex, repeatable, pilot-attention-out-of-the-cockpit tasks which are required for realistic investigation of unintentional loss of control and spin entry.

The results of studies using these evaluation procedures are in the form of time-history records of airplane motions and pilot comments regarding the departure/spin susceptibility of particular configurations and the effects of automatic prevention systems on these characteristics. Some of the more significant results are reviewed in the following section.

Simulation results.- The degraded stability and control characteristics exhibited by many current fighter configurations at high angles of attack are the result of highly complex flow phenomena in the region of stall. Basically, however, these degraded characteristics can generally be attributed to three factors: (a) loss in static and dynamic lateral-directional stability, (b) reduced control effectiveness, and (c) adverse yaw due to roll control. Although not all configurations exhibit all three of these characteristics, poor high-angle-of-attack stability and control encountered by any configuration is most often due to one or more of these three factors. An example of how these factors manifest themselves during an actual simulated flight is shown in figure 81. Above 25° angle of attack, this particular configuration exhibited degraded lateral-directional static stability (C_{l_β} and C_{n_β}) in combination with a high degree of adverse yaw due to roll control. In the flight, the pilot was attempting to make a windup turn with steadily increasing angle of attack. As α increased above 25°, adverse sideslip began to increase slowly as a result of degraded static directional stability and dihedral effect. The adverse sideslip caused the airplane to start rolling out of the turn; in attempting to keep the airplane turning, the pilot applied additional right roll control, which, because of the high adverse yaw, only aggravated the sideslip buildup. Shortly thereafter, the airplane departed to the left and entered an incipient spin. It is obvious that an airplane with these high-angle-of-attack characteristics would be very difficult to handle during combat maneuvering.

Simulation results have clearly indicated that markedly improved tactical effectiveness can be obtained when an airplane is given improved high-angle-of-attack handling qualities such that it can be maneuvered to its limit without danger of departure. The simulation results have also shown that the use of automatic-control concepts to provide these improvements can be highly effective.

Initially, concepts for automatic spin prevention were studied (ref. 57); however, it soon became apparent that although these systems are desirable from a safety viewpoint, much greater improvements in tactical effectiveness can be obtained with systems that prevent departures rather than allowing them to occur. These automatic departure-prevention systems are thus designed to alleviate the primary high-angle-of-attack stability and control problems discussed earlier - degraded lateral-directional stability, reduced control effectiveness, and adverse yaw due to roll control. The remainder of this section discusses one of the primary classes of departure-prevention concepts that have been studied during the Langley simulation efforts and its effects on departure resistance and overall tactical effectiveness of fighter aircraft.

Roll-yaw interconnect systems.- Recently a number of fighter configurations have been developed which are dynamically stable at high angles of attack with no natural tendency to diverge in yaw. However, the designs are subject to control-induced departures from controlled flight as a result of large values of adverse yaw at high angles of attack. These vehicles are well suited for the application of automatic departure-prevention concepts which operate within the normal maneuver envelope of the airplane in order to prevent natural or control-induced departures from controlled flight. The use of such systems does not inhibit maneuvering of the airplane at high angles of attack, and

actually increases the usable maneuverability as well as the pilot's confidence during strenuous maneuvers.

Shown in figure 82 are typical lateral-directional control characteristics for fighter configurations with adverse yaw. The data of figure 82 show the variation with angle of attack of yawing moments produced by ailerons and rudder for right-roll and right-yaw control inputs. The yawing moments produced by ailerons at low angles of attack are favorable (nose right) for right-roll control; however, the moments become adverse (nose left) at high angles of attack. Right-rudder input produces a normal nose-right moment, but at high angles of attack the rudder loses effectiveness because of impingement of the low-energy wake from the partially stalled wing. As can be seen, the magnitudes of the adverse moments due to ailerons are much larger than the corrective moments available from the rudder. When the resulting adverse moments are coupled with low directional stability at high angles of attack, a reversal of roll response occurs; that is, the airplane rolls in a direction opposite to that desired by the pilot.

Shown in figure 83 are calculated time histories which illustrate the roll-reversal phenomenon. The roll response of a typical configuration is shown at an angle of attack of 25° for control inputs of rudder alone and ailerons alone for right-roll control. The response to the rudder input is seen to be quite normal. The airplane yaws to the right, creating nose-right sideslip. The dihedral effect then rolls the airplane to the right, as desired. In contrast to this result, aileron input creates adverse yaw, which causes the airplane to yaw to the left and create sideslip in the opposite direction; the resulting dihedral effect opposes the rolling moment produced by the aileron. After a brief time, the airplane rolls to the left in response to the right-roll control.

As would be expected, the reversed roll response to normal lateral-control-stick inputs presents the pilot with a coordination problem in order to avoid unintentional loss of control and spins. Most fighter pilots adapt to the situation by making the transition from lateral-stick inputs for roll control at low α to rudder-pedal inputs for roll control at high α. The problem becomes one of how to phase these controls in an optimum manner to obtain maximum performance, particularly during the pressure of combat.

From studies in the Langley differential maneuvering simulator, it has been found that configurations which exhibit such characteristics are susceptible to inadvertent departures during vigorous combat maneuvers. Many proposed solutions to the problem were evaluated, and the most effective system involved the lateral-stick-to-rudder interconnect concept shown in figure 84.

Basically, the control system is modified such that deflection of the control stick laterally produces aileron inputs at low angles of attack and rudder inputs at high angles of attack. As shown in the sketch, the ailerons for the example discussed were phased out by $\alpha = 25°$. At that point, lateral stick inputs produced only rudder inputs. In addition, the yawing moments produced by the ailerons above $\alpha = 25°$ were used to advantage in an additional stability augmentation channel which augmented directional stability. This control scheme essentially eliminated inadvertent spins in the simulator.

The net effect of the automatic interconnect scheme on roll performance is illustrated in figure 85. With the basic control system, the roll rate produced by lateral deflection of the control stick reversed near $\alpha = 20^{\circ}$, and the pilot could not maneuver at higher angles of attack with only stick inputs. When the control system was modified with the interconnect, the pilot could maneuver the airplane beyond maximum lift, without fear of unintentional departures, by using only stick inputs.

Correlation with flight results.- As indicated earlier, all the Langley stall/spin simulations performed to date have involved actual current fighter airplane configurations. This situation permits correlation of the simulation results with those obtained in actual flight. In addition, qualitative validation of the simulations is obtained early in the programs by the participation of appropriate individuals to fly the simulator. These individuals include aircraft company as well as military test pilots directly involved with flight testing of the particular study configuration. Results to date have shown good qualitative correlation between simulator and flight results. The simulations have been found to be effective in predicting the general high-angle-of-attack stability and control characteristics of particular configurations; in addition, potential problems as well as benefits of various control schemes identified during the simulations have agreed well with those obtained in flight tests. Thus, an additional benefit of the simulation technique is that it can be used to study the effect of general control schemes, such as normal-acceleration and roll-rate command, on high-angle-of-attack flight characteristics.

SUMMARY OF STATE OF ART

As indicated by the preceding discussions, considerable progress has been made in recent years in research on flight dynamics at high angles of attack. Aerodynamic data have been gathered and analyzed; unique test techniques involving wind-tunnel tests and dynamic models have been developed and correlated with full-scale tests; advanced methods of analysis such as piloted simulation have been successfully employed; and powerful automatic-control-system concepts for automatic spin prevention have been conceived and demonstrated. Research in this area, however, is an ongoing process that changes with the introduction of new configurations and analytical capabilities. A number of extremely important tasks are yet to be accomplished: development of theoretical aerodynamic prediction techniques, validation of motion-calculation procedures, and evaluation and analysis of advanced configurations.

Langley Research Center
National Aeronautics and Space Administration
Hampton, VA 23665
November 22, 1977

REFERENCES

1. Spearman, M. Leroy: Some Factors Affecting the Static Longitudinal and Directional Stability Characteristics of Supersonic Aircraft Configurations. NACA RM L57E24a, 1957.

2. Shortal, Joseph A.; and Maggin, Bernard: Effect of Sweepback and Aspect Ratio on Longitudinal Stability Characteristics of Wings at Low Speeds. NACA TN 1093, 1946.

3. Hagerman, John R.: Wind-Tunnel Investigation of the Effect of Power and Flaps on the Static Longitudinal Stability and Control Characteristics of a Single-Engine High-Wing Airplane Model. NACA TN 1339, 1947.

4. Anderson, Seth B.; and Bray, Richard S.: A Flight Evaluation of the Longitudinal Stability Characteristics Associated With the Pitch-Up of a Swept-Wing Airplane in Maneuvering Flight at Transonic Speeds. NACA Rep. 1237, 1955. (Supersedes NACA RM A51I12.)

5. Sadoff, Melvin; Matterson, Frederick H.; and Havill, C. Dewey: A Method for Evaluating the Loads and Controllability Aspects of the Pitch-Up Problem. NACA RM A55D06, 1955.

6. Sadoff, Melvin; Stewart, John D.; and Cooper, George E.: Analytical Study of the Comparative Pitch-Up Behavior of Several Airplanes and Correlation With Pilot Opinion. NACA RM A57D04, 1957.

7. Campbell, George S.; and Weil, Joseph: The Interpretation of Nonlinear Pitching Moments in Relation to the Pitch-Up Problem. NASA TN D-193, 1959.

8. Sadoff, Melvin: Pitch-Up Problem - A Criterion and Method of Evaluation. NASA MEMO 3-7-59A, 1959.

9. Polhamus, Edward C.: The Deep-Stall Problem of T-Tail Aircraft. Space/Aeronaut., vol. 45, no. 5, May 1966, pp. 106-108.

10. Seckel, Edward: Stability and Control of Airplanes and Helicopter. Academic Press, Inc., c.1964.

11. Coe, Paul L., Jr.; McLemore, H. Clyde; and Shivers, James P.: Effects of Upper-Surface Blowing and Thrust Vectoring on Low-Speed Aerodynamic Characteristics of a Large-Scale Supersonic Transport Model. NASA TN D-8296, 1976.

12. Sadoff, Melvin; and Stewart, John D.: An Analytical Evaluation of the Effects of an Aerodynamic Modification and of Stability Augmenters on the Pitch-Up Behavior and Probable Pilot Opinion of Two Current Fighter Airplanes. NACA RM A57K07, 1958.

13. Taylor, Robert T.; and Ray, Edward J.: Deep-Stall Aerodynamic Characteristics of T-Tail Aircraft. Conference on Aircraft Operating Problems, NASA SP-83, 1965, pp. 113-121.

14. White, Maurice D.; and Cooper, George E.: Simulator Studies of the Deep Stall. Conference on Aircraft Operating Problems, NASA SP-83, 1965, pp. 101-111.

15. Lina, Lindsay J.; and Moul, Martin T.: A Simulator Study of T-Tail Aircraft in Deep Stall Conditions. AIAA Paper No. 65-781, 1965.

16. Fink, Marvin P.; and Freeman, Delma C.: Full-Scale Wind-Tunnel Investigation of Static Longitudinal and Lateral Characteristics of a Light Twin-Engine Airplane. NASA TN D-4983, 1969.

17. Chambers, Joseph R.; and Anglin, Ernie L.: Analysis of Lateral-Directional Stability Characteristics of a Twin-Jet Fighter Airplane at High Angles of Attack. NASA TN D-5361, 1969.

18. Polhamus, Edward C.; and Spreeman, Kenneth P.: Subsonic Wind-Tunnel Investigation of the Effect of Fuselage Afterbody on Directional Stability of Wing-Fuselage Combinations at High Angles of Attack. NACA TN 3896, 1956.

19. Goodman, Alex: Effects of Wing Position and Horizontal-Tail Position on the Static Stability Characteristics of Models With Unswept and 45° Sweptback Surfaces With Some Reference to Mutual Interference. NACA TN 2504, 1951.

20. Goodman, Alex; and Thomas, David F., Jr.: Effects of Wing Position and Fuselage Size on the Low-Speed Static and Rolling Stability Characteristics of a Delta-Wing Model. NACA Rep. 1224, 1955. (Supersedes NACA TN 3063.)

21. Queijo, M. J.; and Wolhart, Walter D.: Experimental Investigation of the Effect of Vertical-Tail Size and Length and of Fuselage Shape and Length on the Static Lateral Stability Characteristics of a Model With 45° Sweptback Wing and Tail Surfaces. NACA Rep. 1049, 1951. (Supersedes NACA TN 2168.)

22. Polhamus, Edward C.; and Sleeman, William C.: The Rolling Moment Due to Sideslip of Swept Wings at Subsonic and Transonic Speeds. NACA TN D-209, 1960.

23. Moul, Martin T.; and Paulson, John W.: Dynamic Lateral Behavior of High-Performance Aircraft. NACA RM L58E16, 1958.

24. Shanks, Robert E.: Investigation of the Low-Subsonic Flight Characteristics of a Model of an All-Wing Hypersonic Boost-Glide Configuration Having Very High Sweep. NASA TN D-369, 1960.

25. Boisseau, Peter C.: Investigation of the Low-Subsonic Flight Characteristics of a Model of a Reentry Vehicle With a Thick Flat 75° Swept Delta Wing and a Half-Cone Fuselage. NASA TN D-1007, 1962.

26. Freeman, Delma C., Jr.: Low-Subsonic Flight and Force Investigation of a Supersonic Transport Model With a Double-Delta Wing. NASA TN D-4179, 1968.

27. Ray, Edward J.; and Hollingsworth, Eddie G.: Subsonic Characteristics of a Twin-Jet Swept-Wing Fighter Model With Maneuvering Devices. NASA TN D-6921, 1973.

28. Chambers, Joseph R.; Gilbert, William P.; and Grafton, Sue B.: Results of Recent NASA Studies on Spin Resistance. Stall/Spin Problems of Military Aircraft, AGARD-CP-199, June 1976, pp. 6-1 - 6-14.

29. Chambers, Joseph R.; Anglin, Ernie L.; and Bowman, James S., Jr.: Effects of a Pointed Nose on Spin Characteristics of a Fighter Airplane Model Including Correlation With Theoretical Calculations. NASA TN D-5921, 1970.

30. Bates, William R.: Static Stability of Fuselages Having a Relatively Flat Cross Section. NACA TN 3429, 1955. (Supersedes NACA RM L9I06a.)

31. Spencer, Bernard, Jr.; and Phillips, W. Pelham: Effects of Cross-Section Shape on the Low-Speed Aerodynamic Characteristics of a Low-Wave-Drag Hypersonic Body. NASA TN D-1963, 1963.

32. Grafton, Sue B.; and Anglin, Ernie L.: Dynamic Stability Derivatives at Angles of Attack From -5° to 90° for a Variable-Sweep Fighter Configuration With Twin Vertical Tails. NASA TN D-6909, 1972.

33. Coe, Paul L., Jr.; Graham, A. Bruce; and Chambers, Joseph R.: Summary of Information on Low-Speed Lateral-Directional Derivatives Due to Rate of Change of Sideslip $\dot{\beta}$. NASA TN D-7972, 1975.

34. Coe, Paul L., Jr.; and Newsom, William A., Jr.: Wind-Tunnel Investigation To Determine the Low-Speed Yawing Stability Derivatives of a Twin-Jet Fighter Model at High Angles of Attack. NASA TN D-7721, 1974.

35. Nguyen, Luat T.: Evaluation of Importance of Lateral Acceleration Derivatives in Extraction of Lateral-Directional Derivatives at High Angles of Attack. NASA TN D-7739, 1974.

36. Bowman, James S., Jr.: Summary of Spin Technology as Related to Light General-Aviation Airplanes. NASA TN D-6575, 1971.

37. Neihouse, Anshal I.; Klinar, Walter J.; and Scher, Stanley H.: Status of Spin Research for Recent Airplane Designs. NASA TR R-57, 1960. (Supersedes NACA RM L57F12.)

38. Letko, William: A Low-Speed Experimental Study of the Directional Characteristics of a Sharp-Nosed Fuselage Through a Large Angle-of-Attack Range at Zero Angle of Sideslip. NACA TN 2911, 1953.

39. Spence, A.; and Trebble, W. J. G.: Low Speed Tunnel Tests on the Flow Structure Behind a Body of Revolution of Fineness Ratio 16 2/3:1. Tech. Note No. Aero. 2406, British R.A.E., Oct. 1955.

40. Fink, P. T.; and Taylor, J.: Some Early Experiments on Vortex Separation. R. & M. No. 3489, British A.R.C., 1967.

41. Ferris, James C.: Static Stability Investigation of a Single-Stage Sounding Rocket at Mach Numbers From 0.60 to 1.20. NASA TN D-4013, 1967.

42. Dunn, Eldon L.: A Low-Speed Experimental Study of Yaw Forces on Bodies of Revolution at Large Angles of Pitch and Zero Angle of Sideslip. TM-1588, U.S. Naval Ord. Test Sta., Mar. 8, 1954.

43. Shanks, Robert E.: Low-Subsonic Measurements of Static and Dynamic Stability Derivatives of Six Flat-Plate Wings Having Leading-Edge Sweep Angles of 70° to 84°. NASA TN D-1822, 1963.

44. Coe, Paul L., Jr.; Chambers, Joseph R.; and Letko, William: Asymmetric Lateral-Directional Characteristics of Pointed Bodies of Revolution at High Angles of Attack. NASA TN D-7095, 1972.

45. Chapman, Gary T.; Keener, Earl R.; and Malcolm, Gerald N.: Asymmetric Aerodynamic Forces on Aircraft Forebodies at High Angles of Attack - Some Design Guides. Stall/Spin Problems of Military Aircraft, AGARD-CP-199, June 1976, pp. 12-1 - 12-9.

46. Polhamus, Edward C.; and Spreeman, Kenneth P.: Effect at High Subsonic Speeds of Fuselage Forebody Strakes on the Static Stability and Vertical-Tail-Load Characteristics of a Complete Model Having a Delta Wing. NASA TN D-903, 1961. (Supersedes NACA RM L57K15a.)

47. Nguyen, Luat T.; Anglin, Ernie L.; and Gilbert, William P.: Recent Research Related to Prediction of Stall/Spin Characteristics of Fighter Aircraft. AIAA Third Atmospheric Flight Mechanics Conference, June 1976, pp. 79-91.

48. Polhamus, Edward C.: Effect of Flow Incidence and Reynolds Number on Low-Speed Aerodynamic Characteristics of Several Noncircular Cylinders With Applications to Directional Stability and Spinning. NASA TR R-29, 1959. (Supersedes NACA TN 4176.)

49. Chambers, Joseph R.; Bowman, James S., Jr.; and Anglin, Ernie L.: Analysis of the Flat-Spin Characteristics of a Twin-Jet Swept-Wing Fighter Airplane. NASA TN D-5409, 1969.

50. Clarkson, M. H.; Malcolm, G. N.; and Chapman, G. T.: Experimental Determination of Post-Stall Rotary Derivatives for Airplane-Like Configurations at Several Reynolds Numbers. AIAA Paper 75-171, Jan. 1975.

51. Chambers, Joseph R.; Anglin, Ernie L.; and Bowman, James S., Jr.: Effects of a Pointed Nose on Spin Characteristics of a Fighter Airplane Model Including Correlation With Theoretical Calculations. NASA TN D-5921, 1970.

52. Bihrle, William, Jr.; and Barnhart, Billy: Effects of Several Factors on Theoretical Predictions of Airplane Spin Characteristics. NASA CR-132521, 1974.

53. Ashworth, B. R.; and Kahlbaum, William M., Jr.: Description and Performance of the Langley Differential Maneuvering Simulator. NASA TN D-7304, 1973.

54. Anglin, Ernie L.; and Scher, Stanley H.: Analytical Study of Aircraft-Developed Spins and Determination of Moments Required for Satisfactory Spin Recovery. NASA TN D-2181, 1964.

55. Greer, H. Douglas: Summary of Directional Divergence Characteristics of Several High-Performance Aircraft Configurations. NASA TN D-6993, 1972.

56. Moore, Frederick L.; Anglin, Ernie L.; Adams, Mary S.; Deal, Perry L.; and Person, Lee H., Jr.: Utilization of a Fixed-Base Simulator To Study the Stall and Spin Characteristics of Fighter Airplanes. NASA TN D-6117, 1971.

57. Gilbert, William P.; and Libbey, Charles E.: Investigation of an Automatic Spin-Prevention System for Fighter Airplanes. NASA TN D-6670, 1972.

TABLE I.- SCALE FACTORS

[Model values are obtained by multiplying airplane values by the scale factors]

	Scale factor
Linear dimension	N
Relative density, $m/\rho\ell^3$	1
Froude number, $V^2/\ell g$	1
Weight or mass	$N^{3\sigma-1}$
Moment of inertia	$N^{5\sigma-1}$
Linear velocity	$N^{1/2}$
Linear acceleration	1
Angular velocity	$N^{-1/2}$
Time	$N^{1/2}$
Reynolds number, $V\ell/\nu$	$N^{1.5}\frac{\nu}{\nu_o}$

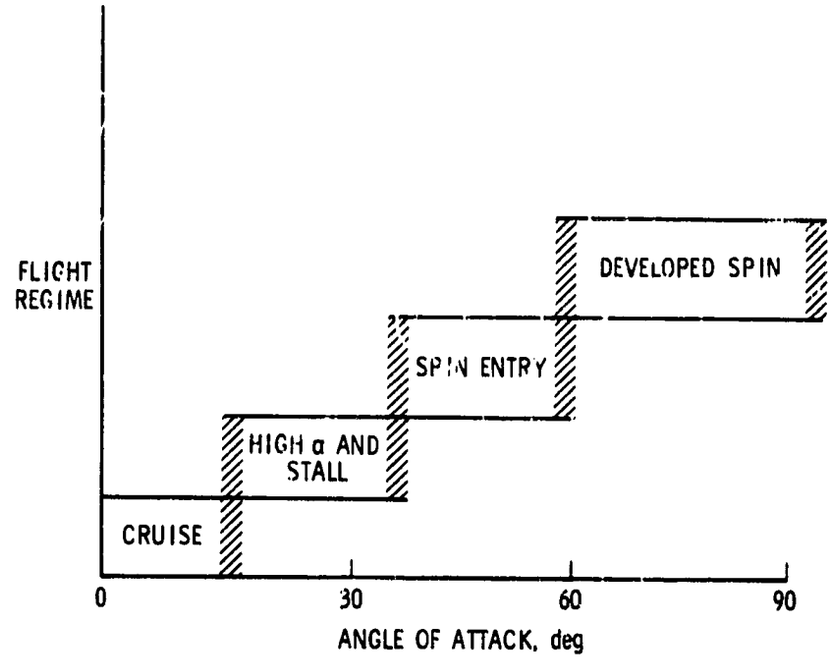

Figure 1.- Relative ranges of angle of attack or various flight regimes for a typical fighter.

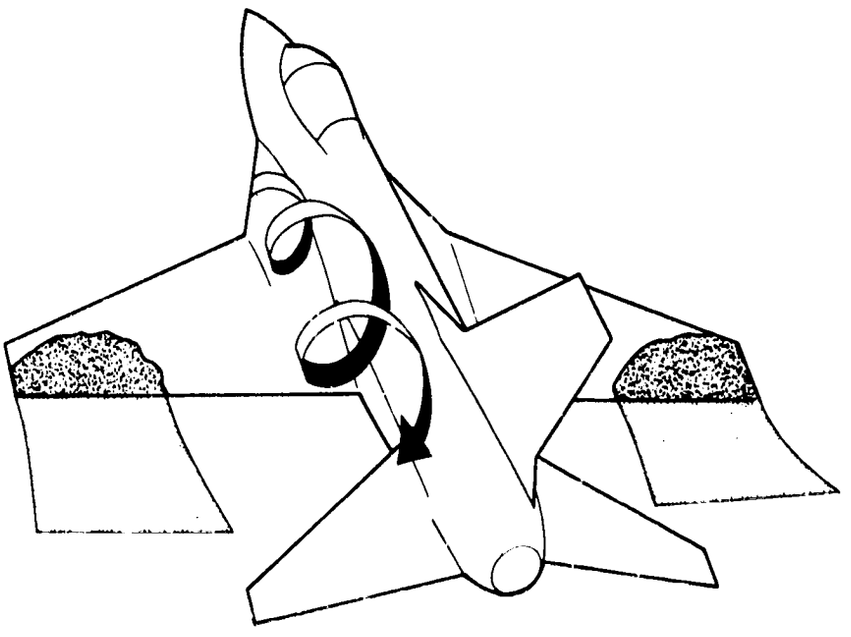

Figure 2.- Illustration of stalled and vortex flows at high α.

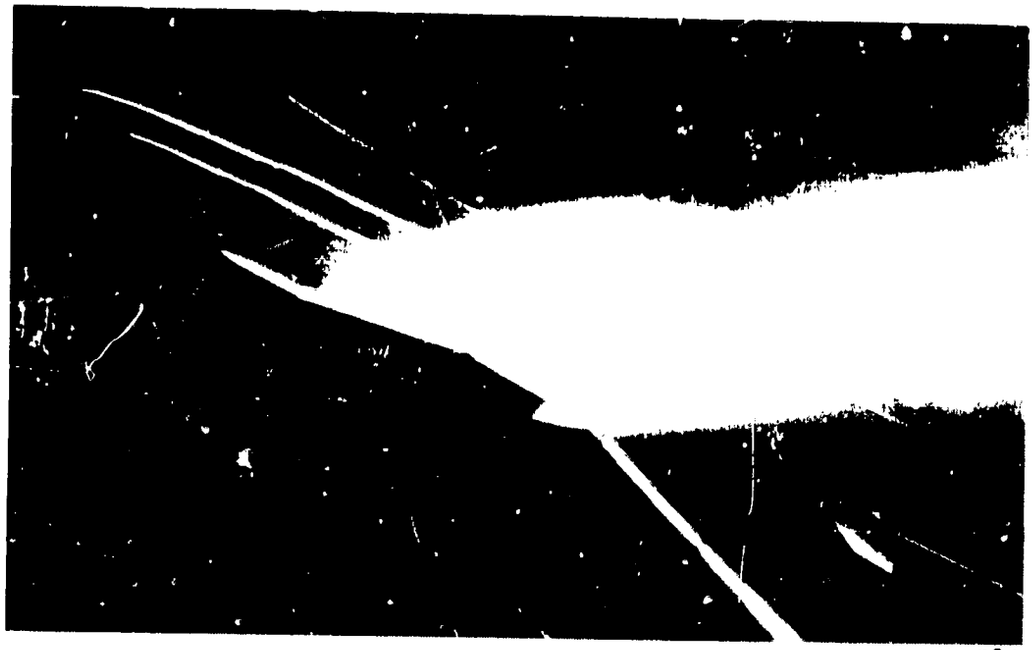

L-77-381

Figure 3.- Stalled-wing wake for fighter model.

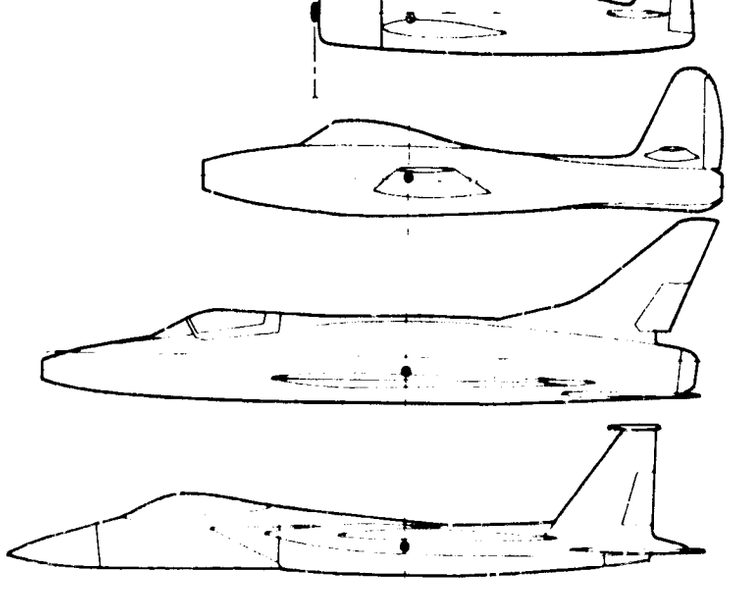

Figure 4.- Evolution in fighter design since World War II.

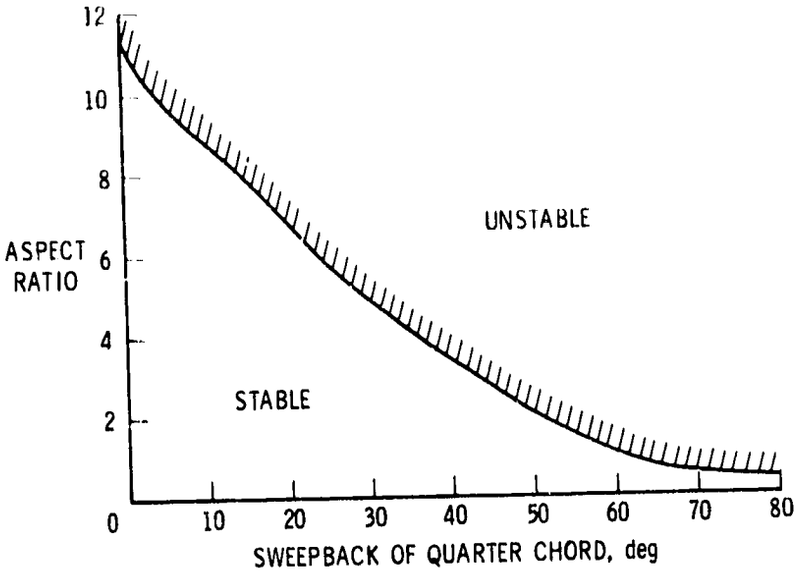

Figure 5.- Effect of wing aspect ratio and sweep on pitch-up tendencies (from ref. 2).

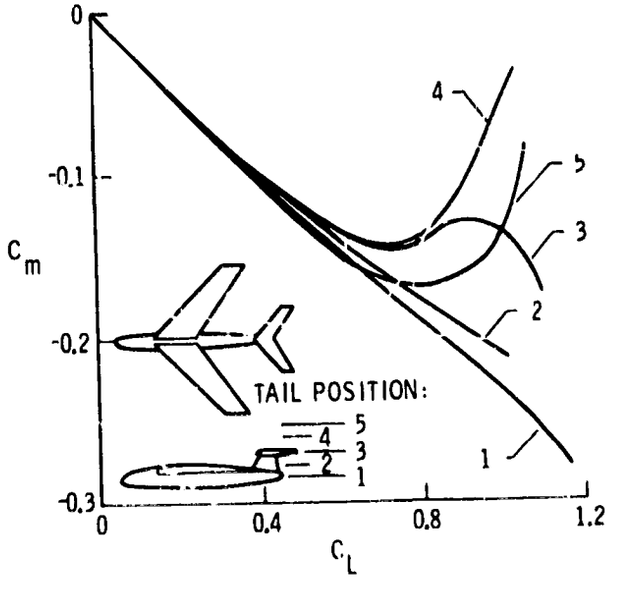

Figure 6.- Effect of horizontal-tail location on pitch-up tendencies.

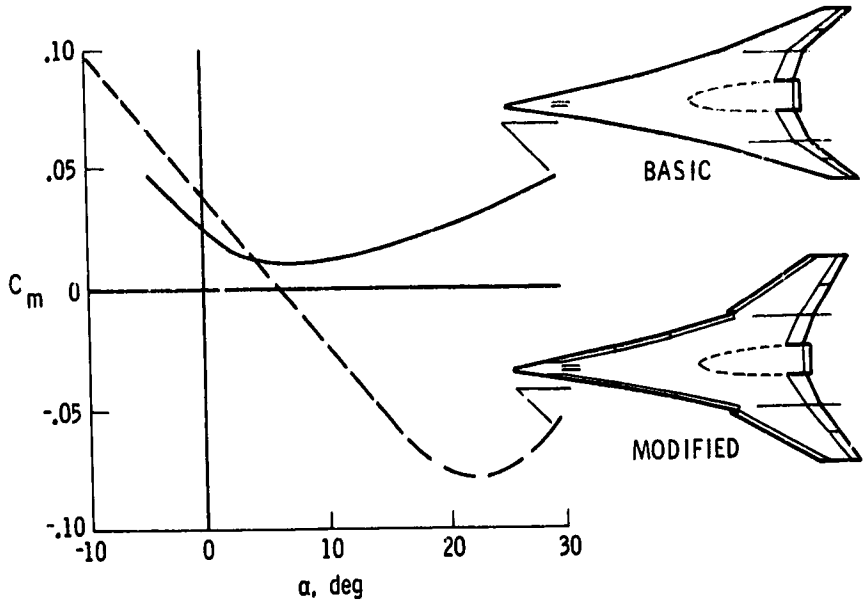

Figure 7.- Longitudinal stability characteristics of supersonic cruise configuration.

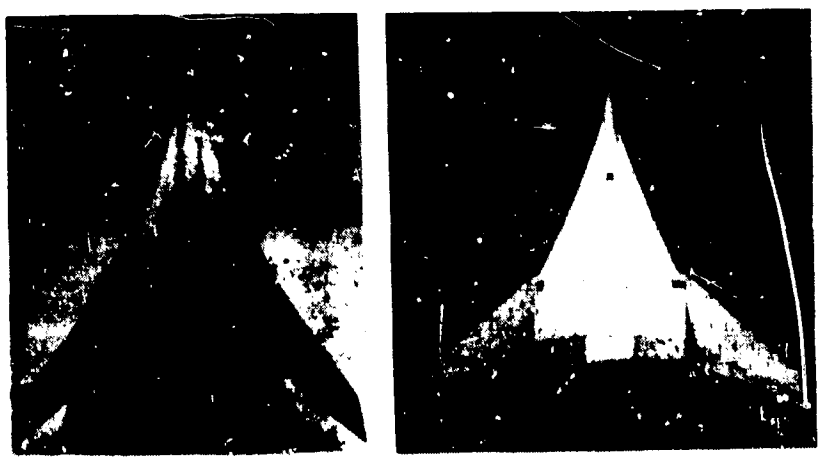

L-77-382

Figure 8.- Tuft flow visualization for the basic and modified models. $\alpha = 6^{\circ}$.

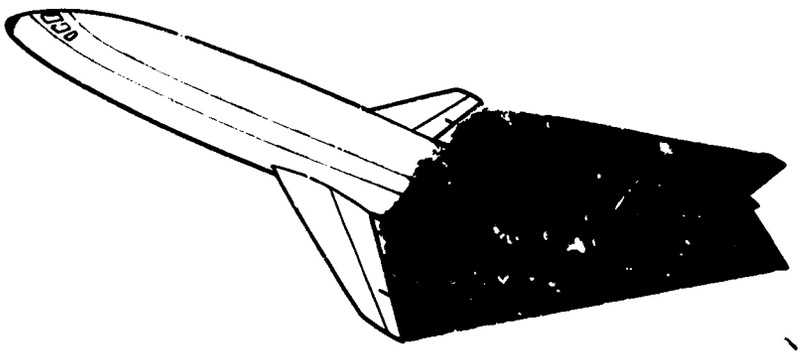

Figure 9.- Illustration of flow conditions producing deep stall.

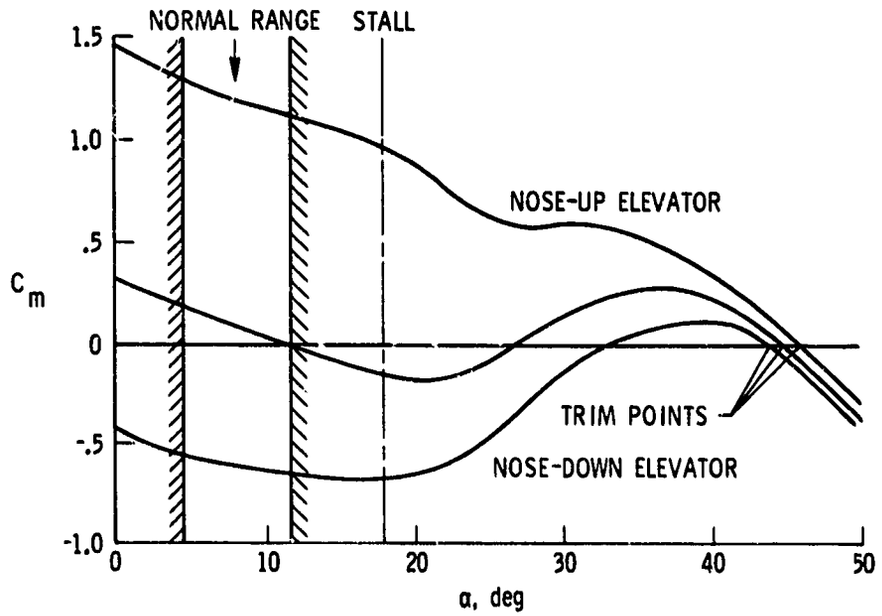

Figure 10.- Longitudinal aerodynamic pitching moments for a configuration with deep stall.

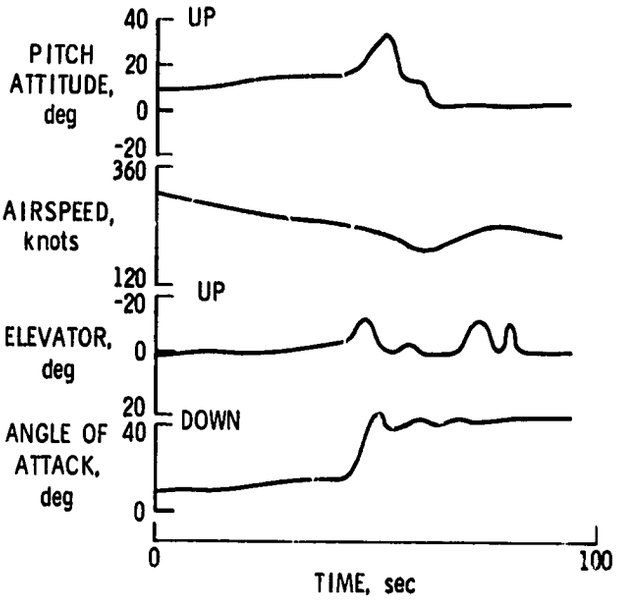

Figure 11.- Time histories of simulated deep stall.

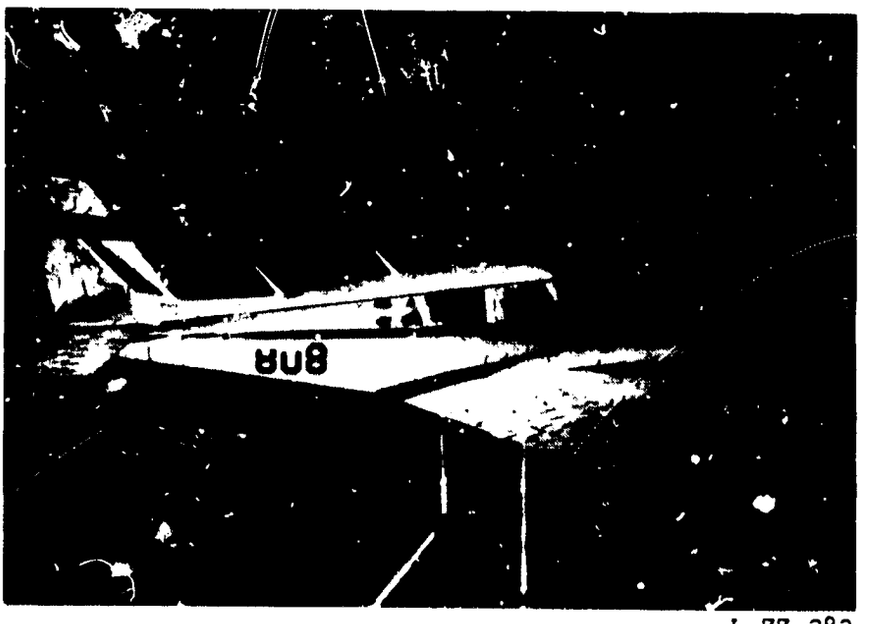

L-77-383

Figure 12.- Light general aviation airplane mounted for tests in the Langley full-scale tunnel.

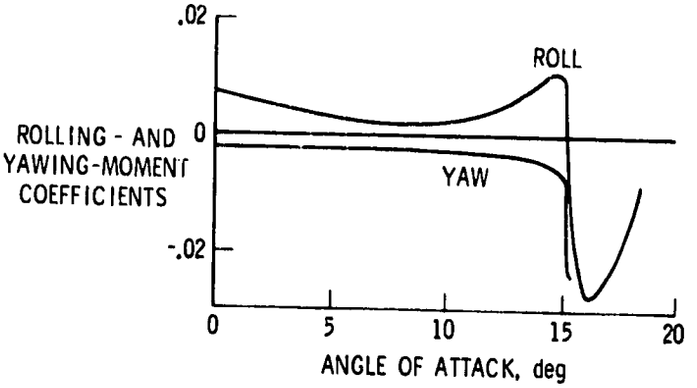

Figure 13.- Asymmetrical rolling- and yawing-moment coefficients at stall.

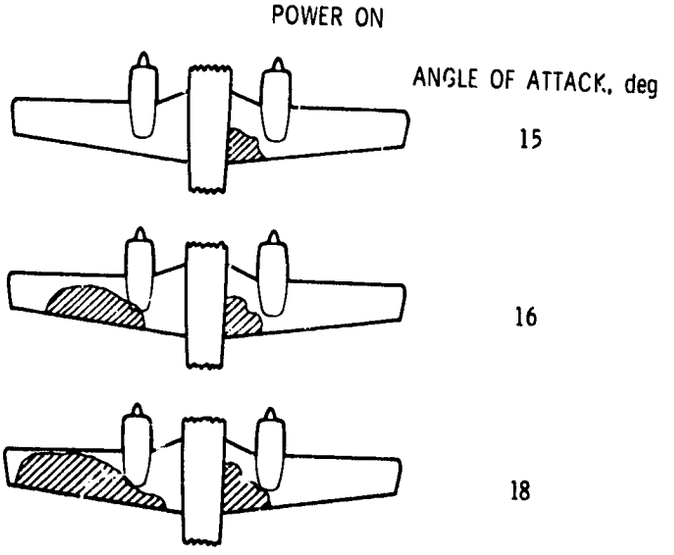

Figure 14.- Stall patterns related to asymmetric moments.

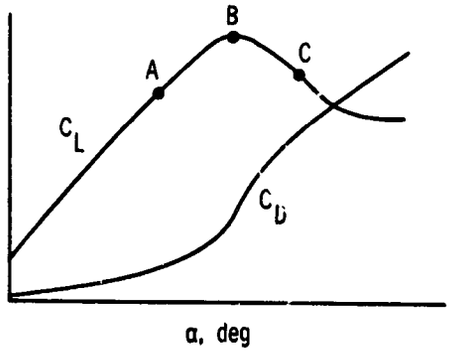

Figure 15.- Typical variations of C_L and C_D with α for unswept wing.

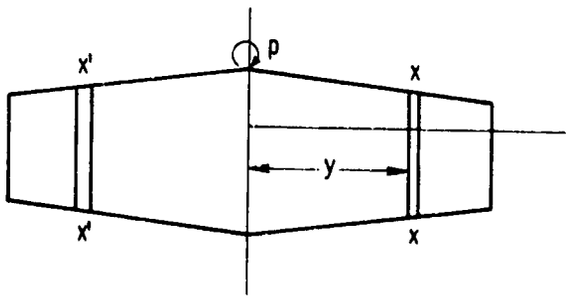

Figure 16.- Unswept wing with rolling motion.

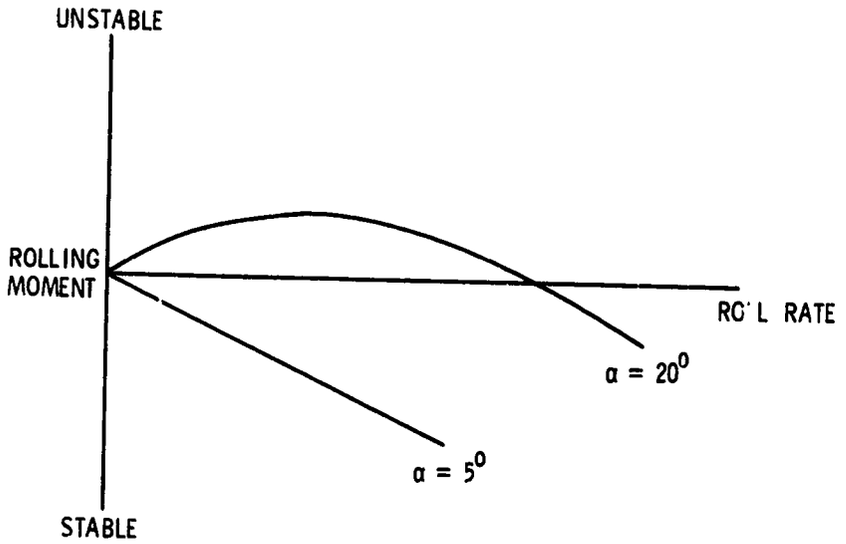

Figure 17.- Nonlinear variation of autorotative rolling moment with roll rate.

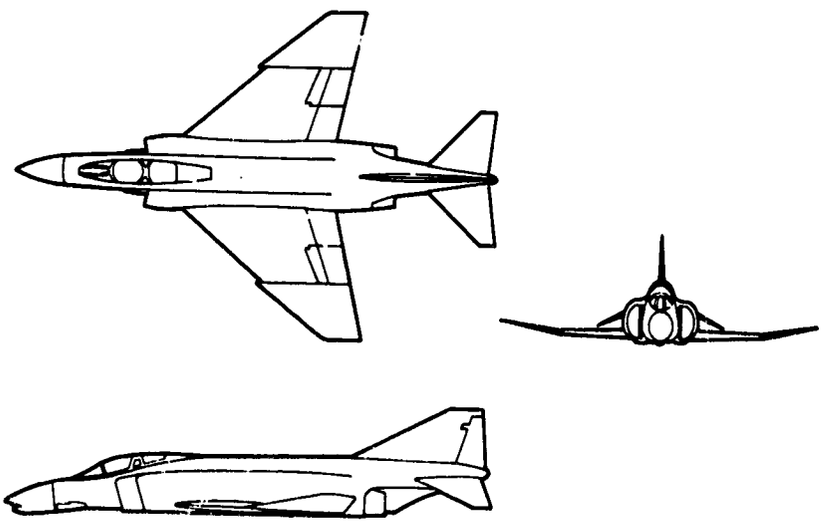

Figure 18.- Sketch of fighter configuration.

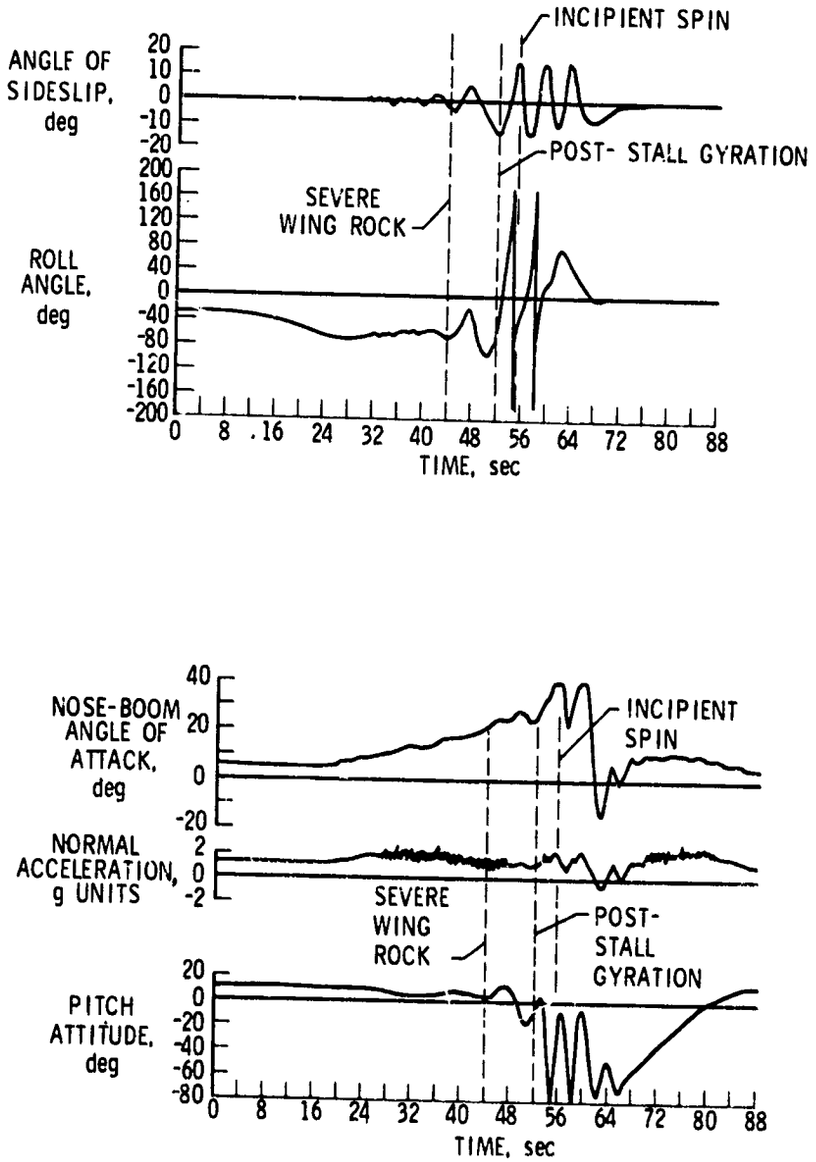

Figure 19.- Time histories of directional divergence.

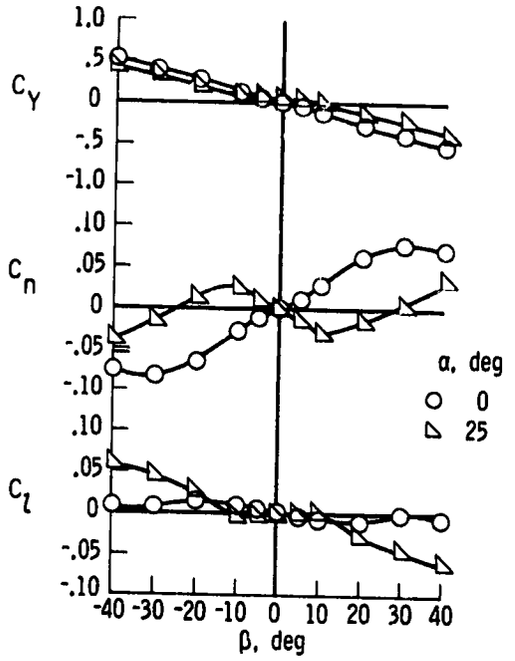

Figure 20.- Variation of static lateral-directional coefficients.

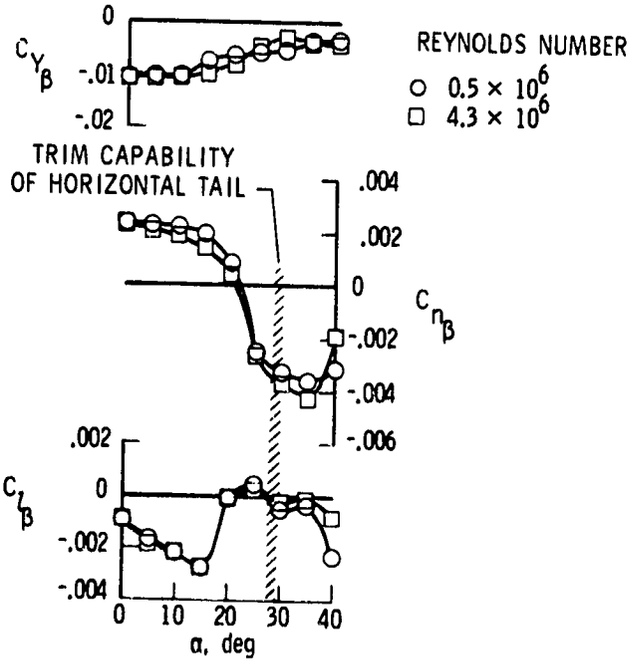

Figure 21.- Static lateral-directional stability derivatives based on $\beta = \pm 5^\circ$.

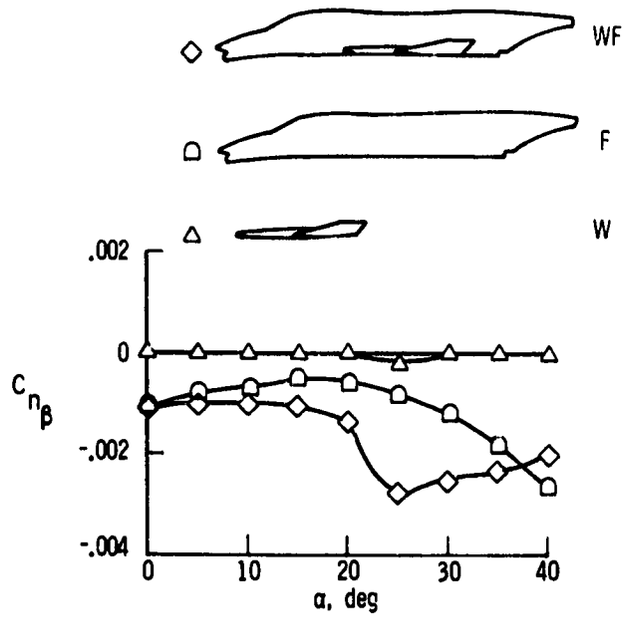

Figure 22.- Effect of wing and fuselage on C_{n_β}.

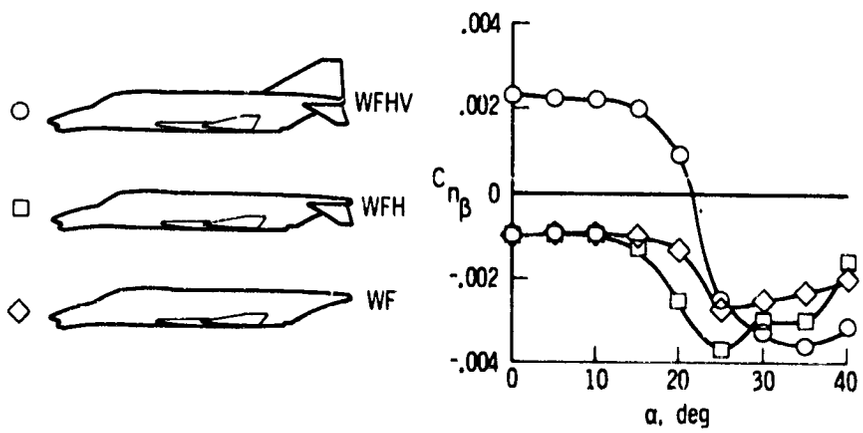

Figure 23.- Effect of vertical and horizontal tails on C_{n_β}.

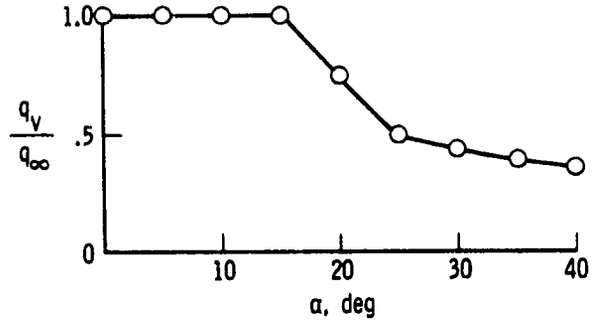

Figure 24.- Results of dynamic-pressure survey at vertical-tail location.

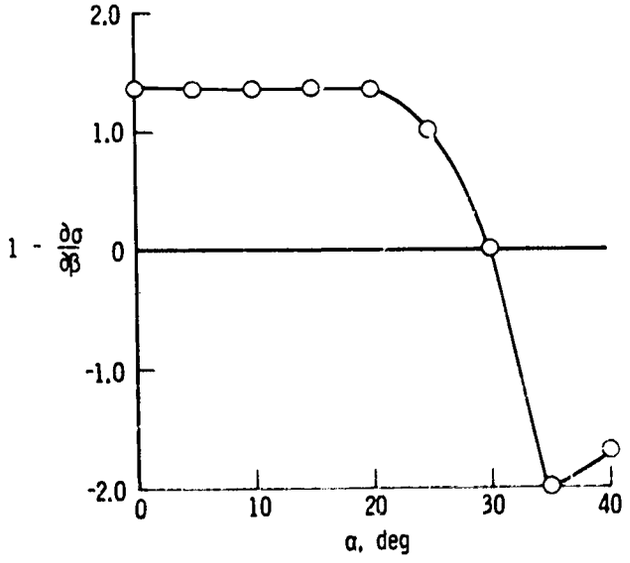

Figure 25.- Results of sidewash measurements at vertical-tail location.

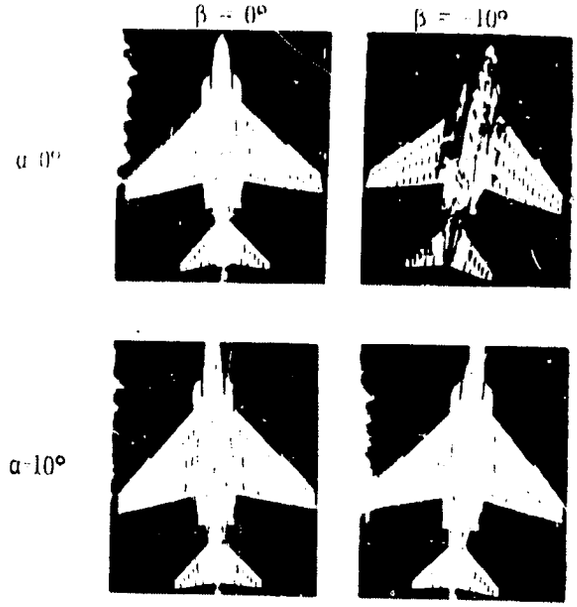

L-77-384

Figure 26.- Tuft flow patterns for low α.

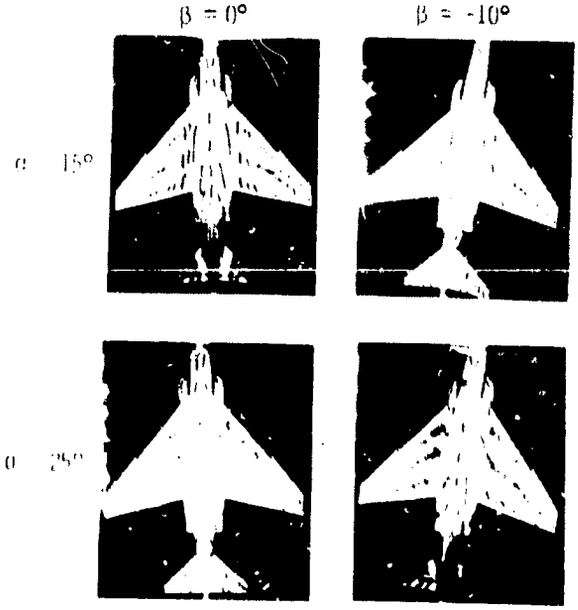

L-77-385

Figure 27.- Tuft flow patterns for high α.

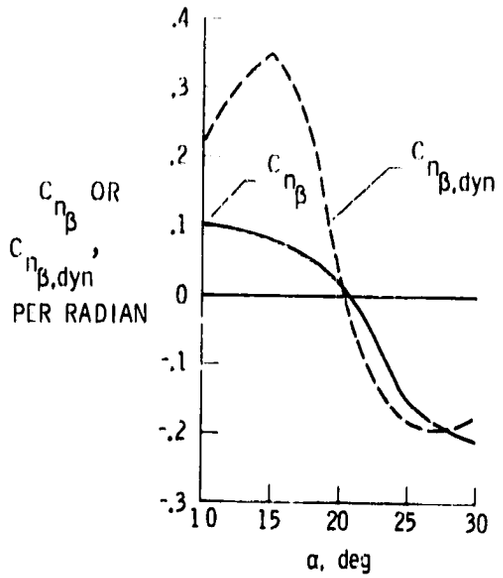

Figure 28.- Variation of static and dynamic directional stability parameters with α.

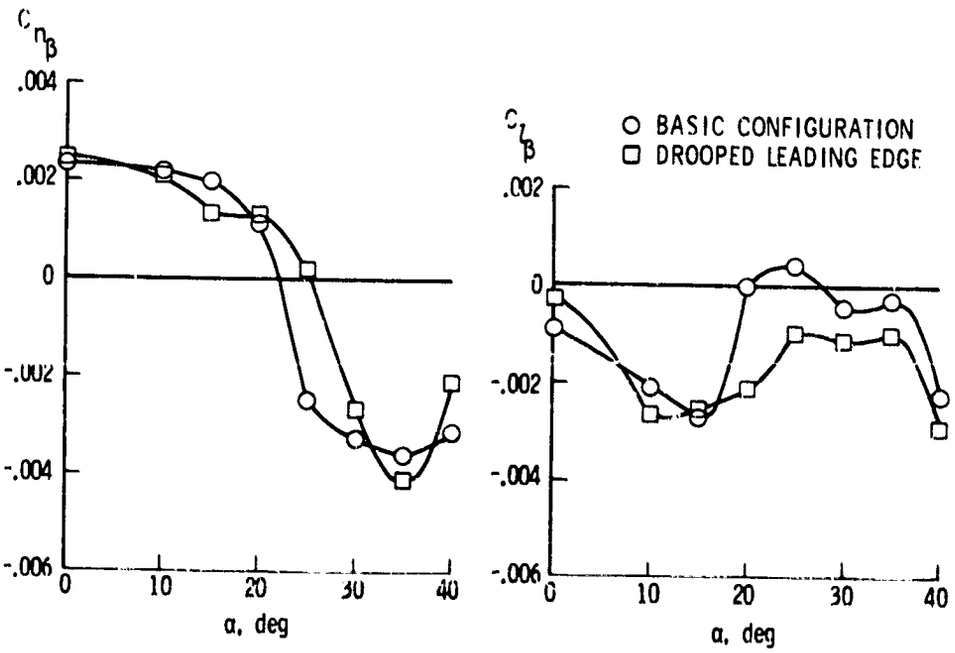

Figure 29.- Effects of 40° wing leading-edge droop on C_{n_β} and C_{l_β}.

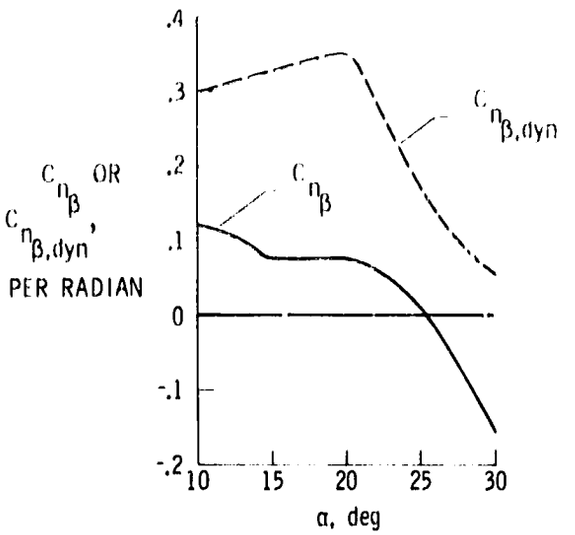

Figure 30.- Effect of leading-edge droop on C_{n_β} and $C_{n_{\beta,dyn}}$.

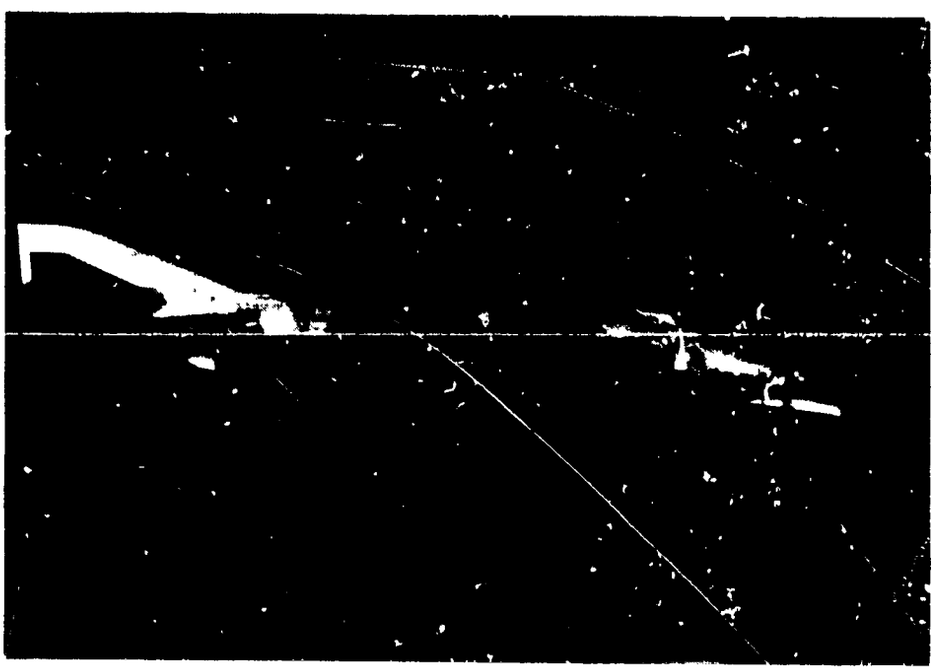

Figure 31.- Airplane with leading-edge slats.

L-72-4473

Figure 32.- Wind-tunnel free-flight model.

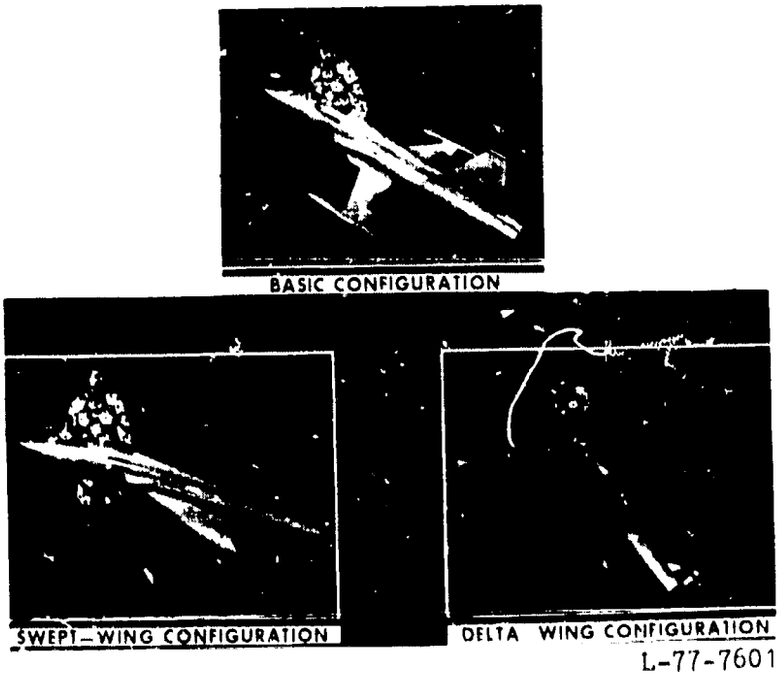

L-77-7601

Figure 33.- Wing configurations tested.

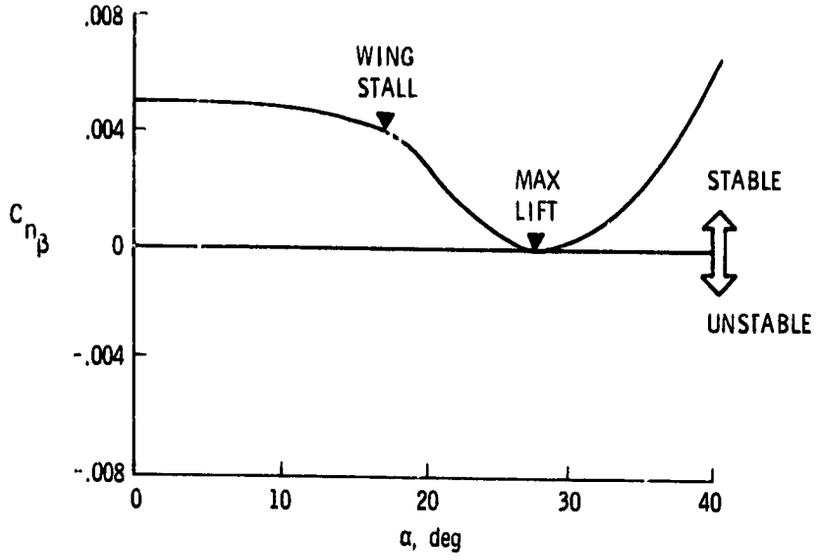

Figure 34.- Static directional stability characteristics of the basic configuration.

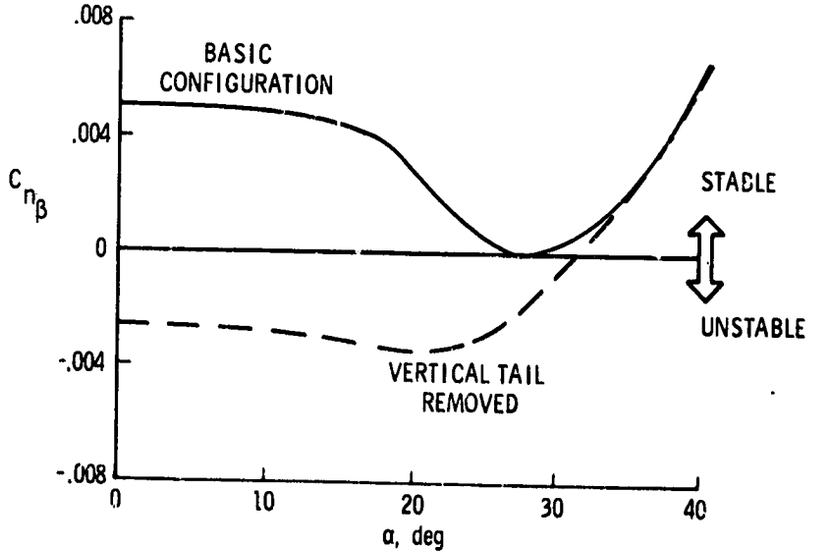

Figure 35.- Contribution of vertical tail to C_{n_β}.

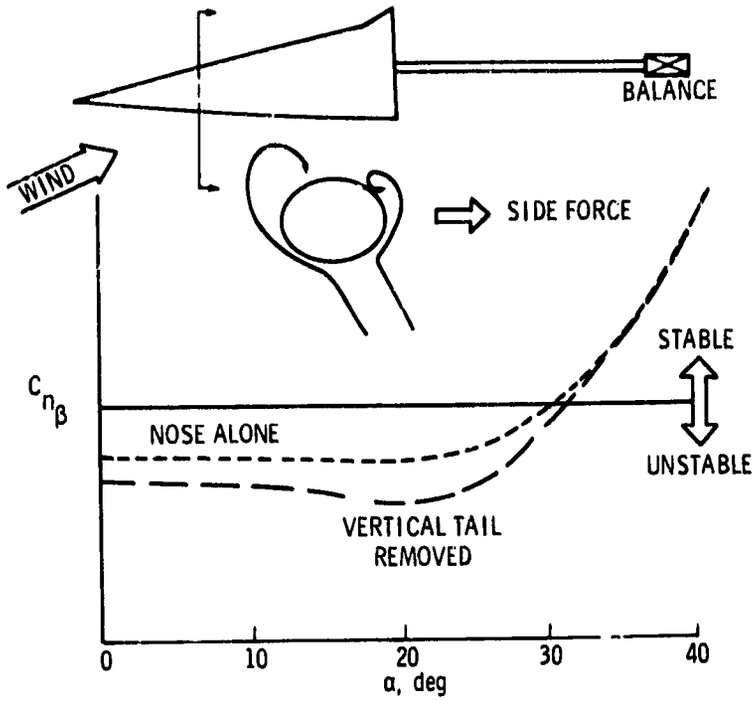

Figure 36.- Results of fuselage-forebody tests.

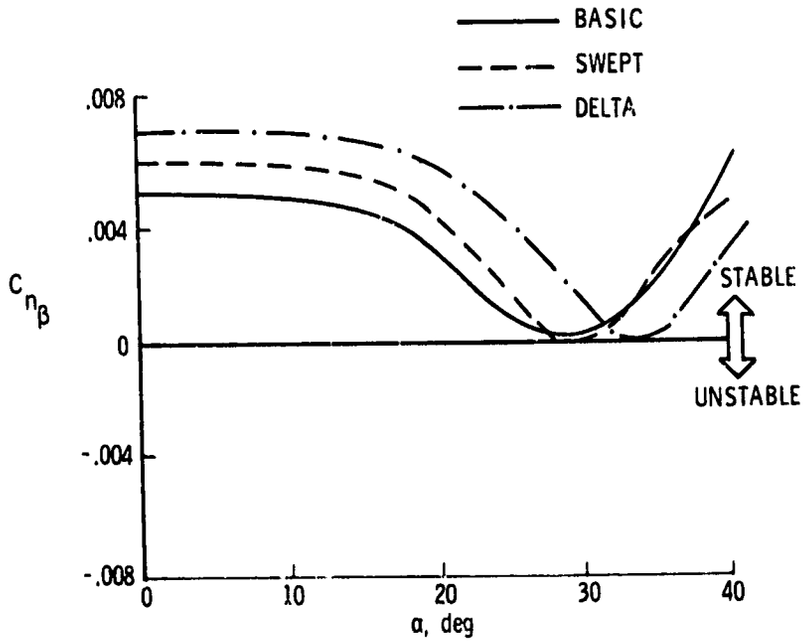

Figure 37.- Static directional stability characteristics of the model with various wings.

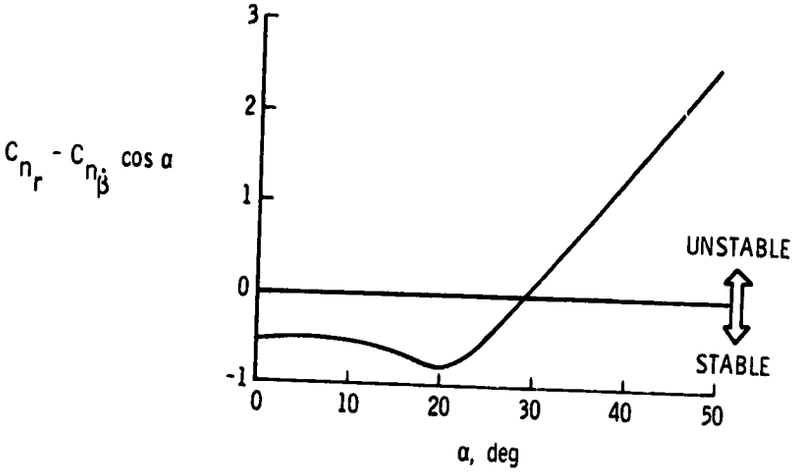

Figure 38.- Variation of damping-in-yaw parameter with α.

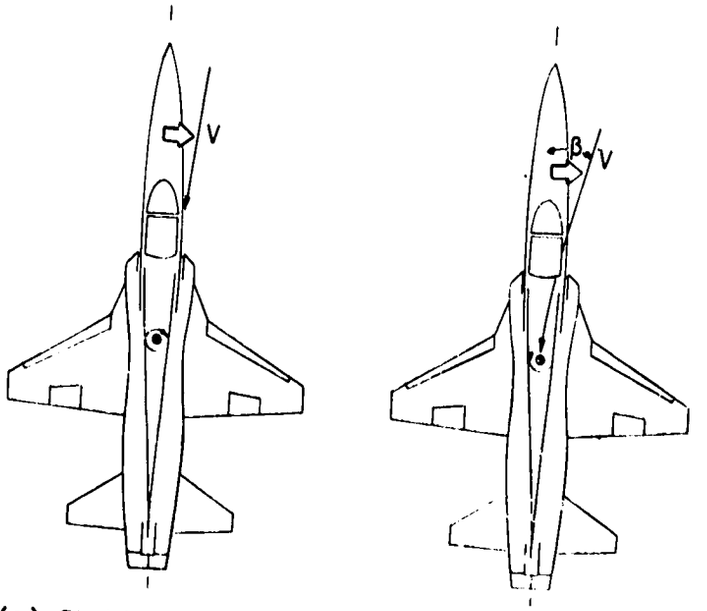

(a) Static, $\beta \neq 0^o$. (b) Yawing, $\beta = 0^o$.

Figure 39.- Cause of unstable damping in yaw.

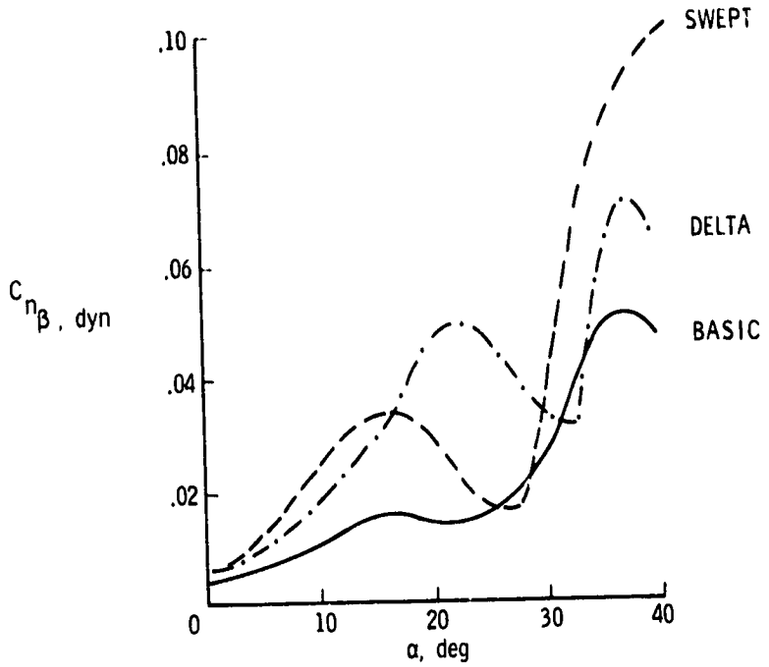

Figure 40.- Variations of $C_{n\beta,dyn}$ for the various configurations.

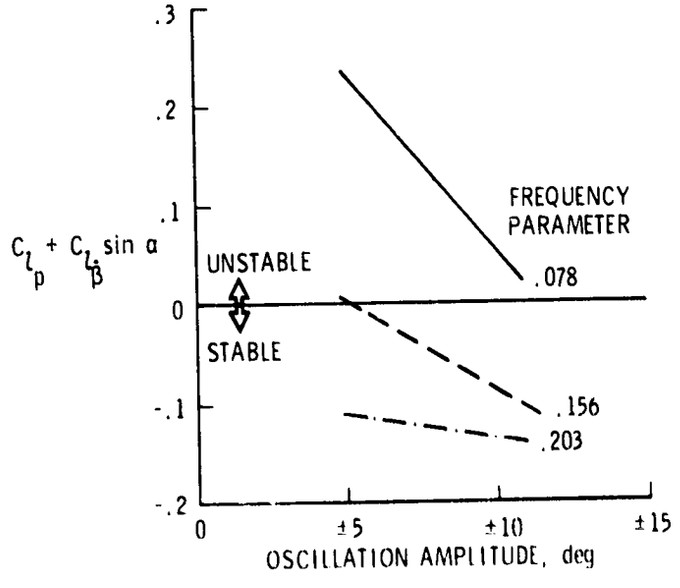

Figure 41.- Variation of damping-in-roll parameter.

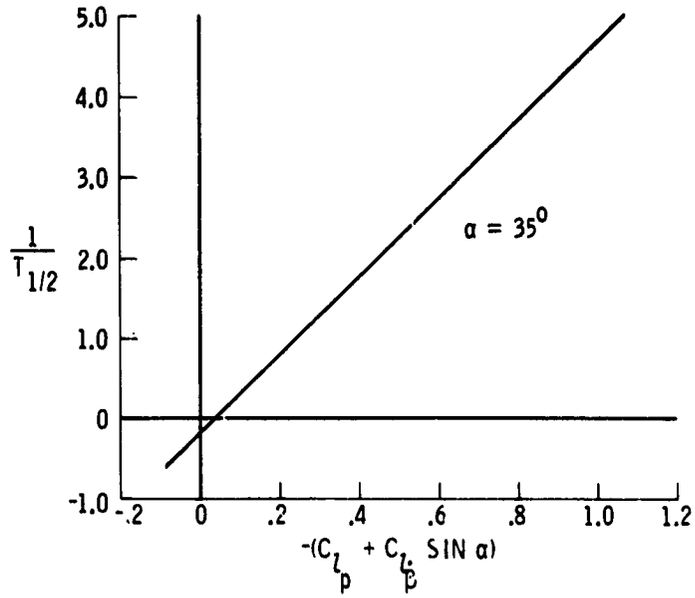

Figure 42.- Effect of damping in roll on damping of lateral oscillation.

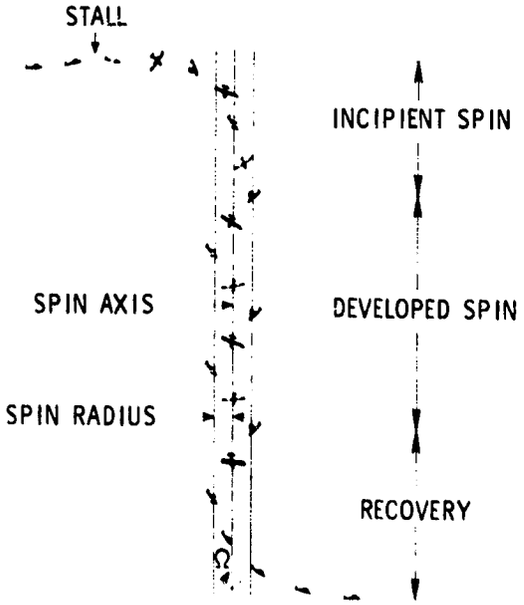

Figure 43.- Various phases of the spin.

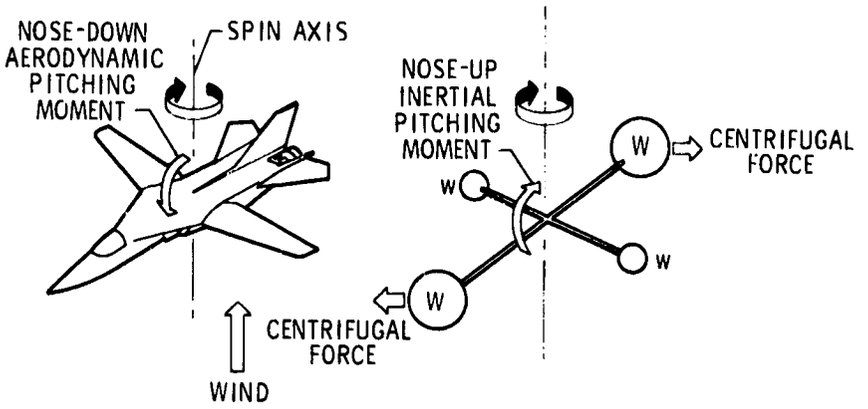

Figure 44.- Aerodynamic and inertial pitching moments in a spin.

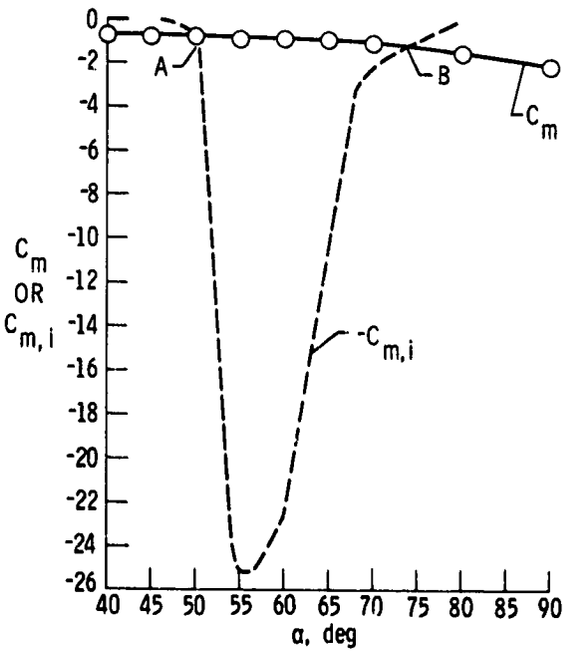

Figure 45.- Variation of aerodynamic and inertial pitching moments with α.

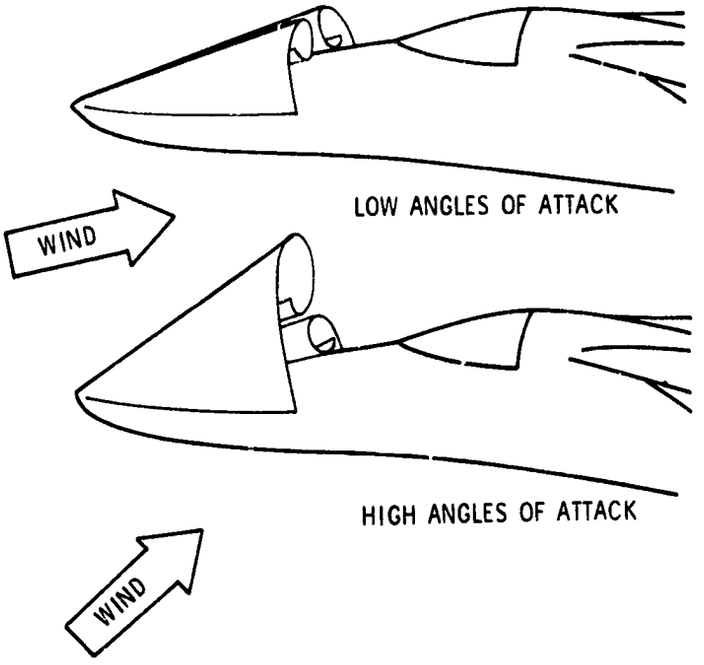

Figure 46.- Sketch of flow separation from pointed nose at low and high angles of attack. $\beta = 0^{o}$.

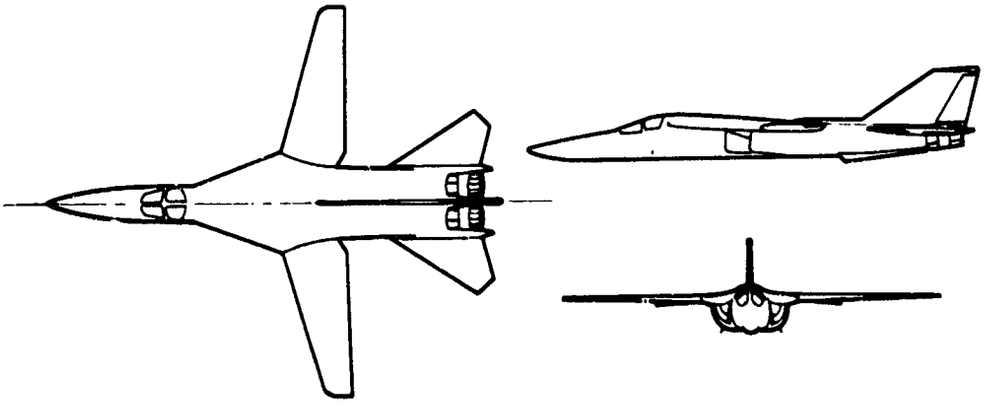

Figure 47.- Sketch of variable-sweep fighter configuration.

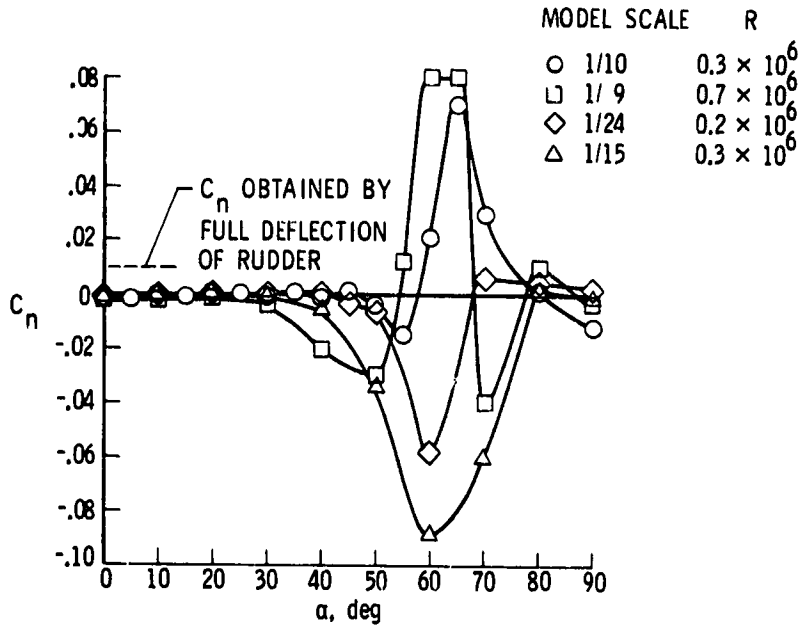

Figure 48.- Variation of C_n with α for four models. $\beta = 0^o$.

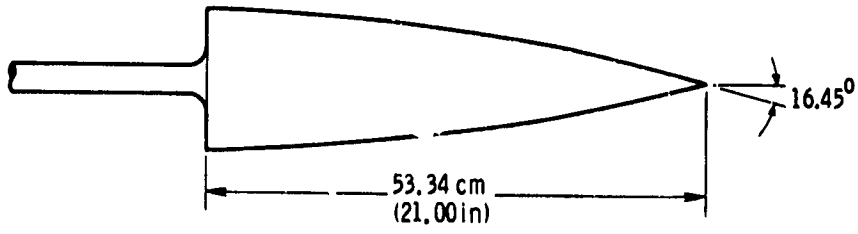

Figure 49.- Sketch of tangent-ogive model.

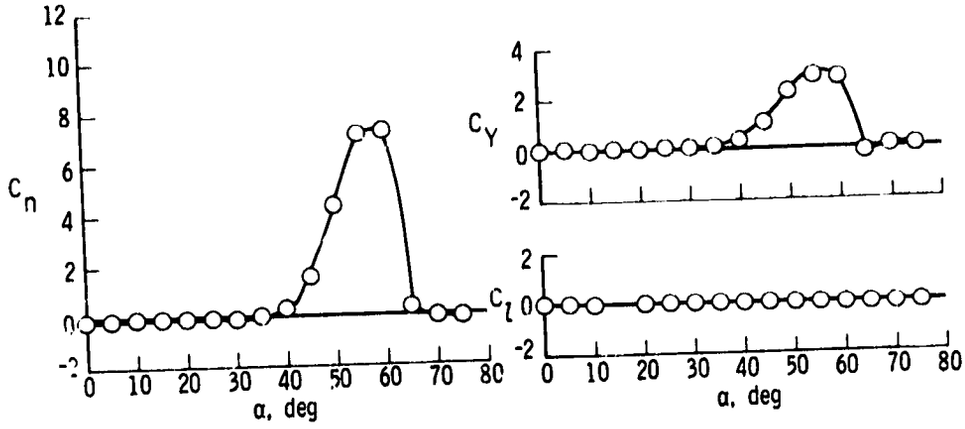

Figure 50.- Asymmetries measured for tangent-ogive model. $\beta = 0^\circ$.

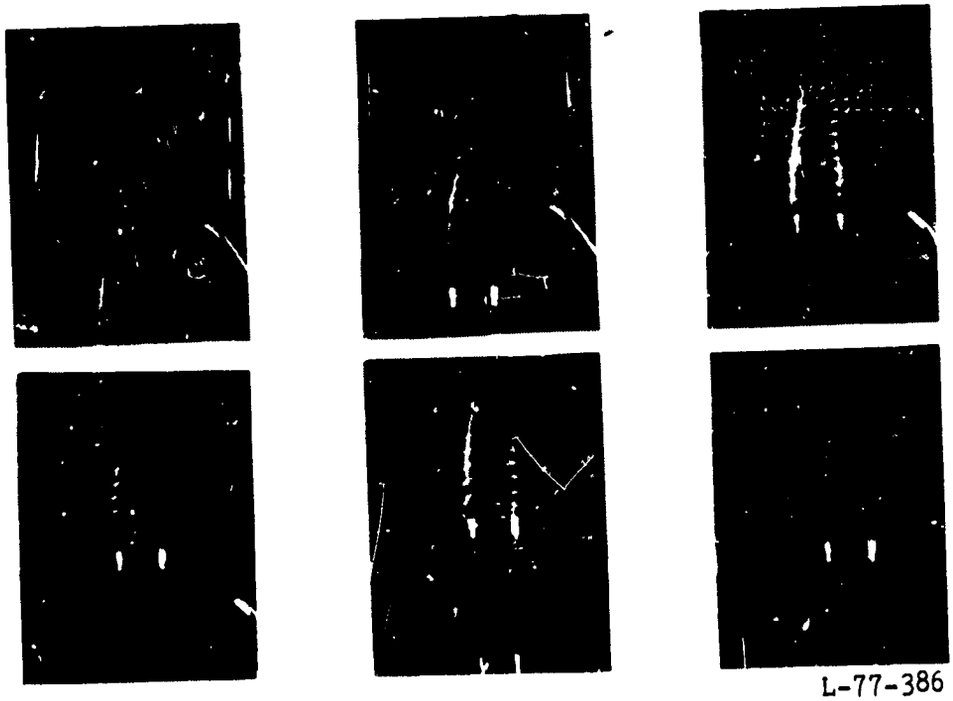

L-77-386

Figure 51.- Tuft flow-visualization results at several downstream locations. $\beta = 0^\circ$; $\alpha = 55^\circ$.

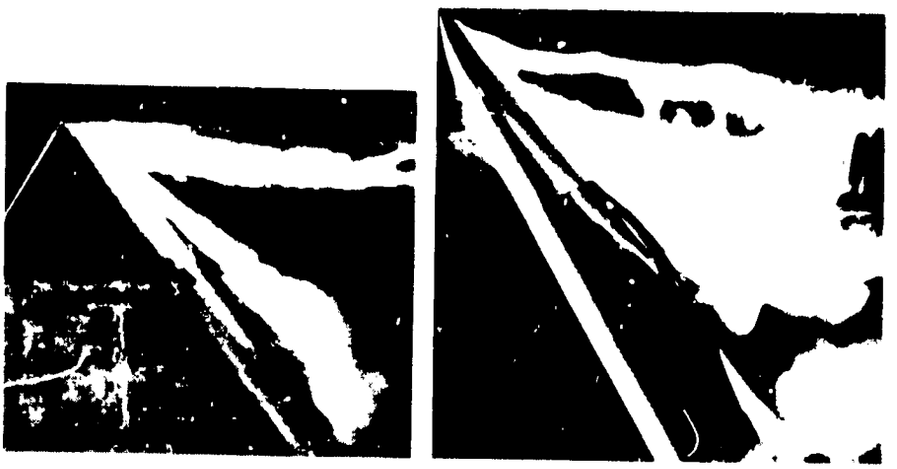

L-77-387

Figure 52.- Smoke flow results for tangent-ogive model and fighter model.

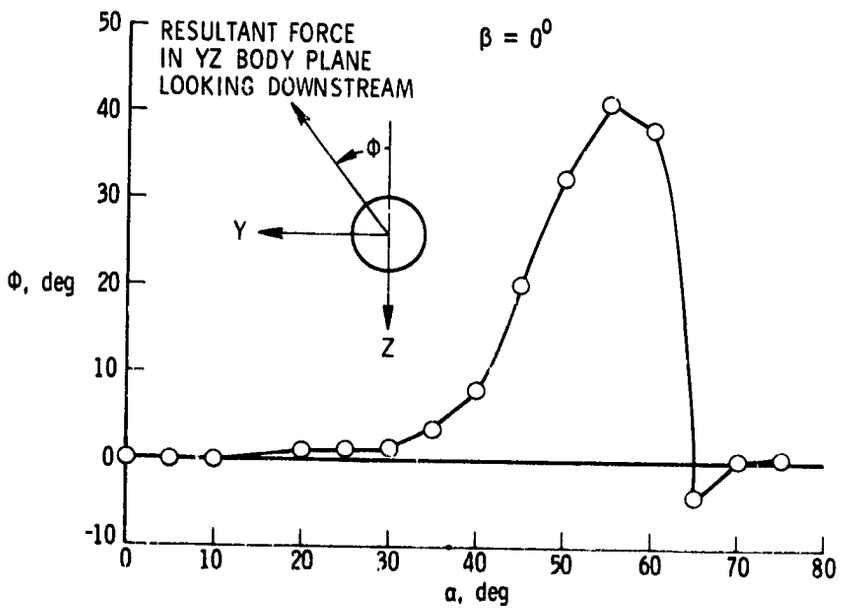

Figure 53.- Inclination of resultant force vector in the YZ-plane.

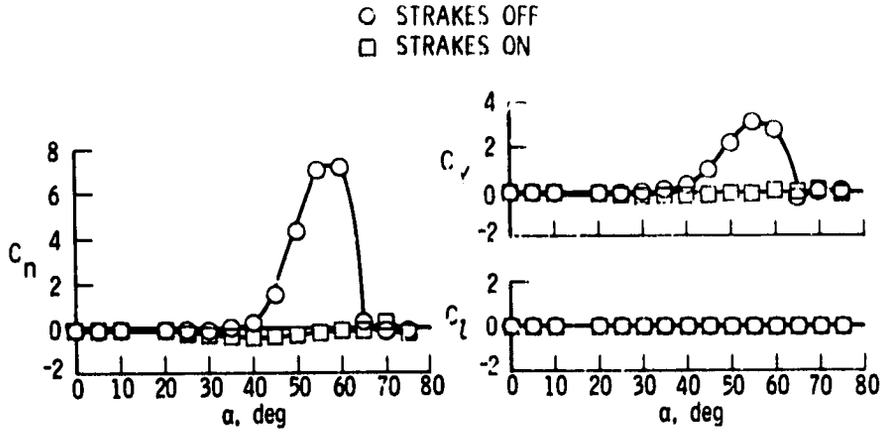

Figure 54.- Effect of nose strakes on asymmetries.

L-73-1596

Figure 55.- Fighter design with nose strakes.

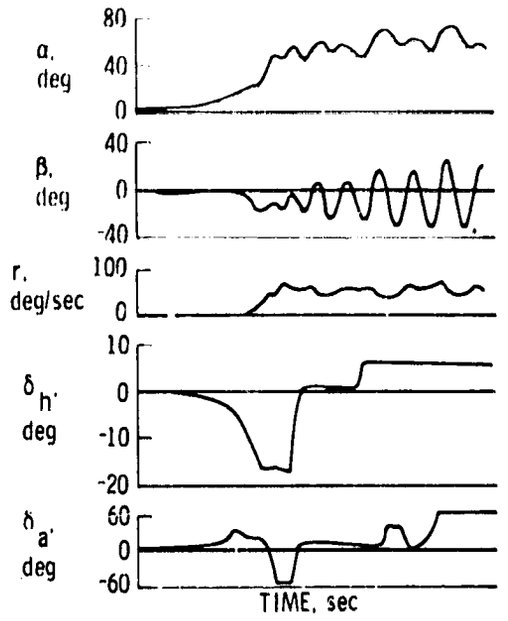

Figure 56.- Typical stall/spin motions.

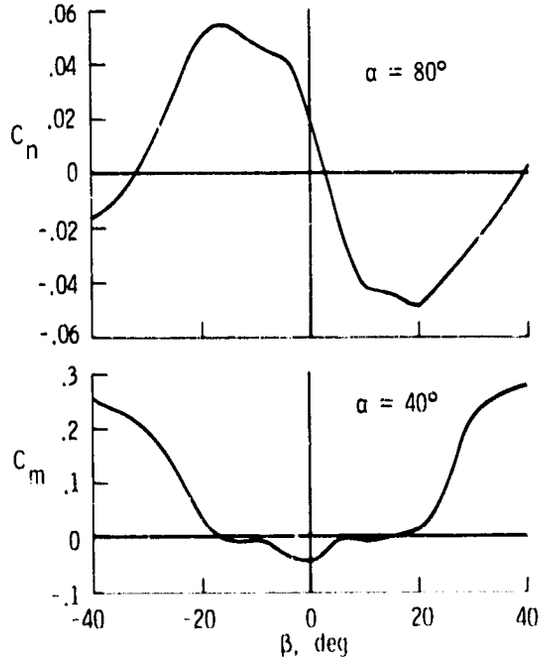

Figure 57.- Typical aerodynamic nonlinearities with β.

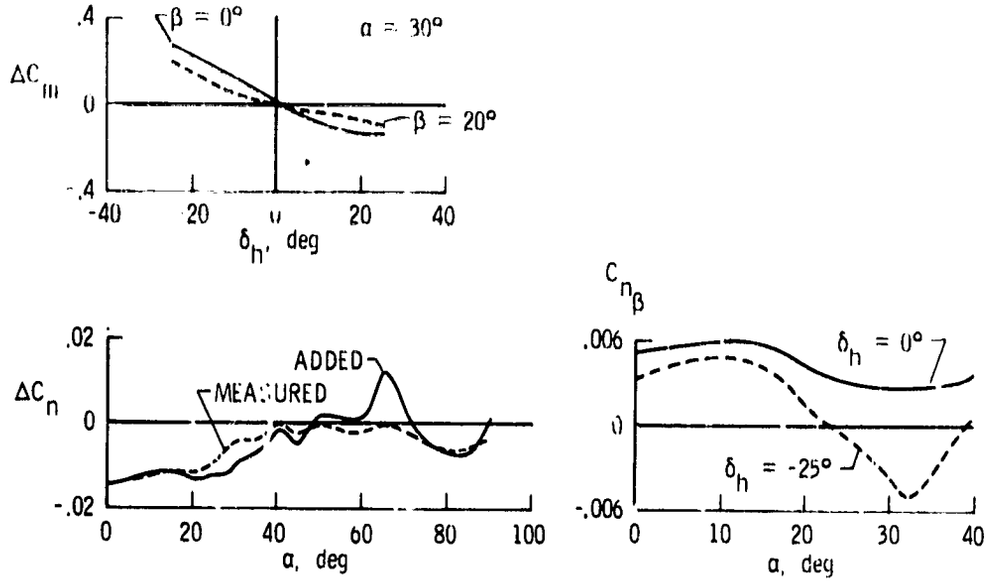

Figure 58.- Control characteristics.

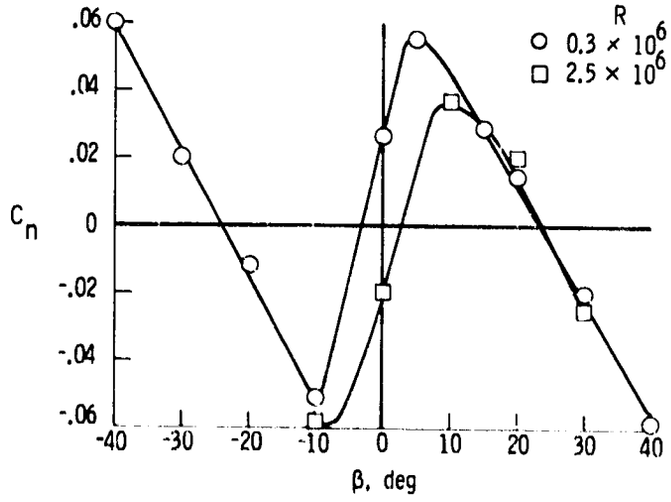

Figure 59.- Nonlinear yawing moments caused by long, pointed nose of fighter model. α = 55°.

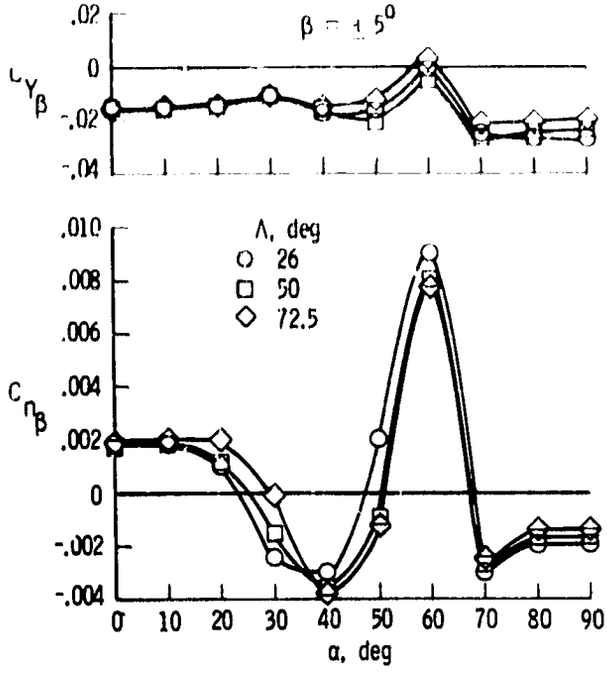

Figure 60.- Variation of C_{n_β} and C_{Y_β} for variable-sweep fighter model.

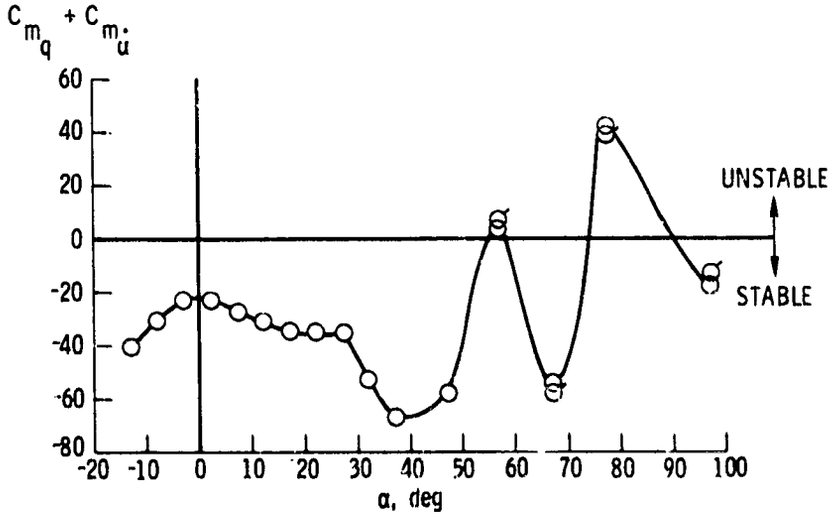

Figure 61.- Damping in pitch of variable-sweep fighter model.

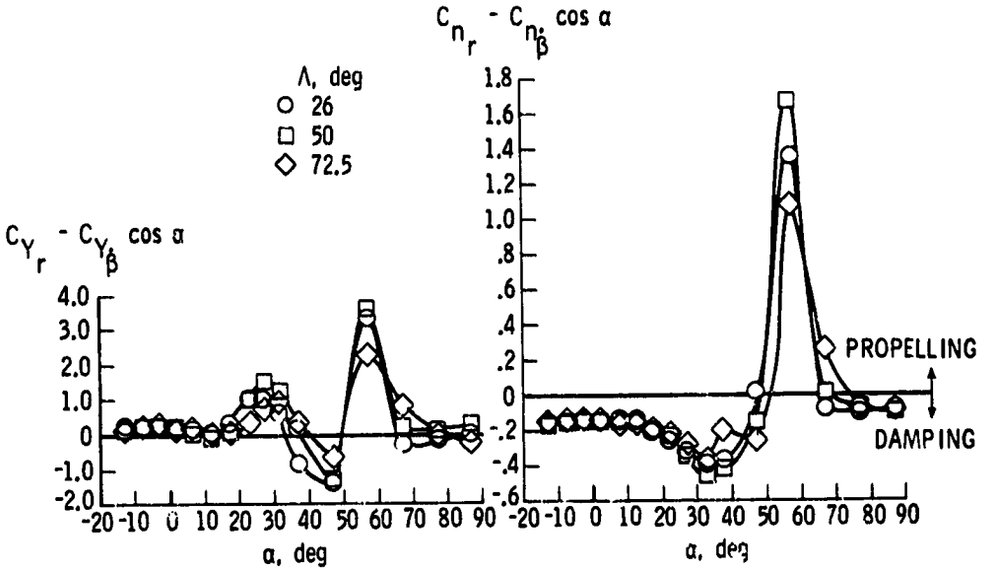

Figure 62.- Damping in yaw of variable-sweep fighter model.

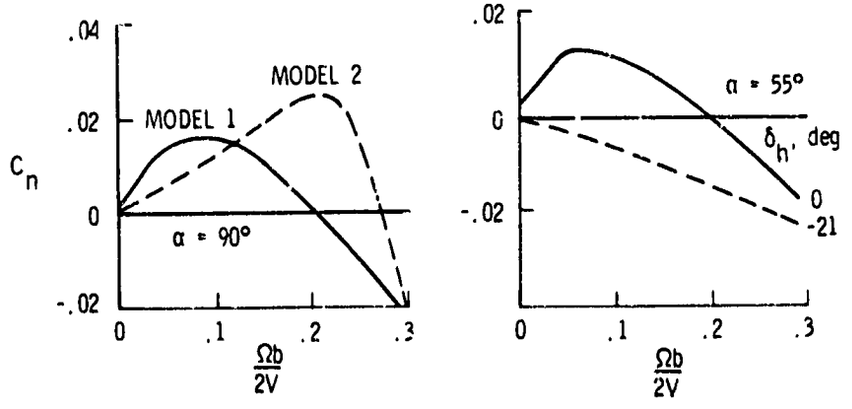

Figure 63.- Results obtained in rotary-spin tests.

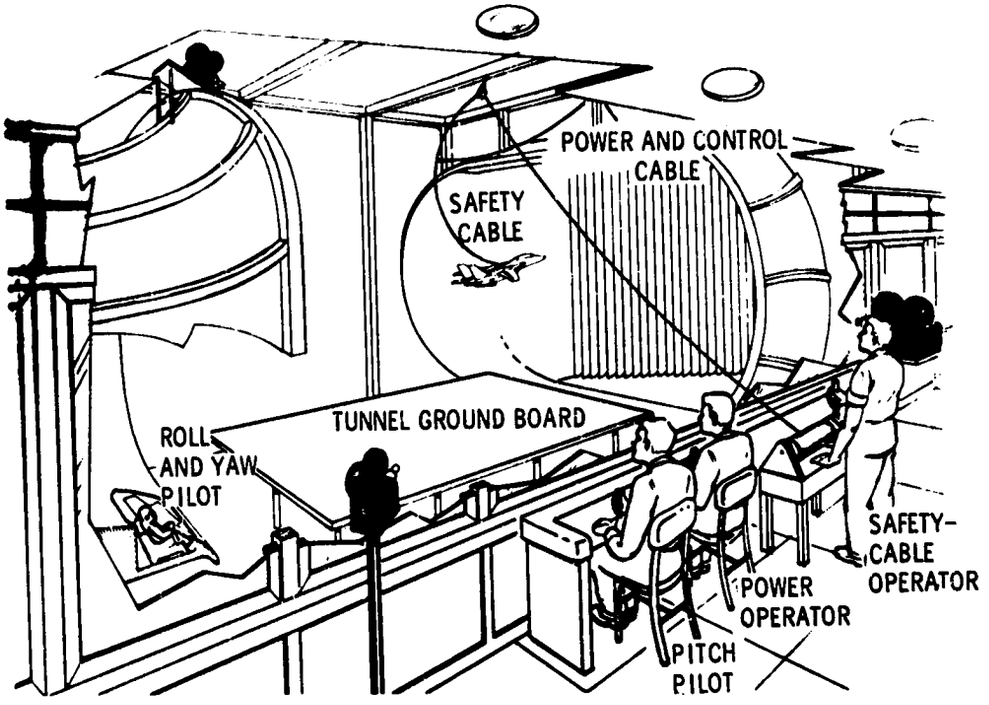

Figure 64.- Test setup for wind-tunnel free-flight model tests.

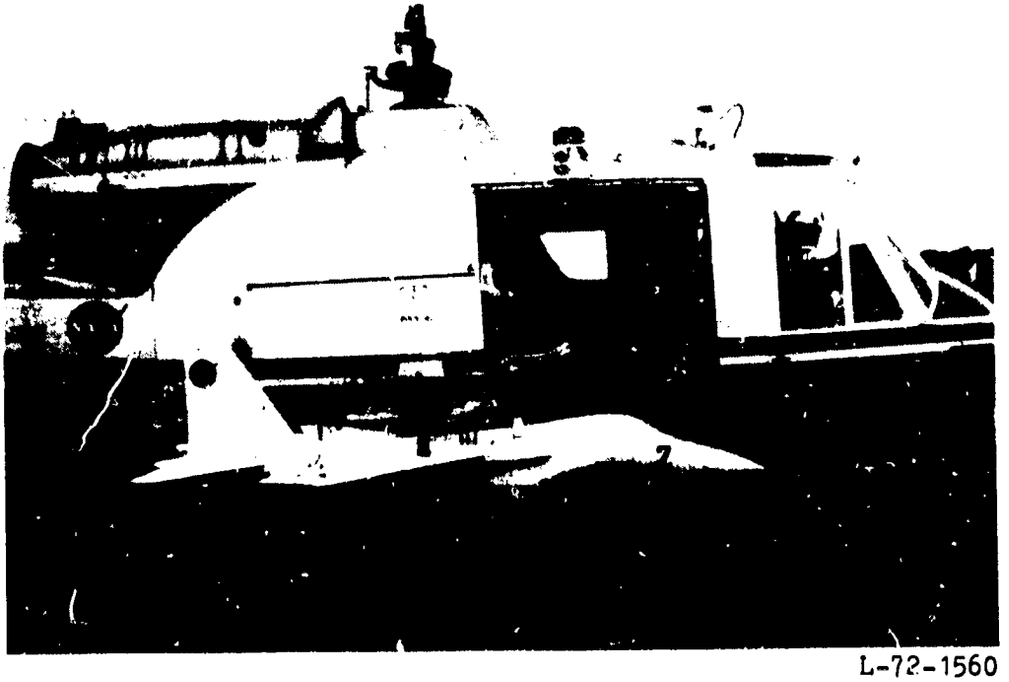

L-72-1560

Figure 65.- Drop model mounted on helicopter.

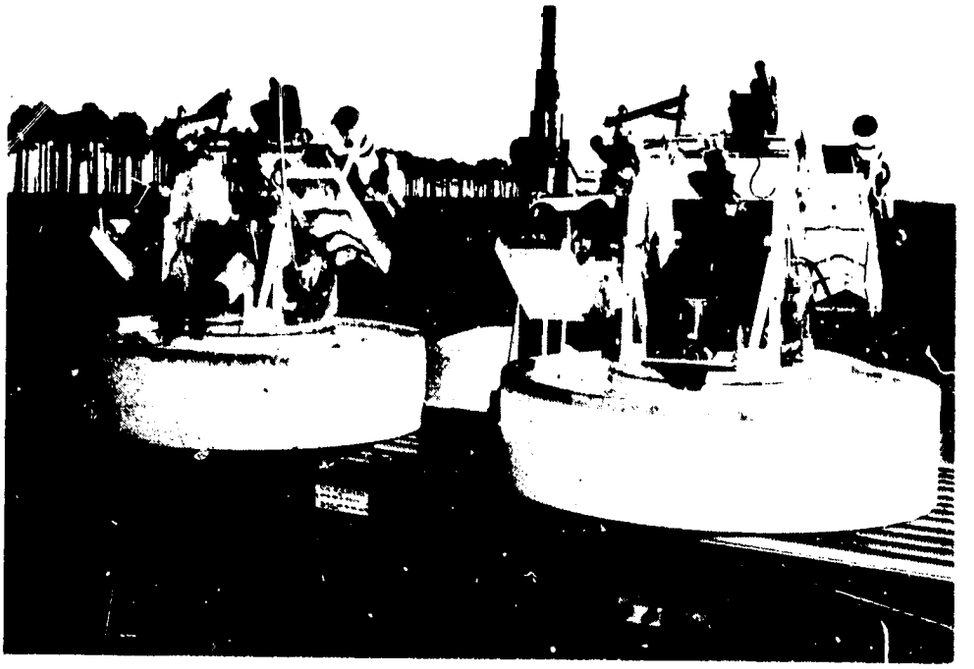

L-66-9183

Figure 66.- Tracking and controlling equipment.

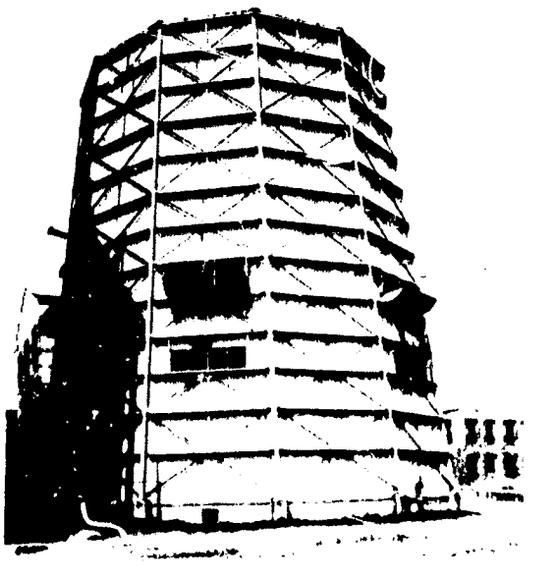

LAL-86257

Figure 67.- External view of Langley spin tunnel.

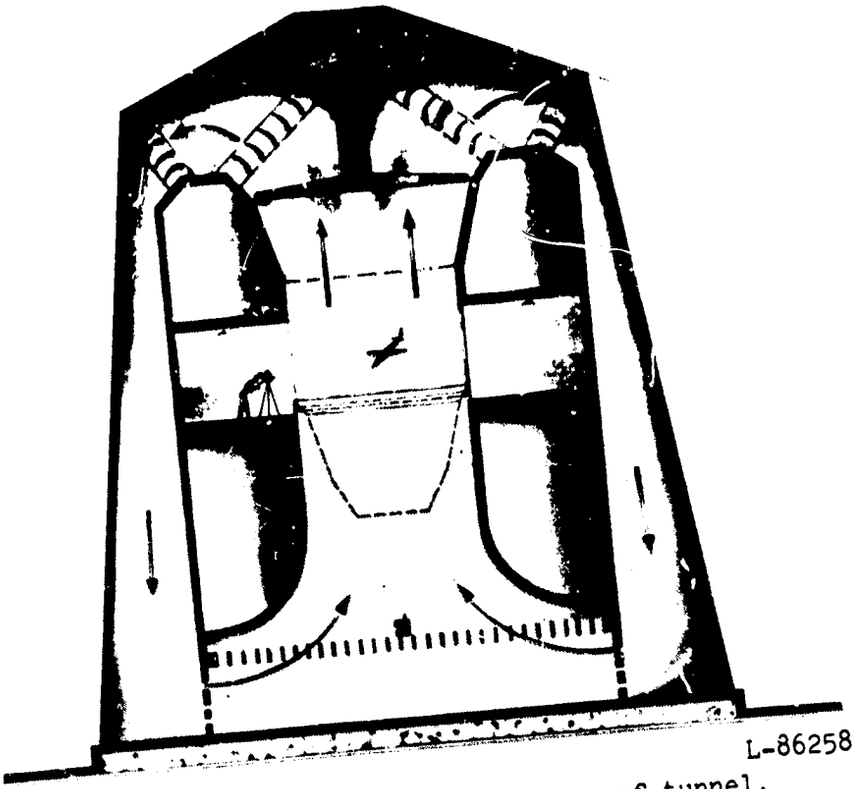

Figure 68.- Cross-sectional view of tunnel.

Figure 69.- Test section of tunnel.

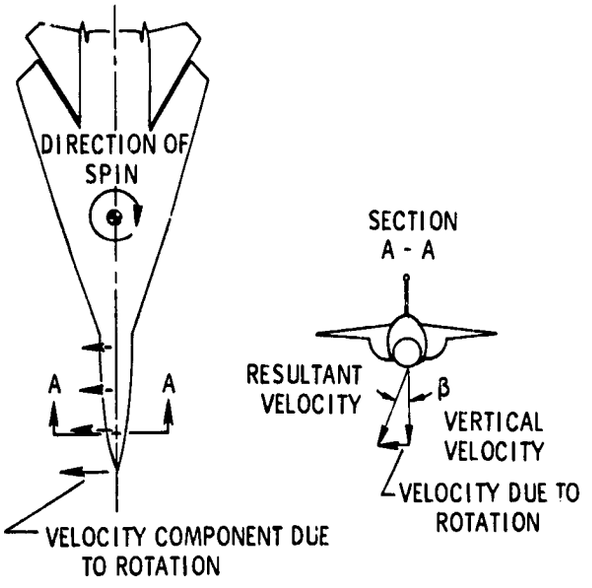

Figure 70.- Plan view of airplane in right spin.

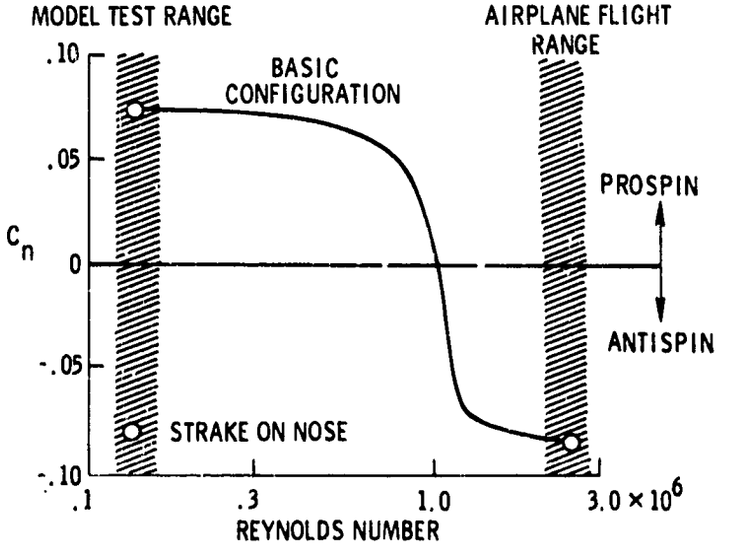

Figure 71.- Variation of C_n with Reynolds number. $\alpha = 80^\circ$; $\beta = 10^\circ$.

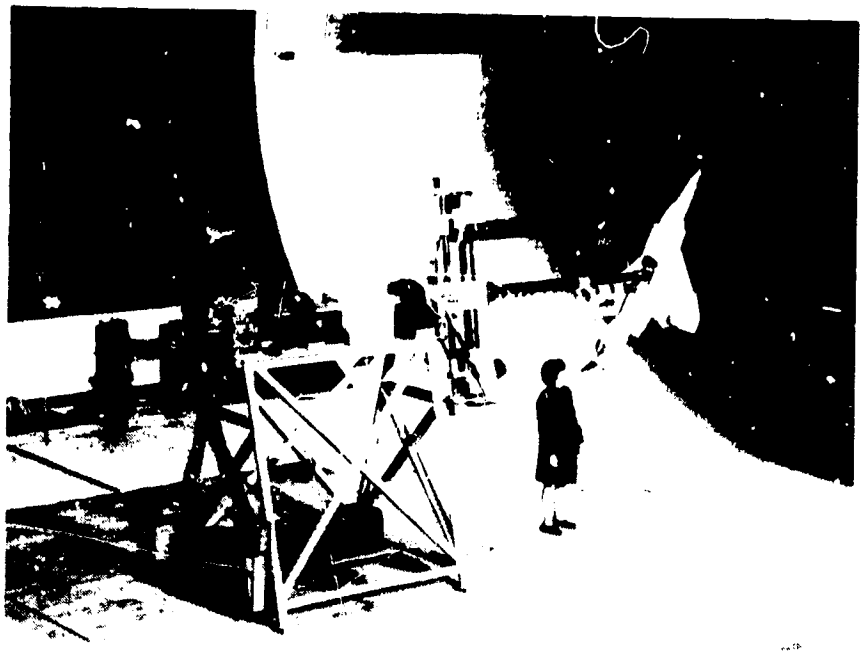

L-73-3701

Figure 72.- Rotary-balance test rig in Langley full-scale tunnel.

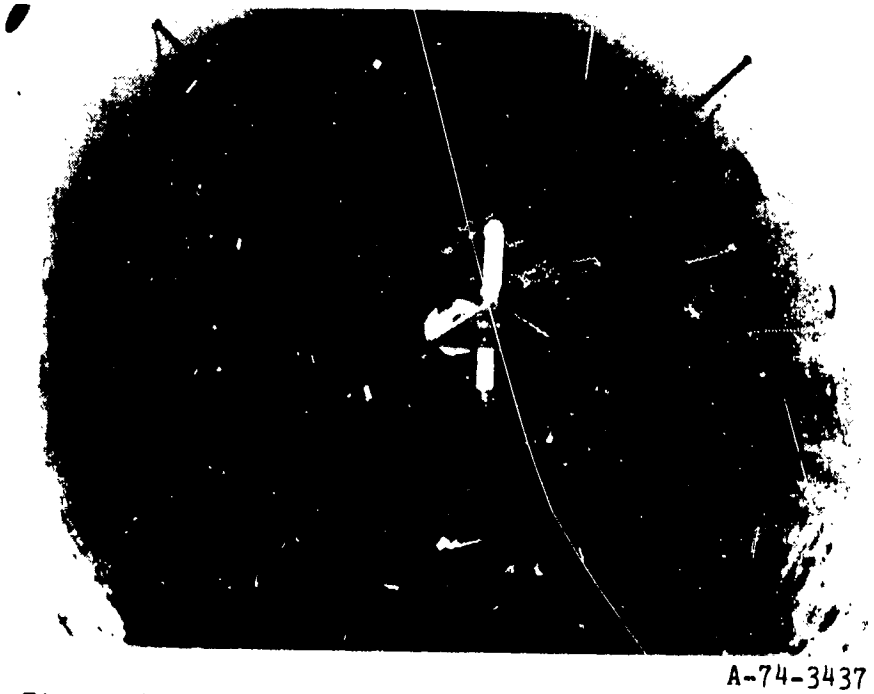

A-74-3437

Figure 73.- Rotary-balance test rig in Ames 12-Foot Pressure Wind Tunnel.

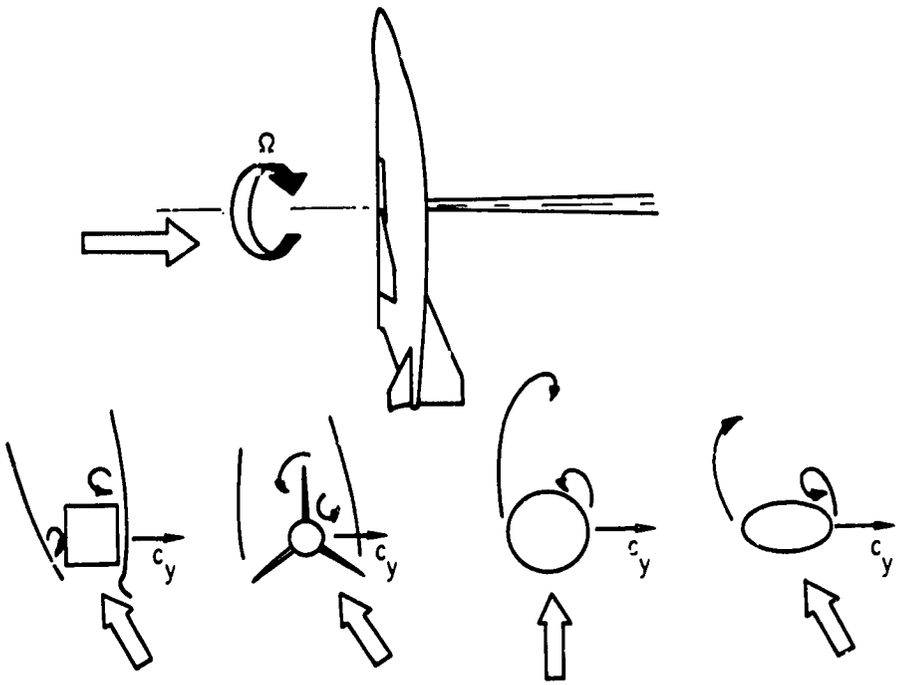

Figure 74.- Some prospin flow mechanisms.

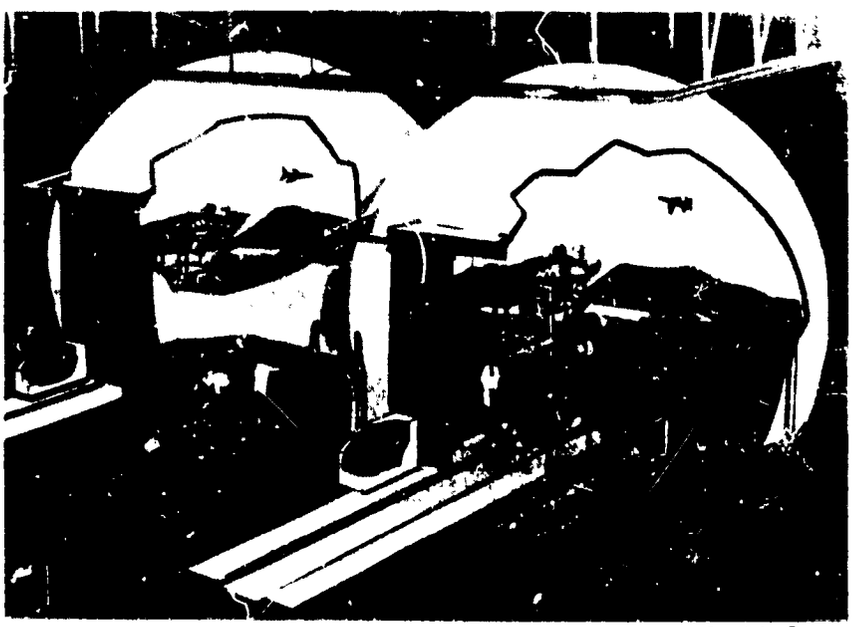

L-71-8700

Figure 75.- Sketch of the Langley differential maneuvering simulator

L-72-1361

Figure 76.- Visual display during simulated engagement.

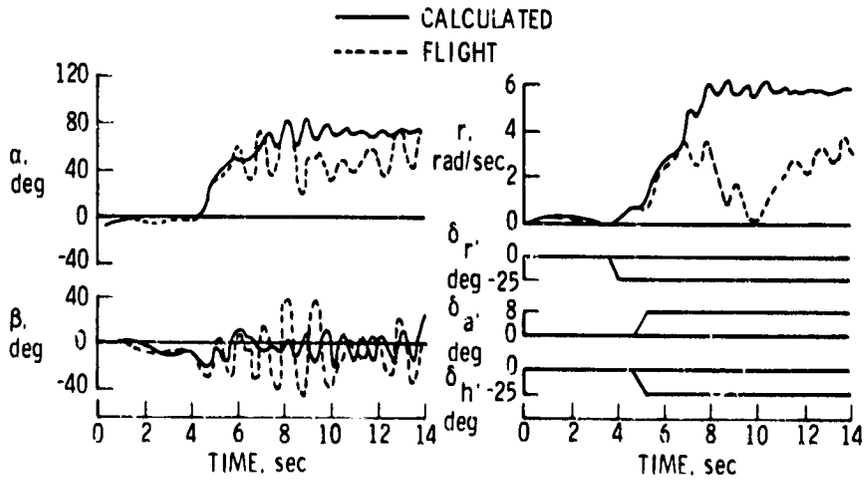

Figure 77.- Correlation of theoretical and experimental flight motions.

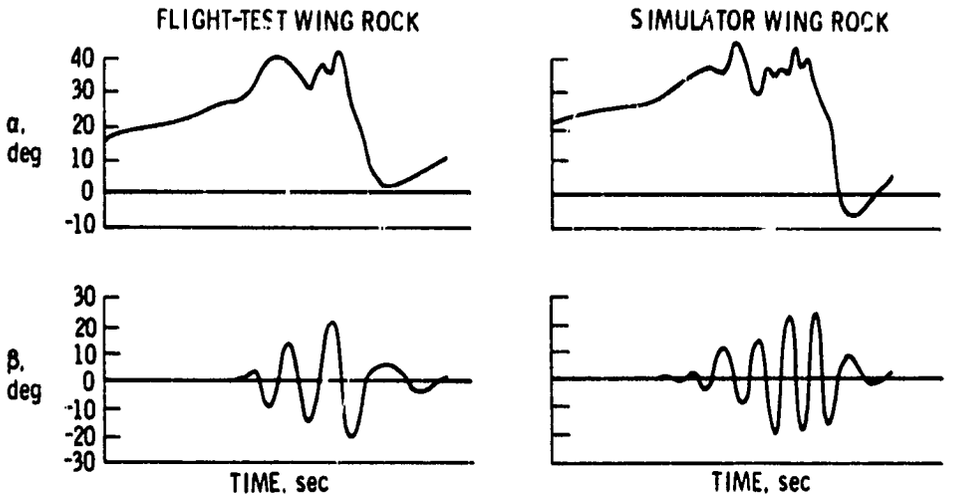

Figure 78.- Correlation of wing-rock motions experienced in flight and in simulation for airplane A.

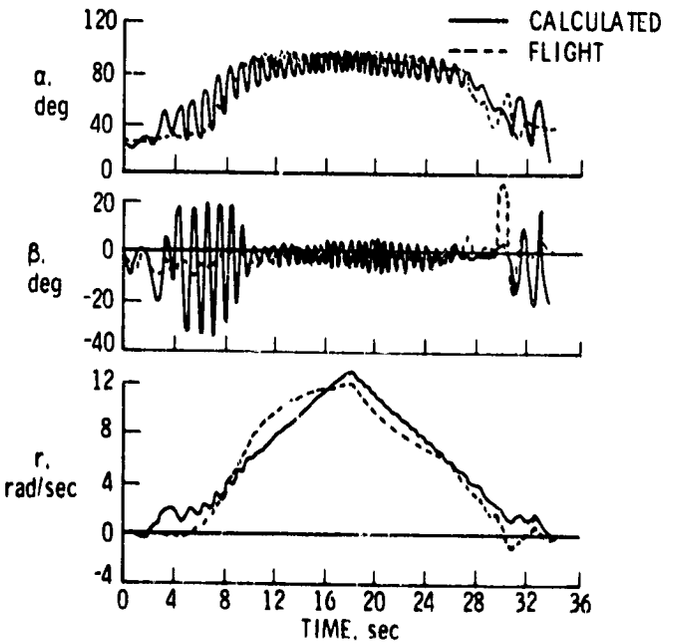

Figure 79.- Correlation of spin-entry motions for airplane B.

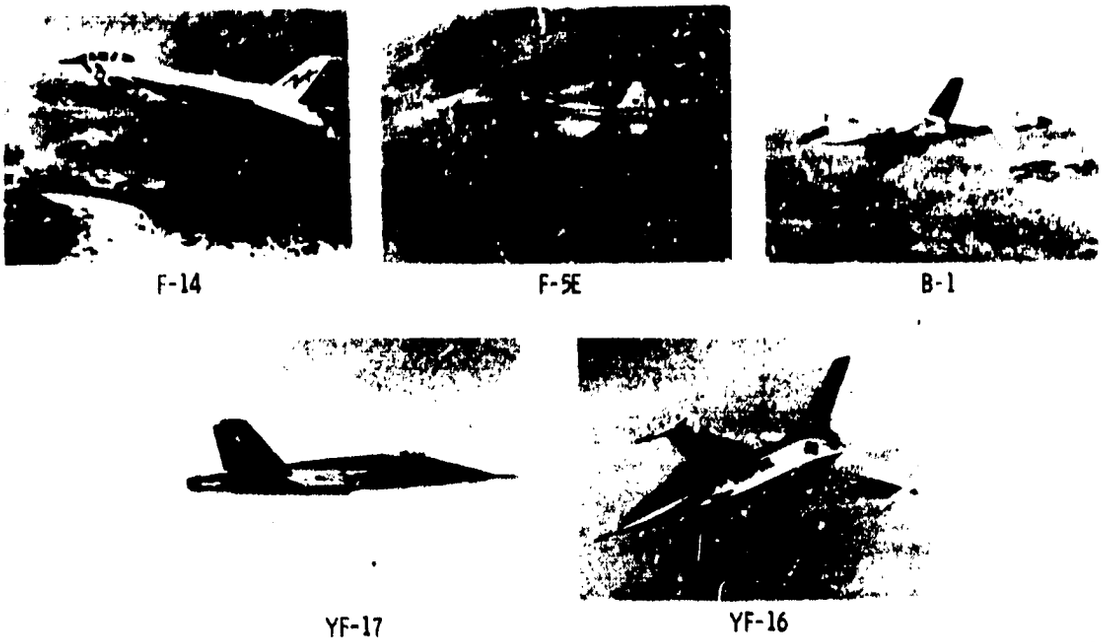

L-77-7598

Figure 80.- Configurations studied in DMS.

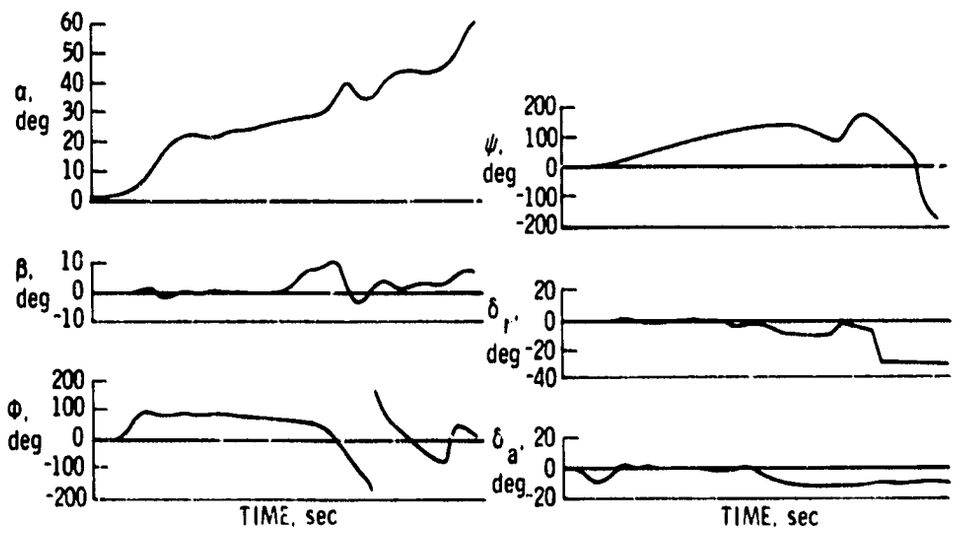

Figure 81.- Effect of degraded high α characteristics on handling qualities.

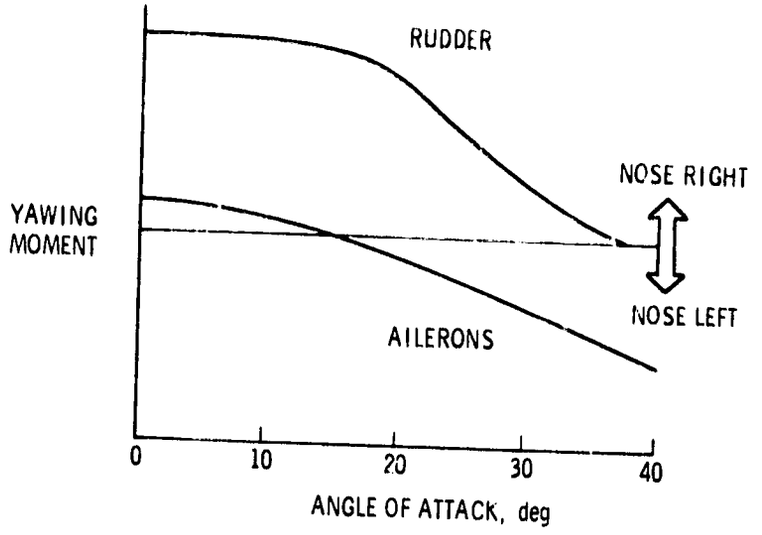

Figure 82.- Yawing moments produced by lateral-directional controls.

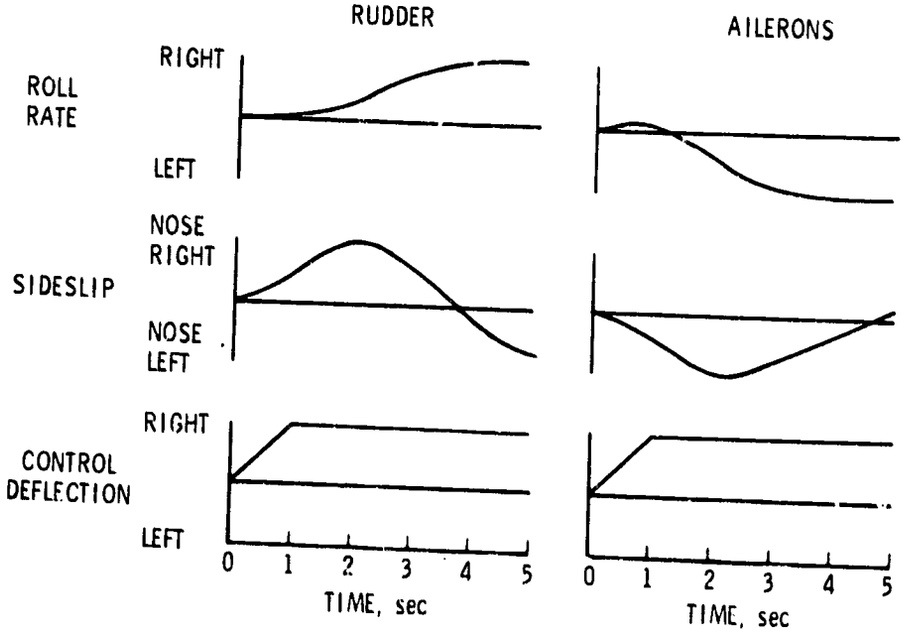

Figure 83.- Illustration of roll-reversal phenomenon. $\alpha = 25^{\circ}$.

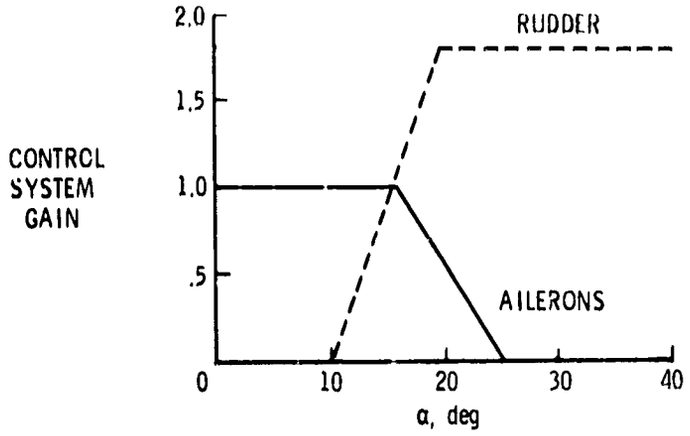

Figure 84.- Lateral-stick-to-rudder interconnect concept.

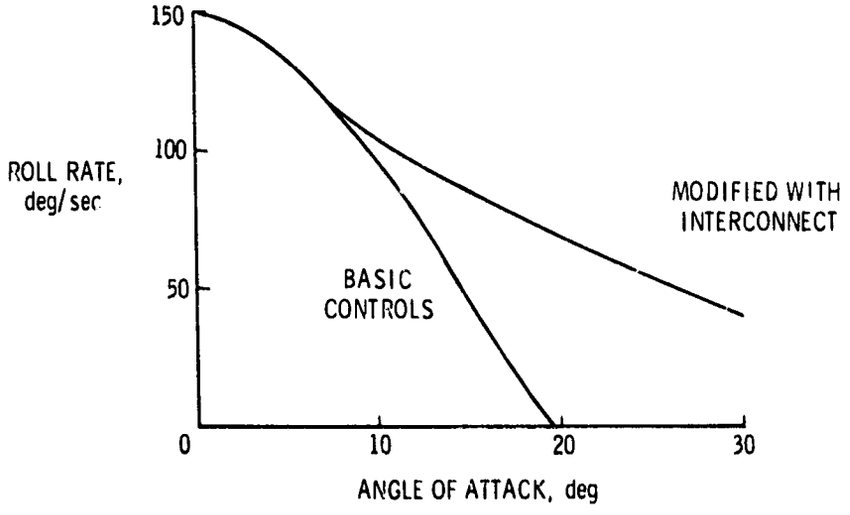

Figure 85.- Effect of interconnect on roll performance.

1. Report No.	2. Government Accession No	3. Recipient's Catalog No
NASA TM-74097		

4. Title and Subtitle	5. Report Date
AERODYNAMIC CHARACTERISTICS OF AIRPLANES AT HIGH ANGLES OF ATTACK	December 1977
	6. Performing Organization Code
7. Author(s)	8. Performing Organization Report No
Joseph R. Chambers and Sue B. Grafton	L-11677
9. Performing Organization Name and Address	10. Work Unit No
NASA Langley Research Center Hampton, VA 23665	505-06-23-01
	11. Contract or Grant No
12. Sponsoring Agency Name and Address	13. Type of Report and Period Covered
National Aeronautics and Space Administration Washington, DC 20546	Technical Memorandum
	14. Sponsoring Agency Code

15. Supplementary Notes

This paper was presented by Joseph R. Chambers at the AGARD/VKI Lecture Series on Aerodynamic Inputs for Problems in Aircraft Dynamics, Rhode-St-Genese, Belgium, April 25-29, 1977.

16. Abstract

The paper provides an introduction to, and a broad overview of, the aerodynamic characteristics of airplanes at high angles of attack. The discussion includes (1) some important fundamental phenomena which determine to a large extent the aerodynamic characteristics of airplanes at high angles of attack; (2) static and dynamic aerodynamic characteristics near the stall; (3) aerodynamics of the spin; (4) test techniques used in stall/spin studies; (5) applications of aerodynamic data to problems in flight dynamics in the stall/spin area; and (6) the outlook for future research in the area. Stall and spin are flight dynamic problems of importance to all aircraft, including general aviation airplanes, commercial transports, and military airplanes. The emphasis in the paper, however, is placed on military configurations and the relative aerodynamic factors which influence the stability and control of such vehicles at high angles of attack.

17. Key Words (Suggested by Author(s))	18. Distribution Statement
Spin Stall/departure Stability	Unclassified - Unlimited Subject Category 02

19. Security Classif. (of this report)	20. Security Classif. (of this page)	21. No. of Pages	22. Price*
Unclassified	Unclassified	42	$4.50

*For sale by the National Technical Information Service, Springfield, Virginia 22161